

Orientifold Planar Equivalence
In Lattice Gauge Theories

Scuola Normale Superiore di Pisa
Classe di Scienze

Tesi di Perfezionamento in Fisica
10 Ottobre 2008

Orientifold Planar Equivalence In Lattice Gauge Theories

Candidato
Agostino Patella

Relatore
Prof. Adriano Di Giacomo

Con questa tesi si conclude la mia avventura pisana, il cui ricordo mi rimarrà prezioso nel cuore. Il pensiero corre a tutti coloro che mi hanno accompagnato in questi otto anni.

Agli amici e colleghi di corso, gli esami preparati insieme sul terrazzo del Fermi nelle afose giornate estive, le passeggiate dal Carducci alla mensa, le volte in cui basta bussare al muro per fare due chiacchiere.

Ai professori, le lezioni seguite e quelle saltate; al mio relatore di molte tesi, gli incontri per fare il punto della situazione.

Ai miei compagni di ufficio, e degli uffici vicini, un pranzo insieme, una discussione di fisica, una battuta, una risata.

Agli amici e fratelli che si sono avvicinati in via Funaioli, gli ospiti più o meno fissi, quelli che semplicemente passavano per cena, per ascoltare musica o per discutere di problemi globali e contaminazioni culturali; a quelli che per tre anni sono stati la mia famiglia.

Agli amici e fratelli di avventure all'aria aperta, compagni di gioie e di fatiche.

Agli amici di serate in birreria, gli amici del divano e del whisky; a quelli con cui non hai bisogno di parlare per essere capito.

Agli amici lontani, quelli da cui rifugiarsi nei momenti bui.

A mia sorella, un caffè pomeridiano, uno sguardo, un abbraccio.

Ai miei genitori, le telefonate serali, la loro costante fiducia.

A tutti va il mio ringraziamento per aver fatto questo pezzo di strada con me.

Contents

| | | |
|----------|-----------------------------------------------------------------------------------|-----------|
| 1 | Introduction | 5 |
| 1.1 | The large- N_c limit of QCD | 6 |
| 1.2 | Aim of the work | 7 |
| 1.3 | Plan of the work | 10 |
| 2 | Planar limits | 13 |
| 2.1 | 't Hooft planar limit | 13 |
| 2.2 | Topological expansion | 16 |
| 2.3 | Orientifold planar limit | 18 |
| 2.4 | Large- N_c limits as Classical Mechanics | 21 |
| 2.5 | Loop equations | 26 |
| 3 | A review of the orientifold planar equivalence | 31 |
| 3.1 | Dictionary between neutral sectors | 32 |
| 3.1.1 | The gauge sector | 32 |
| 3.1.2 | The quark sector of OrientiQCD | 32 |
| 3.1.3 | The gluino sector of AdjQCD | 34 |
| 3.1.4 | Dictionary of observables and symmetries | 35 |
| 3.2 | Relics of SUSY in QCD | 37 |
| 3.3 | The perturbative proof | 38 |
| 3.4 | The nonperturbative proof on the lattice | 42 |
| 3.5 | The role of the C-symmetry | 48 |
| 4 | The equivalence in the strong-coupling and large-mass phase on the lattice | 53 |
| 4.1 | About the Majorana fermion | 55 |
| 4.2 | Hopping expansion | 58 |

| | | |
|----------|-------------------------------------------------------------------|-----------|
| 4.3 | Loop equations | 58 |
| 4.4 | Solution of the loop equations and planar equivalence | 60 |
| 5 | The center symmetry in the planar limit | 63 |
| 5.1 | Potentials for the Polyakov loop | 65 |
| 5.2 | The connected graphs in the large-mass expansion | 67 |
| 5.2.1 | Pure gauge | 68 |
| 5.2.2 | Adjoint fermions | 69 |
| 5.2.3 | Fundamental fermions | 70 |
| 5.2.4 | S/AS fermions | 72 |
| 5.3 | The effective potentials in the large-mass expansion | 77 |
| 5.3.1 | The b_1 coefficient | 78 |
| 5.3.2 | The b_2 coefficient | 79 |
| 5.4 | The center symmetry in the Hamiltonian formalism | 80 |
| 5.5 | Appendix: The planar limit in pure gauge on the lattice | 82 |
| 6 | Breaking of the charge conjugation symmetry | 87 |
| 6.1 | Breaking of discrete symmetries | 88 |
| 6.2 | Baryon currents | 90 |
| 6.3 | The lattice calculation | 92 |
| 7 | Some results in the quenched theory | 97 |
| 7.1 | Setting the scale in the quenched theory | 99 |
| 7.2 | The fermionic condensate at large- N_c | 100 |
| 7.2.1 | Analytical equivalence | 100 |
| 7.2.2 | Separating the $1/N_c$ corrections | 103 |
| 7.2.3 | Details of the simulations | 105 |
| 7.2.4 | Numerical results | 106 |
| 7.2.5 | Extrapolation to $SU(\infty)$ | 111 |
| 7.2.6 | Chiral limit | 111 |
| 7.3 | Mesons at large- N_c | 117 |
| 7.3.1 | Details of the simulations | 117 |
| 7.3.2 | Numerical results | 119 |
| 7.3.3 | Extrapolation to $SU(\infty)$ | 129 |
| 7.3.4 | Discussion | 134 |

| | | |
|----------|----------------------------------------------------|------------|
| 8 | Towards dynamical fermions – the HiRep code | 137 |
| 8.1 | The HMC algorithm | 142 |
| 8.1.1 | Bosonic fields | 142 |
| 8.1.2 | Fermionic fields | 143 |
| 8.2 | $SU(N_c)$ notation | 144 |
| 8.3 | The fermionic action | 145 |
| 8.4 | Molecular dynamics | 146 |
| 8.4.1 | Computation of the force | 146 |
| 8.4.2 | Integration of the Hamilton equations | 149 |
| 8.5 | Metropolis test | 149 |
| 8.6 | Notes on the rational approximations | 149 |
| 8.7 | Conventions used in the code | 150 |
| 8.7.1 | Representations | 150 |
| 8.7.2 | γ matrices | 151 |
| 9 | Conclusions and outlook | 153 |
| | Bibliography | 155 |

Chapter 1

Introduction

For about 35 years, Quantum Chromodynamics (QCD) has withstood the efforts to understand how the well-known microscopic degrees of freedom (strongly) interact and generate the well-known variety of the hadronic world. A large amount of evidences was collected that confirm indeed QCD as the right theory of hadrons. But a satisfactory explanation of the low-energy properties from first principles is still lacking. We do not know how the QCD vacuum looks like; we can explain neither the colour confinement nor the chiral symmetry breaking. Although common lore suggests that QCD in the low-energy regime should be described by some dual weak-coupled theory, we do not know what this theory should be.

The construction of a clear physical picture for the strong interactions might be by itself an excellent reason to go on studying QCD. However, one more and equally important reason must be considered. While the Quantum Field Theory (QFT) is the foundation of the success of the Standard Model of Elementary Particles, and although a large part of the scientific community believes that somehow we need to go beyond QFT to achieve the quantization of Gravity, we cannot claim to fully understand QFT. Basically, we have three different ways to handle (and actually define) QFT:

- approximating it, by means of a perturbative expansion or a semiclassical one, like for the Electroweak Model and all the effective models;
- increasing the number of symmetries, in order to constrain some observables, until these are completely fixed, like for supersymmetric or conformal theories;

- discretizing it on a lattice and to define a continuum limit through an UV renormalization-group fixed point (if it exists), like for QCD-like theories.

Unless so much symmetry exists that the theory is completely determined (but no real system seems to fulfil this requirement), just in the last case we can deal with the full nonperturbative regime of a QFT, avoiding approximations at least in principle.

So QCD-like theories offer a unique workbench. We can define them by a lattice discretization; we can obtain predictions from first principles by numerical simulations; we can use the other techniques in the list above; and finally we can compare the results.

1.1 The large- N_c limit of QCD

One of the possible strategies to attack analytically QCD is to change some parameter and then to try a systematic expansion in order to go back to its original value. When such a procedure is followed, some features of the original theory may be kept, and others may be lost.

In the perturbative expansion any traces of confinement and of chiral symmetry breaking are lost while the high-energy processes are well-described. The expansion in the quark mass (actually m/Λ_{QCD}) retains the main low-energy features of QCD, although in practice it is useful to describe basically the dynamics of the quasi-Goldstone bosons of the chiral symmetry.

A third possibility is to change the number of colours N_c and to study QCD in the limit $N_c = \infty$. This was first proposed in 1974 by 't Hooft [1], who borrowed this idea from the $1/N$ expansion of vector models in Statistical Mechanics. The 't Hooft large- N_c limit has several interesting properties. First, it is a perturbative expansion in the coupling of one-particle states of QCD: meson resonances do not decay, the meson-glueball mixing vanishes. Then, it was understood that it is rather a classical limit: the quantum correlations of observables in the emerging theory vanish. These reasons are enough to state that the large- N_c limit, in spite of the larger and larger number of degrees of freedom, is somehow a simpler theory than the original one.

However, not enough simple to let us penetrate into the vacuum structure of QCD. In the last years, the interest in the large- N_c limit has raised again, mainly thanks to the AdS/CFT correspondence and the orientifold planar equivalence (besides the dimensional reduction and the Eguchi-Kaway-like models, which are evergreen).

The idea of AdS/CFT is that the dual of a gauge theory must be a string theory [2]. Some supports for this conjecture exist for the $\mathcal{N} = 4$ super Yang-Mills, and its dual IIB string theory on the $AdS_5 \times S^5$ space. A strong gauge coupling corresponds to a large string tension; the large- N_c limit corresponds to a weak string coupling. In this regime, the string theory is largely manageable.

The idea of the orientifold planar equivalence [3, 4, 5, 6, 7] is that, if the large- N_c limit of QCD is properly defined by taking fermions in the antisymmetric representation of the gauge group, QCD becomes in this limit equivalent to the $\mathcal{N} = 1$ super Yang-Mills¹. As the number of colours become finite, QCD moves away from the supersymmetric point. I will go deeper into details, being the orientifold planar equivalence the main topic of this work.

1.2 Aim of the work

At the present, the orientifold planar equivalence is a well-established and recognised result. Some analytical predictions for QCD in the large- N_c limit have already been obtained (the quark condensate, the even-odd degeneracy of states, the exact beta function). An exhaustive project about the orientifold planar equivalence should include at least two goals: to extend the analytical results at $N_c = \infty$, and to quantify the $1/N_c$ corrections.

The $1/N_c$ corrections are generally hard to handle analytically. Numerical simulations may help. For instance, the orientifold planar equivalence predicts the coincidence of a subset of the spectra in two gauge theories, the first one with Dirac fermions in the antisymmetric two-index representation, and the second one with Majorana fermions in the adjoint representation; one might simulate this two theories and measure the spectra, then extract the large- N_c limit and compare the corrections.

The project above presents some serious difficulties.

- Simulations are very time-consuming. For the pure gauge at various N_c , the time required for simulations grows roughly like N_c^3 . However, the heat-bath algorithms commonly used for pure gauge simulations are quite fast. The result is that simulations at very large N_c (although not on

¹The idea of the orientifold planar equivalence was borrowed by a string theory model of Sagnotti [8, 9]. In this work, I will completely skip this string theory point of view, and I will focus on the equivalence of field theories. The idea of taking quarks in the antisymmetric representation was firstly elaborated by Corrigan and Ramond [10] in order to study baryons in the planar limit.

large lattices) are available: for instance, in [11], Narayanan and Neuberger present simulations at $N_c = 47$ on a $8^3 \times 6$ lattice². With dynamical fermions, the algorithms are intrinsically slower, since the inversion of the Dirac operator is required. Moreover for fermions in a two-index representation the time required for simulations grows asymptotically like N_c^4 . Some care must be taken of the optimization, the implementation of the fastest available algorithms, and the parallelization.

- The large- N_c limit must be extracted. But it is not possible to know a priori what a large enough value of N_c is. A similar program has already been developed for the large- N_c limit of the Yang-Mills [12, 13, 14, 15, 16, 17, 18, 19, 20, 21, 22]. The simulations show that it is possible to extract reliably the large- N_c limit for a relevant set of observables from data with $N_c = 2, \dots, 8$ and assuming that just the first correction (that is of order $1/N_c^2$ in this case) is present. The same conclusion is reached by measuring the mesonic spectrum in the quenched theory. These results suggest moderate optimism also whether dynamical fermions are simulated. For fermions in the antisymmetric representation, the extraction of the large- N_c limit might be harder, since corrections of order $1/N_c$ (compared with $1/N_c^2$) are expected.

For these reasons that will be discussed in detail later on, even though this work is a part of the general project of evaluating subleading deviations from the orientifold planar equivalence through numerical simulations, the production of the first results will require still some time, probably some months.

Hence, the goal of this work is twofold. The first one is to investigate analytically the orientifold planar equivalence for theories discretized on the lattice, at fixed lattice spacing. In section 3.4, the formal proof of Armoni, Shifman, Veneziano [23] is translated on the lattice and some underlying assumptions are clarified. In chapter 4, a proof of the orientifold planar equivalence on the lattice in the strong-coupling and large-mass phase is provided. In chapter 5, the remnants of the center symmetry in the orientifold planar limit are discussed for the theory on the lattice. In chapter 6, the breaking of the charge conjugation for QCD with one small compact dimension is investigated.

The relevance of these analyses may be better understood in a historical perspective. Since the first work of Armoni, Shifman, Veneziano [4] and for some years, the validity of the orientifold planar equivalence had been questioned.

²The expansion parameter for the pure gauge theory is $1/N_c^2$. I said that $N_c = 47$ is large, in the sense that $1/N_c^2 = 4.5 \times 10^{-4}$ is much smaller than 1.

Thus, some of the works presented here had the aim of clarifying some debated points, arguing in favour of the orientifold planar equivalence. The chronology of the events follows.

| Date | Work |
|---------------|--------------------------------------------------------------------------------------------------------------------------------------------------------------------------------------------------------------------------------------------------------------------------------------------------|
| February 2003 | Armoni, Shifman, Veneziano published their first paper about orientifold planar equivalence [4]. |
| December 2004 | Armoni, Shifman, Veneziano published the detailed proof of the equivalence [23]. |
| July 2005 | Sannino raises the problem of the center symmetry matching between SYM and orientifold QCD [24]. |
| November 2005 | I published the proof of the orientifold planar equivalence in the strong-coupling and large-mass phase on the lattice [25]. |
| August 2006 | Unsal and Ya e pointed out that the orientifold planar equivalence holds if and only if the charge conjugation symmetry is not spontaneously broken [26]; they showed that the equivalence is not valid on a space with one compact dimension and periodic boundary conditions for the fermions. |
| December 2006 | DeGrand and Ho mann published the first simulations about the breaking of the charge conjugation in QCD with compact dimensions [27]. They gave some indications about its restoration at large radius of the compact dimension. |
| October 2006 | Thanks to a private discussion with Armoni, some sufficient conditions were identified for the orientifold planar equivalence to be valid on the lattice beyond the large-mass expansion (see section 3.4). |
| January 2007 | Armoni, Shifman, Veneziano clarified the role of charge conjugation, and the connection with the fermion loop expansion of the action, in their proof [28]. |
| February 2007 | Lucini, Pica and I showed that the breaking of the charge conjugation symmetry implies a baryon current around the compact dimension [29]. This fact strongly supports the restoration picture. |

| Date | Work |
|---------------|-------------------------------------------------------------------------------------------------------------------------------------------------------------|
| December 2007 | Two independent analysis of the center symmetry in the orientifold QCD are developed by Del Debbio and me (unpublished) and by Armoni, Shifman, Unsal [30]. |

The second goal of this work is to develop a parallelized and highly optimized code for simulating dynamical fermions in a general representation. This goal is only partially achieved. A first non-parallel version of the code is already available, and it was used to obtain the results presented in chapter 7. The parallel version is under development. The main features of the code are described in chapter 8 in some details.

1.3 Plan of the work

Chapter 2 is a review of the planar limits of QCD ('t Hooft planar expansion, topological expansion, orientifold expansion). The general formalism of the coherent states and the loop equations are introduced. In this chapter, the notation for the whole work is fixed.

Chapter 3 is a review of the orientifold planar equivalence. The main results are briefly summarized. The dictionary of the observables and symmetries in SYM and orientifold QCD is discussed in some details. A brief review of the perturbative proof, and a discussion of the nonperturbative proof of the orientifold planar equivalence are presented.

The proof of the orientifold planar equivalence on the lattice in the strong-coupling and large-mass phase is the subject of chapter 4.

Chapter 5 is devoted to a discussion of the remnants of the center symmetry in the orientifold QCD in the large- N_c limit, mainly through the computation of the effective potential of the Polyakov loop on the lattice in the large-mass expansion.

Charge conjugation symmetry plays a central role in the proof of the orientifold planar equivalence: the equivalence is valid if and only if the charge conjugation is not spontaneously broken in orientifold QCD. Chapter 6 is an analysis of the C-symmetry in QCD. In particular, it is shown that the C-breaking in QCD with compact dimensions implies the generation of some persistent baryon currents.

From chapter 7, a part devoted mostly to numerical simulations begins. This chapter is an exploratory study of the large- N_c limit of the meson spectrum with quenched fermions in the fundamental representation, and of the the large- N_c limit of the fermionic condensate with quenched fermions in the two-index representations. Some aspects of the orientifold planar equivalence between the quenched theories are discussed.

Finally, in chapter 8 the HiRep code, developed for future simulations with dynamical fermions in a generic representation, is described.

Chapter 2

Planar limits

In order to define a large- N_c (or *planar*) limit of QCD, one must first define a multicoloured version of QCD. More than one procedure are available, as we will see in a while. It is important to remark at this stage that, since more than one multicolour QCD exist, each of those will lead to different large- N_c limit. Therefore, it is quite incorrect to talk about the large- N_c limit of QCD. One should better talk about large- N_c *limits* of QCD, or otherwise one needs to specify which multicolour generalisation of QCD he is considering. In the first three sections, I will give a brief review of three different planar limits of QCD: 't Hooft, topological and orientifold large- N_c limits.

All the large- N_c limits are characterised by the suppression of the quantum fluctuations of the observables. In this sense the large- N_c limits are similar to the $\hbar \rightarrow 0$ limit for the quantum particle. The underlying classical theory can be recovered through the formalism of the coherent states, which is reviewed in section 2.4.

Finally in section 2.5, I will review the Schwinger-Dyson equations for the Wilson loops in the large- N_c limit (the loop equations).

2.1 't Hooft planar limit

The simplest multicolour QCD was proposed by 't Hooft [1].

NQCD: $SU(N_c)$ gauge theory with N_f flavours (N_f is kept fixed) of fermions in the fundamental representation of the gauge group.

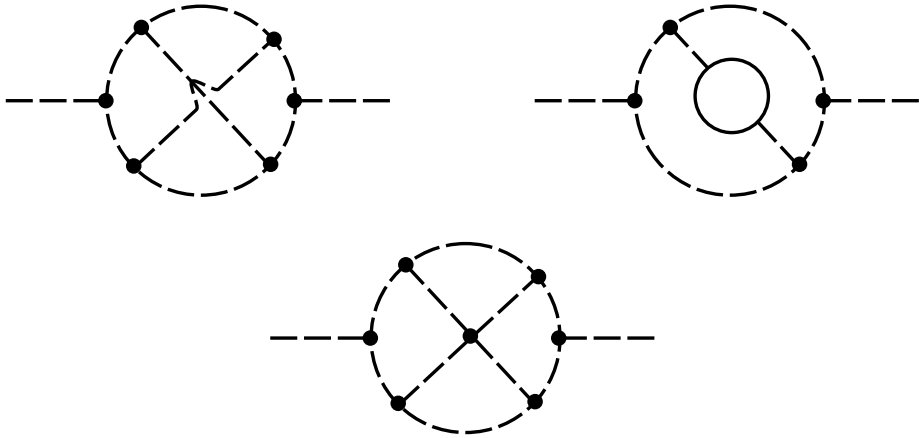


Figure 2.1: Some diagrams for the gluon dressed propagator. The dashed lines are the gluons, the full lines are the quarks, the circles are the three or four-gluon vertices. In the first row, two subleading contributions. The first diagram is non planar; the second one is planar, but contains a hole (i.e. a quark loop). In the second row, a leading contribution.

By perturbative arguments 't Hooft pointed out the following facts.

- The 't Hooft coupling $\lambda = g^2 N_c$ must be kept fixed, as N_c increases, in order to have a non-trivial beta function in the $N_c = \infty$ limit.
- The expansion in $1/N_c$ rearranges the diagrams of perturbation theory according to their topology. In the $N_c = \infty$ limit, only planar diagrams survive. For this reason, the large- N_c limit is also known as *planar limit*. In general, each diagram may be interpreted as a polyhedron, whose faces are the loops containing gluon propagators; purely fermionic loops are interpreted as holes in the surface. If χ is the Euler characteristic of the polyhedron, then the diagram is of order N_c^χ (figure 2.1).
- As a consequence of the previous point, each quark loop contributes with a $1/N_c$ suppression.

The most remarkable properties of the 't Hooft planar limit derive from a hierarchy of connected correlation functions of gauge-invariant operators, which

I am going to explain. Let O_i denote a set of gauge-invariant operators that have a finite large- N_c limit. For simplicity, I have in mind operators that cannot be written as the product of two pieces, that are separately gauge-invariant. It is possible to choose the normalization of the fields in such a way that the Lagrangian is:

$$\mathcal{L} = -\frac{N_c}{2\lambda} \text{tr} F_{\mu\nu} F^{\mu\nu} + \sum_{f=1}^{N_f} \bar{\psi}_f (i\mathcal{D} - m_f) \psi_f . \quad (2.1)$$

For instance, O_i may be chosen among the following operators:

$$\left. \begin{aligned} & \frac{1}{N_c} \bar{\psi} \gamma_\mu \psi(x), \quad \frac{1}{N_c} \text{tr} F_{\mu\nu} F^{\mu\nu}(x), \quad \frac{1}{N_c} \text{tr} \text{Pexp} \left\{ i \oint_\alpha A_\mu(x) dx^\mu \right\}, \\ & \frac{1}{N_c} \bar{\psi}(x) \text{Pexp} \left\{ i \int_x^y A_\mu(z) dz^\mu \right\} \psi(y), \quad \frac{1}{N_c} \bar{\psi} F_{\mu\nu} \psi(x) . \end{aligned} \right\} \quad (2.2)$$

When it will be useful, I will split the operators O_i into a set of pure gluonic operators G_i and mesonic operators H_i (I will not consider baryonic operators for the moment).

In the planar limit, the expectation value of the product of some operators O_i factorizes (*factorization property*):

$$\langle O_1 \cdots O_k \rangle \simeq \langle O_1 \rangle \cdots \langle O_k \rangle . \quad (2.3)$$

Moreover, the N_c asymptotic behaviour of the connected correlation functions can be computed:

$$\langle G_1 \cdots G_r \rangle_c \propto N_c^{2-2r} \quad (2.4a)$$

$$\langle H_1 \cdots H_s \rangle_c \propto N_c^{1-s} \quad (2.4b)$$

$$\langle G_1 \cdots G_r H_1 \cdots H_s \rangle_c \propto N_c^{1-2r-s} . \quad (2.4c)$$

Let us focus on the two-points functions. Since $\langle G_1 G_2 \rangle_c$ is of order of N_c^{-2} , clearly the operator $\hat{G}_i = N_c G_i$ creates a glueball state with normalization of order 1. Similarly, since $\langle H_1 H_2 \rangle_c$ is of order of N_c^{-1} , it is clear that the operator $\hat{H}_i = N_c^{1/2} H_i$ creates a meson state with normalization of order 1. Moreover, it can be shown that both \hat{G}_i and \hat{H}_i create only one-particle states from the vacuum [31].

A list of some interesting properties of the 't Hooft planar limit follows.

Meson and glueball resonances are stable. The s -meson interaction vertex $\langle \hat{H}_1 \cdots \hat{H}_s \rangle_c$ is of order $N^{1-\frac{s}{2}}$. Each additional meson gives a $1/\sqrt{N_c}$ suppression. The mixed vertex $\langle \hat{G}_1 \cdots \hat{G}_r \hat{H}_1 \cdots \hat{H}_s \rangle_c$ is of order $N_c^{1-r-\frac{s}{2}}$, and the r -glueball vertex $\langle \hat{G}_1 \cdots \hat{G}_r \rangle_c$ is of order N_c^{1-r} . Thus each additional glueball gives a $1/N_c$ suppression. The dominant interaction vertices are the three-particle ones; but still all the interaction vertices vanish in the planar limit. Therefore, mesons and glueballs cannot decay at $N_c = \infty$.

Scalar isosinglet mesons and glueballs do not mix. The mixing amplitude $\langle \hat{H} \hat{G} \rangle_c$ is of order $1/\sqrt{N_c}$.

Axial anomaly turns off. In the planar limit, the η' mass vanishes. At the NLO, the Witten-Veneziano formula [32, 33] holds:

$$m_{\eta'}^2 = \frac{2N_f}{F_\pi^2} \int \langle Q(x)Q(0) \rangle_{YM} d^4x. \quad (2.5)$$

The pion decay constant F_π is of order $\sqrt{N_c}$, while the susceptibility of the topological charge $Q(x)$ is of order 1, so the η' mass is of order $1/\sqrt{N_c}$.

Baryons mass goes to infinity. A baryon is a bound state of N_c quarks. By a heuristic argument, which is precised in [31], the mass of a baryon is given by the sum of the quark masses, the kinetic energy of the quarks and the quark-pairs potential energy. The first two terms are clearly proportional to N_c ; the potential energy is given by the sum over all the pairs (that are of order N_c^2) of the quark-pair interaction (that is of order $1/N_c$). Altogether, the baryon mass is of order N_c .

2.2 Topological expansion

A different generalisation of QCD to N_c colours was proposed by Veneziano [34]. It is based on the idea of Witten [35] and 't Hooft [36]. It is based on the idea of Witten [35] and 't Hooft [36]. It is based on the idea of Witten [35] and 't Hooft [36].

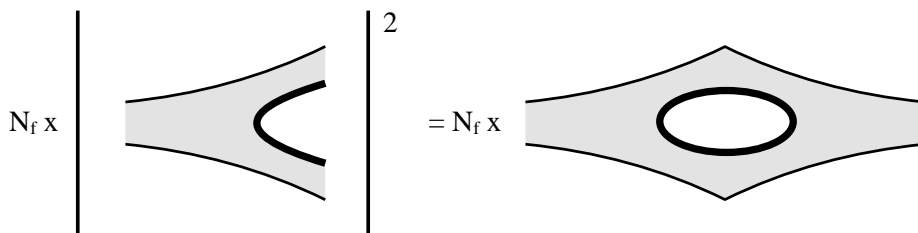


Figure 2.2: Schematically, the decay width of the channel $1 \rightarrow 2$ mesons. The squared norm of the amplitude corresponds to a graph with (at least) one loop ($\propto 1/N_c$). To obtain the width, a sum over all the possible outgoing mesons is required ($\propto N_c$). Hence, the width is of order 1.

suppressed anymore. Indeed, a single flavour propagating in a loop gives still rise to a $1/N_c$ factor, but we have to sum over $N_f = uN_c$ equal contributors.

Here, some properties of the topological planar limit follow.

Meson and glueball resonances decay. By adding a meson in the final states, the amplitude takes a factor $1/\sqrt{N_c}$, thus the width takes a $1/N_c$. But one more meson means a quark line propagating among the final states. Thus, the total width takes an extra N_c per quark line, when summing over all the flavours (figure 2.2). Finally, the decay by meson production is allowed at the leading order.

Scalar isosinglet mesons and glueballs do not mix. The mixing amplitude $\langle \hat{H}\hat{G} \rangle_c$ remains of order $1/\sqrt{N_c}$ (no sum over flavour must be performed).

Axial $U(1)$ is anomalous. The η' mass does not vanish. The Witten-Veneziano formula gives a non-zero contribution to the leading order of the η' mass in the topological expansion. However, some other contributions must be added, and the Witten-Veneziano formula does not hold in the topological expansion.

Baryons mass goes to infinity. It works exactly like in the 't Hooft large- N_c limit.

2.3 Orientifold planar limit

The last version of multicoloured QCD I will consider can be understood on the basis of the following simple fact: the antifundamental representation of the group $SU(3)$ coincides with the antisymmetric two-index one. In fact, thanks to the invariance of the fully skew-symmetric ϵ_{ijk} tensor, a one-to-one unitary map exists between the two representations:

$$\begin{aligned} \bar{q}_i &= \frac{1}{2} \epsilon_{ijk} Q^{jk} & Q^{jk} &= \epsilon^{ijk} \bar{q}_i \\ \bar{q} &\rightarrow U^* \bar{q} & Q &\rightarrow U Q U^T. \end{aligned} \quad (2.6)$$

The field describing quarks and antiquarks can be equivalently thought as a vector or as an antisymmetric matrix in the colour space. I want to stress that it does not make any difference at $N_c = 3$, but we obtain completely different theories at $N_c \neq 3$. Thus, Armoni, Shifman and Veneziano in 2003 [3] proposed the orientifold QCD.

OrientiQCD: $SU(N_c)$ gauge theory with n_f flavours of fermions in the antisymmetric representation and $n_f^{(F)}$ flavours (both $n_f^{(F)}$ and n_f are kept fixed) of fermions in the fundamental representation of the gauge group.

By perturbative arguments, the following facts are established.

- The one-loop beta function of the 't Hooft coupling $\lambda = g^2 N_c$ is:

$$\beta(\lambda) = -\frac{\lambda^2}{8\pi^2} \left\{ \frac{11}{3} - n_f \frac{2N_c - 4}{3N_c} - n_f^{(F)} \frac{2}{3N_c} \right\}, \quad (2.7)$$

it remains finite if λ is kept fixed as N_c increases.

- Since quarks have two indices, quark loops are not suppressed in the planar limit.
- The expansion in $1/N_c$ rearranges the diagrams of perturbation theory according to their topology, like in the 't Hooft expansion. But now, fermionic loops are faces and not holes in the diagrams. In the $N_c = \infty$ limit, only planar diagrams survive (figure 2.3).

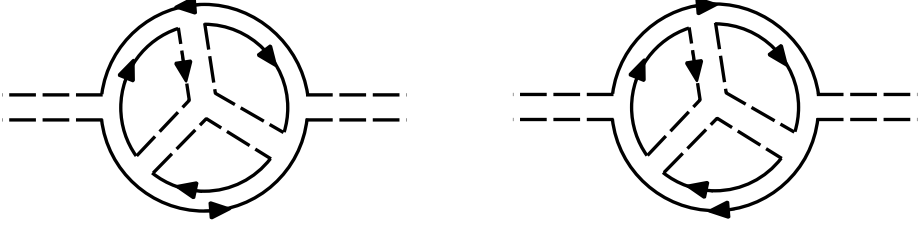


Figure 2.3: Some diagrams for the gluon dressed propagator, in the double lines notation. The dashed double lines are the gluons, the full double lines are the quarks. Double parallel lines mean the adjoint representation, double opposite lines mean the antisymmetric representation. Both diagrams are leading contributions.

I want to explore the hierarchy of the connected correlation functions of gauge-invariant operators. Again, let O_i denote a set of gauge-invariant operators, that have a finite large- N_c limit, and that cannot be split into two pieces which are separately gauge-invariant. For instance, O_i may be chosen among the following operators (ψ is the fermion in the antisymmetric representation):

$$\begin{aligned} & \frac{1}{N_c^2} \bar{\psi} \gamma_\mu \psi(x), \quad \frac{1}{N_c} \text{tr} F_{\mu\nu} F^{\mu\nu}(x), \quad \frac{1}{N_c} \text{tr} \text{Pexp} \left\{ i \oint_\alpha A_\mu(x) dx^\mu \right\}, \\ & \frac{1}{N_c^2} \bar{\psi}(x) \text{As} \left[\text{Pexp} \left\{ i \int_x^y A_\mu(z) dz^\mu \right\} \right] \psi(y), \quad \frac{1}{N_c^2} \bar{\psi} \text{As} [F_{\mu\nu}] \psi(x). \end{aligned} \quad (2.8)$$

As before, I will denote G_i the gluonic operators and H_i the mesonic operators.

As in the 't Hooft planar limit, the expectation value of the product of some operators O_i factorizes (*factorization property*):

$$\langle O_1 \cdots O_k \rangle \simeq \langle O_1 \rangle \cdots \langle O_k \rangle. \quad (2.9)$$

Since quarks and gluons have the same weight in the planar limit, the N_c asymptotic behaviour of the connected correlation functions is different from the 't Hooft large- N_c :

$$\langle G_1 \cdots G_r \rangle_c \propto N_c^{2-2r} \quad (2.10a)$$

$$\langle H_1 \cdots H_s \rangle_c \propto N_c^{2-2s} \quad (2.10b)$$

$$\langle G_1 \cdots G_r H_1 \cdots H_s \rangle_c \propto N_c^{2-2r-2s}. \quad (2.10c)$$

By analyzing the two-points functions, we conclude that the operator $\hat{G}_i = N_c G_i$ creates a glueball state with normalization of order 1; and the operator $\hat{H}_i = N_c H_i$ creates a meson state with normalization of order 1. Both \hat{G}_i and \hat{H}_i create only one-particle states from the vacuum.

From a phenomenological point of view, the 't Hooft planar limit underestimates the quark term in the action. The orientifold expansion have it in common with the topological expansion, to be a possible remedy to that problem.

Meson and glueball resonances are stable. Indeed, each additional meson and each additional glueball to an interaction vertex give a $1/N_c$ suppression. The dominant interaction vertexes are the three-particle ones, and those are of order $1/N_c$. Therefore, mesons and glueballs cannot decay at $N_c = \infty$.

Scalar isosinglet mesons and glueballs mix. Indeed, the mixing amplitude $\langle \hat{H}\hat{G} \rangle_c$ is of order 1.

Axial $U(1)$ is anomalous. The Witten-Veneziano formula is not valid with fermions in a two-index representation. Moreover (through the orientifold planar equivalence) it can be shown that the η' mass stays different from zero in the planar limit.

Some baryons survive. Indeed, baryons can be constructed by contracting one antisymmetric fermion with two fundamental fermions.

However, from a theoretical point of view, the orientifold planar limit opens new perspectives thanks to the *orientifold planar equivalence*. Armoni, Shifman and Veneziano argued that each Dirac fermion in the antisymmetric representation can be replaced by a Majorana fermion in the adjoint representation, in the planar limit [4, 3, 5]. Therefore, in the planar limit OrientiQCD is equivalent to the following theory:

AdjQCD: $SU(N_c)$ gauge theory with n_f flavours of Majorana fermions in the adjoint representation of the gauge group.

For the moment, I want to focus on two simple consequences that make the orientifold planar limit attractive:

- in the planar limit, the confinement in OrientiQCD is associated with the existence of a center symmetry;

- for $n_f = 1$ massless fermion in the antisymmetric representation, Ori-entiQCD becomes supersymmetric in the planar limit; the value of the chiral condensate and the even-odd degeneracy in the bosonic spectrum are predicted.

2.4 Large- N_c limits as Classical Mechanics

The factorization of the expectation values of products of gauge-invariant operators is a common property of the large- N_c limits. If G is a gauge-invariant operator, the factorization property implies:

$$\frac{\langle \Delta G^2 \rangle}{\langle G \rangle^2} = \frac{\langle G^2 \rangle}{\langle G \rangle^2} - 1 \rightarrow 0. \quad (2.11)$$

Therefore, the quantum fluctuations are suppressed and a Classical Mechanics should be somehow recovered. The functional integral measure should be concentrated on a single gauge orbit, called the master orbit. The ground state should be represented by a set of classical configurations of the fields (which are vectors and matrices with infinite components!), connected to each other by some gauge transformations. Although this idea is quite old, any attempt to compute the master orbit was unsuccessful.

An alternate way to understand the Classical Mechanics underlying the large- N_c limit of gauge theories was proposed by 't Hooft in 1981 [35]. The proposed mechanism is analogous to emerging of Classical Mechanics in the $\hbar \rightarrow 0$ limit for the point particle. I want to briefly review it, without pretending to go deep in the details. The following formalism will be used in reviewing the proof of the orientifold planar equivalence by Unsal and 't Hooft (see section 3.5), and in the analysis of the center symmetry (see chapter 5).

In the Quantum Mechanics of the point particle, the coherent states are characterised by the fact that their uncertainties in both position and momentum vanish as $\hbar \rightarrow 0$. A set of coherent states can be generated applying the Heisenberg group (the group of translations in position and momentum spaces) to an initial coherent state (for instance, a real Gaussian state with center in the origin and width proportional to $\sqrt{\hbar}$). This set is overcomplete. The overlap between two coherent states vanishes in the $\hbar \rightarrow 0$ limit; in other words, the coherent states become orthogonal. Roughly speaking, the coherent states are the classical states; the classical observables are defined by two properties: their expectation value on the coherent states must have a finite limit and they must

become diagonal with respect to the set of coherent states as $\hbar \rightarrow 0$. The commutator of two classical observables defines the Poisson brackets in the $\hbar \rightarrow 0$ limit. The position, the momentum, the Hamiltonian are classical observables. If $|\xi(\hbar)\rangle$ is the coherent state that defines the classical state ξ in the $\hbar \rightarrow 0$ limit, the value of the Hamiltonian at ξ is:

$$h(\xi) = \lim_{\hbar \rightarrow 0} \langle \xi(\hbar) | H | \xi(\hbar) \rangle = \frac{p^2(\xi)}{2m} + V(x(\xi)). \quad (2.12)$$

The ground state in the $\hbar \rightarrow 0$ limit is the minimum of the classical Hamiltonian $h(\xi)$.

The same philosophy may be applied to the large- N_c limit of a gauge theory, with a complication. Because of the gauge symmetry, the physical states are gauge-invariant; it is natural to look for a classical Hamiltonian written as a function of only gauge-invariant classical observables. Let us focus on $U(N_c)$ Yang-Mills discretized on the lattice. The Yang-Mills construction schematically follows.

Spatial lattice. The three-dimensional space is discretized as a lattice \mathcal{L} . Two nearest neighbour sites $x, y \in \mathcal{L}$ are connected by a link $\alpha = \langle xy \rangle$; $\bar{\alpha}$ denotes the reversed link. $\mathcal{L}_+^+, \mathcal{L}_-^+, \mathcal{L}_\square$ will be the sets of respectively the positive, the negative and all the links. Similarly, $\mathcal{L}_\square^+, \mathcal{L}_\square^-, \mathcal{L}_\square$ will be the sets of respectively the positive, the negative and all the plaquettes. Finally, \mathcal{C} as the set of all the closed paths, and \mathcal{C}_α as the set of all the closed path starting with the link α .

Quantum structure. The kinematic variables associated with the link α are the parallel transport $U_\alpha \in U(N_c)$ and its conjugate momentum $E_\alpha \in \mathfrak{u}(N_c)$, which is the flux of electric field through a surface of area a^2 orthogonal to α . The algebra of these operators is defined by the following relations (for each $\alpha \in \mathcal{L}_+^+$):

$$E_{\bar{\alpha}}^{A\dagger} = E_\alpha^A, \quad E_{\bar{\alpha}}^A = -\text{Adj}[U_\alpha]^{AB} E_\alpha^B, \quad U_\alpha^\dagger = U_{\bar{\alpha}} \quad (2.13a)$$

$$[E_\alpha^A, E_\alpha^B] = if^{ABC} E_\alpha^C, \quad [E_{\bar{\alpha}}^A, E_{\bar{\alpha}}^B] = if^{ABC} E_{\bar{\alpha}}^C, \quad (2.13b)$$

$$[E_\alpha^A, U_\alpha] = -T^A U_\alpha, \quad [E_{\bar{\alpha}}^A, U_\alpha] = U_\alpha T^A, \quad (2.13c)$$

$$[E_{\bar{\alpha}}^A, E_\alpha] = 0 \quad (2.13d)$$

while variables on different links commute.

If x is a site in the lattice, the electric flux through a small closed surface surrounding the site is given by $\sum_{y|\langle xy \rangle \in \mathcal{L}_+} E_{\langle xy \rangle}$; this is the generator of

the gauge transformation in x . The Hamiltonian is:

$$H = \frac{\lambda N_c}{a} \sum_{\alpha \in \mathcal{L}^\pm} \text{tr} E_\alpha^2 + \frac{2N_c}{\lambda a} \sum_{p \in \mathcal{L}^\pm} \Re \text{tr} U(p), \quad (2.14)$$

where $E_\alpha = 1/N_c \sum_A T^A E_\alpha^A$ and $U(p)$ is the parallel transport along the plaquette identified by p . In general, if Γ is a path, $U(\Gamma)$ is the parallel transport along Γ .

The states can be represented as wave functions $\Psi(U)$ on the space of all the link variables $\{U_\alpha\}$. The operator U_α acts multiplicatively on these wave functions. If d_α^A is the left Lie derivative with respect to the link variable U_α in direction T^A :

$$d_\alpha^A \Psi(U_\alpha) = \lim_{\omega \rightarrow 0} \frac{\Psi(e^{-i\omega T^A} U_\alpha) - \Psi(U)}{\omega}, \quad (2.15)$$

the operator E_α^A is represented by $-id_\alpha^A$. Finally, the operator E_α^A is proportional to the right Lie derivative:

$$E_\alpha^A \Psi(U_\alpha) = i \lim_{\omega \rightarrow 0} \frac{\Psi(U_\alpha e^{-i\omega T^A}) - \Psi(U)}{\omega}. \quad (2.16)$$

Coherence group. The coherence group is the analogous of the Heisenberg group for the point particle. It is parametrized by the following functions:

- a set of gauge-invariant unitary diffeomorphisms $\phi_\alpha(U) \in U(N_c)$, one per each link α ;
- a gauge-invariant hermitian diffeomorphism $\psi(U) \in \mathfrak{u}(N_c)$; it will be convenient to decompose it as a sum of closed paths

$$\psi(U) = \sum_{\Gamma \in \mathcal{C}} \psi_\Gamma U(\Gamma). \quad (2.17)$$

The generic element $V(\phi, \psi)$ of the coherence group is a unitary operator on the Hilbert space and it is defined through its action on the link variables and their conjugate momenta:

$$V U_\alpha V^\dagger = \phi_\alpha(U) U_\alpha \equiv \Phi_\alpha(U) \quad (2.18a)$$

$$V E_\alpha^A V^\dagger = [J^{-1}(U)]_{\alpha\beta}^{AB} \times \left\{ E_\beta^B - d_\beta^B \left[N^2 \text{tr} \psi(U) + \frac{i}{2} \log J(U) \right] \right\}, \quad (2.18b)$$

where $J_{\alpha\beta}^{AB}(U)$ is the Jacobian matrix of the change of variables $U \rightarrow \Phi(U)$:

$$J_{\alpha\beta}^{AB}(U) = 2i \operatorname{tr} [(d_{\alpha}^A \Phi_{\beta})(U) \Phi(U)^{\dagger} T^B] , \quad (2.19)$$

and $J(U)$ is the relative Jacobian determinant.

It can be shown [35] that the set of operators $V(\phi, \psi)$ is closed under composition and inversion, and that the coherence group acts irreducibly over the Hilbert space. Finally, the representation of the generic element $V(\phi, \psi)$ on the wave functions is computed:

$$\hat{V}(\phi, \psi) \Psi(U) = \frac{1}{\sqrt{J(U)}} e^{iN^2 \operatorname{tr} \psi(U)} \Psi(\Phi(U)) . \quad (2.20)$$

It is useful to identify the Lie algebra of the coherence group, as the set of the following operators:

$$\Lambda(a, b) = iN_c \operatorname{tr} \left\{ a(U) + \sum_{\alpha \in \mathcal{L}^{\pm}} [E_{\alpha} b_{\alpha}(U) + b_{\alpha}(U) E_{\alpha}] \right\} , \quad (2.21)$$

where $a(U) = \sum_{\Gamma \in \mathcal{C}} a_{\Gamma} U(\Gamma)$ and $b_{\alpha}(U) = \sum_{\Gamma \in \mathcal{C}_{\alpha}} b_{\alpha, \Gamma} U(\Gamma)$ must be hermitian.

Coherent states. The coherent states can be obtained by applying the elements of the coherence group to the state characterised by the constant wave function $\Psi_0(U) = 1$. The coherent states are written as:

$$\Psi_{\psi, \phi}(U) = \frac{1}{\sqrt{J(U)}} e^{iN^2 \operatorname{tr} \psi(U)} . \quad (2.22)$$

If properly normalized, the elements of the coherence algebra have finite expectation values on the coherent states:

$$\lambda(a, b) = \lim_{N_c \rightarrow \infty} \frac{1}{N_c^2} \langle \Psi_{\psi, \phi} | \Lambda(a, b) | \Psi_{\psi, \phi} \rangle . \quad (2.23)$$

Canonical structure. The coefficients ψ_{Γ} of the decomposition in the equation (2.17) and the expectation values of the Wilson loops

$$W_{\Gamma} = \frac{1}{N_c} \langle \Psi_{\psi, \phi} | \operatorname{tr} U(\Gamma) | \Psi_{\psi, \phi} \rangle \quad (2.24)$$

identify the coherent state $\Psi_{\psi,\phi}$. These observables have a well-defined large- N_c limit and can be chosen as coordinates of the classical phase space. Moreover, it can be shown that W_Γ and ψ_Γ are canonically conjugate.

Classical Hamiltonian. The classical Hamiltonian is given by the large- N_c limit of the expectation value of the quantum Hamiltonian on the coherent states:

$$\begin{aligned} h(\psi, W) &= \lim_{N_c \rightarrow \infty} \frac{1}{N_c^2} \langle \Psi_{\psi,\phi} | H | \Psi_{\psi,\phi} \rangle = \\ &= \frac{\lambda}{4} \psi_\Gamma^\dagger \Omega_{\Gamma,\Gamma'} \psi_\Gamma + \lambda \omega_\Gamma^\dagger \Omega_{\Gamma,\Gamma'}^{-1} \omega_\Gamma - \frac{1}{\lambda} \sum_{p \in \mathcal{L}_\Gamma^\dagger} (W_p + W_p^\dagger), \end{aligned} \quad (2.25)$$

where the matrix Ω and the vector ω are defined as:

$$\Omega_{\Gamma,\Gamma'} = - \lim_{N_c \rightarrow \infty} \frac{2}{N_c} \langle \Psi_{\psi,\phi} | [d_\alpha^A \text{tr} U(\Gamma)]^\dagger d_\alpha^A \text{tr} U(\Gamma') | \Psi_{\psi,\phi} \rangle, \quad (2.26a)$$

$$\omega_\Gamma = - \lim_{N_c \rightarrow \infty} \frac{2}{N_c^2} \langle \Psi_{\psi,\phi} | d_\alpha^A d_\alpha^A \text{tr} U(\Gamma) | \Psi_{\psi,\phi} \rangle. \quad (2.26b)$$

What changes by introducing fermions in the adjoint representation? The simplest lattice fermions are the staggered ones, since these are local and do not involve gamma matrices. The quantum Hamiltonians for the matter is:

$$H_f = N_c \left\{ m \sum_x \xi(x) \text{tr} (\psi(x)^\dagger \psi(x)) + \frac{\kappa}{2i} \sum_{\alpha=\langle xy \rangle} \eta(\alpha) \text{tr} (\psi(x)^\dagger U_\alpha \psi(y) U_\alpha^\dagger) \right\}, \quad (2.27)$$

where the fermion field obeys the anticommutation rules:

$$\{\psi_{ij}(x), \psi_{kl}(y)^\dagger\} = \frac{1}{N_c} \delta_{ik} \delta_{jl} \delta_{xy}. \quad (2.28)$$

The Hilbert space is given by the tensor product of the Hilbert space of pure gauge times the fermionic Fock space.

The elements of the coherence algebra are decorated Wilson loops, which are Wilson loops with the insertion of fermionic fields. To synthetically describe these decorated Wilson loop, it is useful to extend the original lattice in the

following way: the extended lattice $\hat{\mathcal{L}}$ has the same points as the original lattice; from each point, n_f extra links, connecting the point with itself, emanate. This n_f extra directions will be identified by the versors e_i (with $i = 1, \dots, n_f$). The link variables associated to the extended lattice are:

$$\hat{U}_{\hat{\alpha}} = \begin{cases} U_{\alpha} & \text{if } \hat{\alpha} = \alpha \\ \psi_i(x) & \text{if } \hat{\alpha} = (x, +e_i) \\ \psi_i(x)^\dagger & \text{if } \hat{\alpha} = (x, -e_i) \end{cases} . \quad (2.29)$$

The set of all the closed paths in the extended lattice will be denoted by $\hat{\mathcal{C}}$ ($\hat{\mathcal{C}}_\alpha$ identify the set of the closed paths starting with the link α). The coherence algebra is defined as the set of all the operators:

$$\Lambda(a, b) = iN_c \text{tr} \left\{ a(U, \psi) + \sum_{\alpha \in \hat{\mathcal{L}}^\pm} [E_\alpha b_\alpha(U, \psi) + b_\alpha(U, \psi) E_\alpha] \right\} , \quad (2.30)$$

where $a(U, \psi) = \sum_{\Gamma \in \hat{\mathcal{C}}} a_\Gamma \hat{U}(\Gamma)$ and $b_\alpha(U, \psi) = \sum_{\Gamma \in \hat{\mathcal{C}}_\alpha} b_{\alpha, \Gamma} \hat{U}(\Gamma)$ must be hermitian.

The construction of the coherent states and of the classical Hamiltonian follows the same lines as for the pure gauge theory. It is useful to point out for the future (for details see [36]) that the Hamiltonian can be written as a sum of elements of the coherence algebra, and the classical Hamiltonian is defined also in this case as:

$$h(\Psi) = \lim_{N_c \rightarrow \infty} \frac{1}{N_c^2} \langle \Psi | H | \Psi \rangle . \quad (2.31)$$

2.5 Loop equations

The expectation values of Wilson loops satisfy a closed set of infinite equations in the large- N_c limits. These loop equations are the Schwinger-Dyson equations for the Wilson loops [37, 38]. These equations will be useful in the proof of the orientifold planar equivalence in the strong-coupling and large-mass phase on the lattice (see chapter 4).

Let us focus on the simple case of pure $U(N_c)$ Yang-Mills on the lattice. The setup for this section is the formalism of the functional integral on the Euclidean space-time, discretized as a four-dimensional lattice.

Let $U(\Gamma)$ be the parallel transport along the closed path Γ and define the Wilson loops as:

$$W(\Gamma) = \frac{1}{N_c} \text{tr} U(\Gamma) . \quad (2.32)$$

It is convenient to introduce the left Lie derivatives with respect each link variable:

$$d_\alpha^A U_\beta = -iT^A U_\alpha \delta_{\alpha\beta} . \quad (2.33)$$

Since the Haar measure is invariant under left-multiplication, the integral of the Lie derivative of anything must vanish. In particular,

$$\int d_\alpha^A \left[e^{-S(U)} d_\alpha^A W(\Gamma) \right] dU = 0 . \quad (2.34)$$

Introducing the Wilson action

$$S[U] = \frac{N_c^2}{\lambda} \sum_{p \in \mathcal{L}_\square} \left(1 - \frac{1}{N_c} \text{tr} U(p) \right) , \quad (2.35)$$

where p is the generic (either positive or negative) plaquette, differentiating and summing over the index A (this sum is not explicitly written), we obtain

$$\frac{1}{N_c} \langle d_\alpha^A d_\alpha^A W(\Gamma) \rangle + \frac{N_c}{\lambda} \sum_{p \in \mathcal{L}_\square} \langle d_\alpha^A W(\Gamma) d_\alpha^A W(p) \rangle = 0 . \quad (2.36)$$

The loop equations are precisely the previous ones (for each α), once the derivatives are explicitly computed and the large- N_c is taken. The final result will be given in equation (2.47), while in what follows I will give a sketch of the proof.

Concentrate on the first term of the previous equation. Assume that the path Γ goes through the link α only once. I will write $\Gamma \equiv \alpha\Gamma_1$ to indicate that the two paths are equal modulo redefining the starting point. Thus,

$$d_\alpha^A W(\Gamma) = \frac{1}{N_c} d_\alpha^A \text{tr} U_\alpha U(\Gamma_1) = -\frac{i}{N_c} \text{tr} T^A U(\alpha\Gamma_1) . \quad (2.37)$$

By using the completeness of the T^A matrices $\sum_A T_{ij}^A T_{kl}^A = \frac{1}{2} \delta_{il} \delta_{jk}$,

$$\frac{1}{N_c} \sum_A d_\alpha^A d_\alpha^A W(\Gamma) = -\frac{1}{N_c^2} \sum_A \text{tr} T^A T^A U(\alpha\Gamma_1) = -\frac{1}{2N_c} \text{tr} U(\Gamma) = -\frac{1}{2} W(\Gamma) . \quad (2.38)$$

In this case, the second derivative of the Wilson loop is simply proportional to the Wilson loop itself. Assume now that the path Γ goes through the link α twice, $\Gamma \equiv \alpha\Gamma_1\alpha\Gamma_2$. The derivative has two terms, and the second derivative

has four terms:

$$d_\alpha^A W(\Gamma) = -\frac{i}{N_c} [\text{tr } T^A U(\alpha\Gamma_1\alpha\Gamma_2) + \text{tr } U(\alpha\Gamma_1)T^A U(\alpha\Gamma_2)] \quad (2.39)$$

$$\begin{aligned} \frac{1}{N_c} \sum_A d_\alpha^A d_\alpha^A W(\Gamma) &= -\frac{1}{N_c^2} \sum_A [\text{tr } (T^A)^2 U(\alpha\Gamma_1\alpha\Gamma_2) + \\ &+ 2 \text{tr } T^A U(\alpha\Gamma_1)T^A U(\alpha\Gamma_2) + \text{tr } U(\alpha\Gamma_1)(T^A)^2 U(\alpha\Gamma_2)] = \\ &= -\frac{1}{2} [2W(\Gamma) + 2W(\alpha\Gamma_1)W(\alpha\Gamma_2)] . \end{aligned} \quad (2.40)$$

Consider now the case in which the path Γ goes through the link α and the reversed link $\bar{\alpha}$, $\Gamma \equiv \alpha\Gamma_1\bar{\alpha}\Gamma_2$. The Lie derivative acts on $U_{\bar{\alpha}}$ as:

$$d_{\bar{\alpha}}^A U_{\bar{\beta}} = +iU_{\bar{\alpha}} T^A \delta_{\alpha\beta} . \quad (2.41)$$

It is easy to verify that the second derivative is:

$$\frac{1}{N_c} \sum_A d_\alpha^A d_\alpha^A W(\Gamma) = -\frac{1}{2} [2W(\Gamma) - 2W(\Gamma_1)W(\Gamma_2)] . \quad (2.42)$$

The generalisation to a path Γ , going $C_\alpha(\Gamma)$ times through the links α or $\bar{\alpha}$, is straightforward:

$$\begin{aligned} -\frac{2}{N_c} \sum_A d_\alpha^A d_\alpha^A W(\Gamma) &= C_\alpha(\Gamma)W(\Gamma) + \sum_{\substack{\Gamma_1, \Gamma_2 \in \mathcal{C} \\ \Gamma \equiv \alpha\Gamma_1\alpha\Gamma_2}} W(\alpha\Gamma_1)W(\alpha\Gamma_2) + \\ &+ \sum_{\substack{\Gamma_1, \Gamma_2 \in \mathcal{C} \\ \Gamma \equiv \bar{\alpha}\Gamma_1\bar{\alpha}\Gamma_2}} W(\Gamma_1\bar{\alpha})W(\Gamma_2\bar{\alpha}) - \sum_{\substack{\Gamma_1, \Gamma_2 \in \mathcal{C} \\ \Gamma \equiv \alpha\Gamma_1\bar{\alpha}\Gamma_2}} W(\Gamma_1)W(\Gamma_2) . \end{aligned} \quad (2.43)$$

This equation will be schematically written as:

$$\begin{aligned} -\frac{2}{N_c} \sum_A d_\alpha^A d_\alpha^A W(\Gamma) &= C_\alpha(\Gamma)W(\Gamma) + \\ &+ \left\{ \sum_{\substack{\text{self-intersections} \\ \text{with parallel link}}} - \sum_{\substack{\text{self-intersections} \\ \text{with opposite link}}} \langle W(\Gamma_1) \rangle \langle W(\Gamma_2) \rangle \right\} , \end{aligned} \quad (2.44)$$

where it is understood that the closed path Γ is self-intersecting and the intersection point splits it into two closed paths Γ_1 and Γ_2 ; the sum runs over all the possible pairs of Γ_1 and Γ_2 .

Consider now the second term of the equation (2.36), and let α be a link that belongs both to the path Γ and the plaquette p . Computing the derivatives and summing over the index A , one obtains:

$$\begin{aligned}
 N_c \sum_A \sum_{p \in \mathcal{L}_\square} d_\alpha^A W(\Gamma) d_\alpha^A W(p) &= \frac{1}{N_c} \times \\
 &\times \sum_A \left\{ \sum_{\substack{\Gamma_1 \in \mathcal{C} \\ \Gamma \equiv \alpha \Gamma_1}} (-i) \text{tr} T^A U(\alpha \Gamma_1) + \sum_{\substack{\Gamma_1 \in \mathcal{C} \\ \Gamma \equiv \bar{\alpha} \Gamma_1}} i \text{tr} T^A U(\Gamma_1 \bar{\alpha}) \right\} \times \\
 &\times \left\{ \sum_{\substack{p \in \mathcal{L}_\square \\ p \equiv \alpha p_1}} (-i) \text{tr} T^A U(\alpha p_1) + \sum_{\substack{p \in \mathcal{L}_\square \\ p \equiv \bar{\alpha} p_1}} i \text{tr} T^A U(p_1 \bar{\alpha}) \right\} = \\
 &= \sum_{\substack{\Gamma_1 \in \mathcal{C} \\ \Gamma \equiv \alpha \Gamma_1}} \left\{ -\frac{1}{2} \sum_{\substack{p \in \mathcal{L}_\square \\ p \equiv \alpha p_1}} W(\alpha \Gamma_1 \alpha p_1) + \frac{1}{2} \sum_{\substack{p \in \mathcal{L}_\square \\ p \equiv \bar{\alpha} p_1}} W(\Gamma_1 p_1) \right\} + \\
 &+ \sum_{\substack{\Gamma_1 \in \mathcal{C} \\ \Gamma \equiv \bar{\alpha} \Gamma_1}} \left\{ \frac{1}{2} \sum_{\substack{p \in \mathcal{L}_\square \\ p \equiv \alpha p_1}} W(\Gamma_1 p_1) - \frac{1}{2} \sum_{\substack{p \in \mathcal{L}_\square \\ p \equiv \bar{\alpha} p_1}} W(\Gamma_1 \bar{\alpha} p_1 \bar{\alpha}) \right\}. \quad (2.45)
 \end{aligned}$$

This equation will be schematically written as:

$$\begin{aligned}
 -2N_c \sum_A \sum_{p \in \mathcal{L}_\square} d_\alpha^A W(\Gamma) d_\alpha^A W(p) &= \\
 &= \left\{ \sum_{\substack{\Gamma \text{ and } p \in \mathcal{L}_\square \text{ join} \\ \text{with parallel link}}} - \sum_{\substack{\Gamma \text{ and } p \in \mathcal{L}_\square \text{ join} \\ \text{with opposite link}}} \langle W(\Gamma p) \rangle \right\}, \quad (2.46)
 \end{aligned}$$

where it is understood that the closed paths Γ and p have some intersection, and it is possible to open and glue the two paths in the intersection point to obtain the compound path Γp ; the sum runs over all the paths p (here, plaquettes) and over all the intersection points of Γ and p .

Putting altogether in the equation (2.36), using that the expectation value of two Wilson loops factorizes in the large- N_c limit, and summing over all the

links of the path Γ , we obtain the loop equations:

$$\begin{aligned}
 |\Gamma| \langle W(\Gamma) \rangle + \left\{ \sum_{\substack{\text{self-intersections} \\ \text{with parallel link}}} - \sum_{\substack{\text{self-intersections} \\ \text{with opposite link}}} \langle W(\Gamma_1) \rangle \langle W(\Gamma_2) \rangle \right\} = \\
 = -\frac{1}{\lambda} \left\{ \sum_{\substack{\Gamma \text{ and } p \in \mathcal{L}_\square \text{ join} \\ \text{with parallel link}}} - \sum_{\substack{\Gamma \text{ and } p \in \mathcal{L}_\square \text{ join} \\ \text{with opposite link}}} \langle W(\Gamma p) \rangle \right\}, \quad (2.47)
 \end{aligned}$$

where $|\Gamma|$ is the length of the path.

In the loop equations, just the expectation values of Wilson loops are involved. Unfortunately, we have no guarantee for the uniqueness of the solution, since we are dealing with a system of infinite quadratic equations. The physical picture of this fact is simple. The loop equations (in the limit of continuum time) must be equivalent to the static Hamilton equation derived from the Hamiltonian (2.25). A solution of the loops equations corresponds to some stationary state of the Hamiltonian. Of course, only the absolute minimum of the Hamiltonian is the real vacuum of the theory.

Nevertheless, the loop equations are useful to compute the solution in the strong-coupling phase. In this case, we know that the absolute minimum can be expanded in powers of the inverse of the coupling constant in a neighborhood of $\lambda = \infty$. Since the insertion of one more plaquette is weighted with a λ^{-1} factor, this kind of solution is unique and can be computed iteratively.

As λ decreases, it might happen that the strong-coupling solution becomes just a relative minimum of the Hamiltonian and another absolute minimum appears. This mechanism is realised in the solvable two-dimensional theory [39]. Two solutions of the loop equations are known. One can be obtained through a strong-coupling expansion and the other through a weak-coupling expansion. These two solutions are well-defined for each value of the coupling constant. But in a strong-coupling region, the solution obtained through strong-coupling expansion corresponds to the real vacuum of the theory. While lowering the coupling, a third order phase transition occurs at some point and the other solution becomes the lower energy one.

In conclusion, the loop equations are sufficient to characterise the pure gauge theory in the strong-coupling phase in the large- N_c limit. But outside of the strong-coupling phase this is not true, and the knowledge of the Hamiltonian is also required.

Chapter 3

A review of the orientifold planar equivalence

The orientifold planar equivalence is the equivalence in a common sector (the *neutral* sector) of the following theories in the large- N_c limit:

OrientiQCD : $SU(N_c)$ gauge theory with n_f flavours of Dirac fermions in the antisymmetric two-index representation and $n_f^{(F)}$ flavours (both $n_f^{(F)}$ and n_f are kept fixed) of Dirac fermions in the fundamental representation of the gauge group;

AdjQCD : $SU(N_c)$ gauge theory with n_f flavours of Majorana fermions in the adjoint representation of the gauge group.

The neutral sector is defined by bosonic, single-trace, gauge-invariant, \mathcal{C} -even observables (\mathcal{C} is the charge conjugation symmetry). A dictionary between the observables in the neutral sectors of the two theories will be compiled in section 3.1 [5].

At $N_c = 3$ the OrientiQCD becomes the usual QCD. The equivalence is valid for any number of flavours and for any value of the masses of the fermions. Moreover, if $n_f = 1$ and the fermion in the antisymmetric representation is massless, the OrientiQCD is equivalent to $\mathcal{N} = 1$ super Yang-Mills (SYM) in the planar limit. Some analytical results of SYM can be transferred to QCD up to corrections of order $1/N_c$, as we will see in section 3.2 [3].

Even with massive fermions, the colour confinement and the area law for the Wilson loops are consequences of the center symmetry in the AdjQCD.

The deconfinement transition is characterised by the spontaneous breaking of this symmetry. An identical mechanism must be realised in the planar limit of the OrientiQCD. The approximate center symmetry of OrientiQCD and the effective potential for the Polyakov loop will be discussed in chapter 5 [24, 30].

In the present chapter, a brief review of the proofs (both perturbative and non-perturbative) of the orientifold planar equivalence will be presented [5, 23, 26]. In the next chapter, I will discuss in details the proof of the orientifold planar equivalence on the lattice in the strong-coupling and large-mass phase [25].

3.1 Dictionary between neutral sectors

3.1.1 The gauge sector

The kinematics of the gauge sector is the same in the two theories. In order to identify the neutral sector, it is sufficient to see how single-trace gauge-invariant operators transform under charge conjugation symmetry. The transformation law for the gauge field $A_\mu(x) = \sum_A A_\mu^A T^A$ follows:

$$\mathcal{C}^\dagger A_\mu(x) \mathcal{C} = -A_\mu^T(x) = \bar{\mathbb{F}}[A_\mu(x)] , \quad (3.1)$$

where $\bar{\mathbb{F}}$ denotes the antifundamental representation of the gauge group. Clearly, the operators:

$$\text{tr } F_{\mu\nu} F^{\mu\nu} \quad \text{tr } \tilde{F}_{\mu\nu} F^{\mu\nu} \quad (3.2)$$

are \mathcal{C} -even. While, if Γ is a closed path, the Wilson loop $W(\Gamma)$ transforms as:

$$\mathcal{C}^\dagger W(\Gamma) \mathcal{C} = W(\Gamma)^* , \quad (3.3)$$

therefore only its real part belongs to the neutral sector.

3.1.2 The quark sector of OrientiQCD

Since the bilinears of fermions in the fundamental representations contribute only to the subleading order, I will focus only on the Dirac fermions ψ_i (with $i = 1, \dots, n_f$) in the antisymmetric representation. Under spatial parity and

charge conjugation, ψ transforms as¹:

$$\mathcal{P}^\dagger \psi(x_0, \vec{x}) \mathcal{P} = \gamma_0 \psi(x_0, -\vec{x}) , \quad (3.8a)$$

$$\mathcal{C}^\dagger \psi(x_0, \vec{x}) \mathcal{C} = i\gamma_2 \gamma_0 \bar{\psi}^T(x_0, \vec{x}) . \quad (3.8b)$$

The generic local gauge-invariant fermionic bilinear is obtained by contracting the $\psi_j \bar{\psi}_i$ with a product of gamma matrices and a flavour matrix M_{ij} . The rules of transformation for the bilinears are:

$$\mathcal{P}^\dagger \bar{\psi} \Gamma M \psi(x_0, \vec{x}) \mathcal{P} = \bar{\psi} \gamma_0 \Gamma M \gamma_0 \psi(x_0, -\vec{x}) , \quad (3.9a)$$

$$\mathcal{C}^\dagger \bar{\psi} \Gamma M \psi(x_0, \vec{x}) \mathcal{C} = (-1)^{\#\Gamma} \bar{\psi} \bar{\Gamma} M^T \psi(x_0, \vec{x}) , \quad (3.9b)$$

where Γ is a product of $\#\Gamma$ gamma matrices, and $\bar{\Gamma} = \gamma_0 \Gamma^\dagger \gamma_0$.

In order to obtain eigenstates of the charge conjugation, it is useful to choose M as a real symmetric S or an imaginary antisymmetric R . The transformation properties of hermitian combinations under parity and charge conjugation are listed:

¹The notations for the current chapter follow. The Minkowskian metric tensor is $g_{\mu\mu} = (1, -1, -1, -1)$. The matrices for the two-component spinor algebra are:

$$\sigma_\mu = (\mathbf{1}_2, \vec{\sigma}) , \quad \bar{\sigma}_\mu = (\mathbf{1}_2, -\vec{\sigma}) , \quad (3.4)$$

$$\eta_{\mu\nu} = \frac{i}{4} (\sigma_\mu \bar{\sigma}_\nu - \sigma_\nu \bar{\sigma}_\mu) , \quad \bar{\eta}_{\mu\nu} = \frac{i}{4} (\bar{\sigma}_\mu \sigma_\nu - \bar{\sigma}_\nu \sigma_\mu) , \quad (3.5)$$

where σ_i are the 2×2 Pauli matrices. The gamma matrices are

$$\gamma_\mu = \begin{pmatrix} 0 & \sigma_\mu \\ \bar{\sigma}_\mu & 0 \end{pmatrix} , \quad \gamma_5 = \begin{pmatrix} \mathbf{1}_2 & 0 \\ 0 & -\mathbf{1}_2 \end{pmatrix} . \quad (3.6)$$

Finally it is useful to introduce the matrices:

$$\sigma_{\mu\nu} = \frac{i}{4} [\gamma_\mu, \gamma_\nu] = \begin{pmatrix} \eta_{\mu\nu} & 0 \\ 0 & \bar{\eta}_{\mu\nu} \end{pmatrix} . \quad (3.7)$$

| Observable | \mathcal{P} | \mathcal{C} |
|-------------------------------------|------------------------|---------------|
| $\bar{\psi}S\psi$ | +1 | +1 |
| $i\bar{\psi}\gamma_5S\psi$ | -1 | +1 |
| $\bar{\psi}\gamma_\mu S\psi$ | $g_{\mu\mu}$ | -1 |
| $\bar{\psi}\gamma_\mu\gamma_5S\psi$ | $-g_{\mu\mu}$ | +1 |
| $\bar{\psi}\sigma_{\mu\nu}S\psi$ | $g_{\mu\mu}g_{\nu\nu}$ | -1 |
| $\bar{\psi}R\psi$ | +1 | -1 |
| $i\bar{\psi}\gamma_5R\psi$ | -1 | -1 |
| $\bar{\psi}\gamma_\mu R\psi$ | $g_{\mu\mu}$ | +1 |
| $\bar{\psi}\gamma_\mu\gamma_5R\psi$ | $-g_{\mu\mu}$ | -1 |
| $\bar{\psi}\sigma_{\mu\nu}R\psi$ | $g_{\mu\mu}g_{\nu\nu}$ | +1 |

3.1.3 The gluino sector of AdjQCD

Let λ_i with $i = 1, \dots, n_f$ be the two-component Majorana fermions in the adjoint representation of the gauge group. Under spatial parity and charge conjugation, λ transforms as:

$$\mathcal{P}^\dagger \lambda_A(x_0, \vec{x}) \mathcal{P} = \sigma_2 \lambda_A^*(x_0, -\vec{x}), \quad (3.10a)$$

$$\mathcal{C}^\dagger \lambda_A(x_0, \vec{x}) \mathcal{C} = \alpha_A \lambda_A(x_0, \vec{x}), \quad (3.10b)$$

where $\alpha_A = -2 \text{tr}(T_A^T T_A)$ is a sign, that assure that the gluino obeys the same law of transformation as the gauge field:

$$\mathcal{C}^\dagger \sum_A \lambda_A(x_0, \vec{x}) T_A \mathcal{C} = - \sum_A \lambda_A(x_0, \vec{x}) T_A^T. \quad (3.11)$$

Clearly all the possible single-trace gauge-invariant fermionic bilinears, that do not involve the insertion of the gauge field, are invariant under charge conjugation. In order to obtain an identification with the bilinears of the OrientiQCD, it is useful to consider the transformation properties of hermitian combinations under parity. As in the previous subsection, S is a real symmetric matrix in the flavour space and R is real antisymmetric.

| Observable | \mathcal{P} |
|-----------------------------------------------------------------------------------------------------------|--------------------------|
| $i\lambda^T \sigma_2 S \lambda - i\lambda^\dagger \sigma_2 S \lambda^*$ | +1 |
| $\lambda^T \sigma_2 S \lambda + \lambda^\dagger \sigma_2 S \lambda^*$ | -1 |
| $\lambda^\dagger \bar{\sigma}_\mu S \lambda$ | $-g_{\mu\mu}$ |
| $\lambda^\dagger \bar{\sigma}_\mu R \lambda$ | $g_{\mu\mu}$ |
| $i\lambda^T \sigma_2 \eta_{\mu\nu} R \lambda - i\lambda^\dagger \bar{\eta}_{\mu\nu} \sigma_2 R \lambda^*$ | $g_{\mu\mu} g_{\nu\nu}$ |
| $\lambda^T \sigma_2 \eta_{\mu\nu} R \lambda + \lambda^\dagger \bar{\eta}_{\mu\nu} \sigma_2 R \lambda^*$ | $-g_{\mu\mu} g_{\nu\nu}$ |

3.1.4 Dictionary of observables and symmetries

Putting altogether the results of the previous two sections, and providing that the fields are normalized the same way in the actions, a table of correspondence between operators follows². From the equality of the correlation functions of these operators, particles in the common sector can be identified.

| Operator in OrientiQCD | Operator in AdjQCD | J^P | States (if $n_f=2$) |
|-------------------------------------|-----------------------------------------------------------------------------------------------------------------------|-------|------------------------------------------------|
| $\Re W(\Gamma)$ | $\Re W(\Gamma)$ | 0^+ | \mathcal{P} -even glueballs |
| $\bar{\psi}\psi$ | $\frac{i}{2}\lambda^T\sigma_2\lambda - \frac{i}{2}\lambda^\dagger\sigma_2\lambda^*$ | 0^+ | $ \sigma\rangle$ |
| $-i\bar{\psi}\gamma_5\psi$ | $\frac{i}{2}\lambda^T\sigma_2\lambda + \frac{i}{2}\lambda^\dagger\sigma_2\lambda^*$ | 0^- | $ \eta\rangle$ |
| $\bar{\psi}S\psi$ | $\frac{i}{2}\lambda^T\sigma_2S\lambda - \frac{i}{2}\lambda^\dagger\sigma_2S\lambda^*$ | 0^+ | $ a_0\rangle$ |
| $-i\bar{\psi}\gamma_5S\psi$ | $\frac{i}{2}\lambda^T\sigma_2S\lambda + \frac{i}{2}\lambda^\dagger\sigma_2S\lambda^*$ | 0^- | $ \pi^0\rangle, \pi^+\rangle + \pi^-\rangle$ |
| $\bar{\psi}\gamma_\mu R\psi$ | $\lambda^\dagger\bar{\sigma}_\mu R\lambda$ | 1^- | $i \rho^+\rangle - i \rho^-\rangle$ |
| $\bar{\psi}\gamma_\mu\gamma_5\psi$ | $\lambda^\dagger\bar{\sigma}_\mu\lambda$ | 1^+ | $ h_1\rangle$ |
| $\bar{\psi}\gamma_\mu\gamma_5S\psi$ | $\lambda^\dagger\bar{\sigma}_\mu S\lambda$ | 1^+ | $ b_1^0\rangle, b_1^+\rangle + b_1^-\rangle$ |
| $\bar{\psi}\sigma_{\mu\nu}R\psi$ | $\frac{i}{2}\lambda^T\sigma_2\eta_{\mu\nu}R\lambda - \frac{i}{2}\lambda^\dagger\bar{\eta}_{\mu\nu}\sigma_2R\lambda^*$ | 1^+ | $i b_1^+\rangle - i b_1^-\rangle$ |

Moreover, in the massless case the vectorial fermionic bilinears are the Noether currents of the flavour symmetry. Therefore a matching between symmetries is also possible.

AdjQCD The symmetry breaking pattern is:

$$SU(n_f) \times \mathbf{Z}_{2N_c n_f} \rightarrow O(n_f) \times \mathbf{Z}_2. \quad (3.13)$$

The first $\mathbf{Z}_{2N_c n_f}$ comes from the anomalous $U(1)_R$ ³. Since the generators of these symmetries are fermionic bilinears and those belong to the neutral

²The exact matching of the normalizations is obtained by substituting

$$\psi \rightarrow \frac{1}{\sqrt{2}} \begin{pmatrix} \lambda \\ -i\sigma_2\lambda^* \end{pmatrix}, \quad \bar{\psi} \rightarrow \frac{1}{\sqrt{2}} (i\lambda^T\sigma_2, \lambda^\dagger) \quad (3.12)$$

in the bilinears of the OrientiQCD. The factor $1/\sqrt{2}$ gives the right matching of the number of degrees of freedom in the bilinears.

³The general formula for the axial anomaly in a gauge theory with one Weyl fermion in the representation \mathbf{R} , is:

$$\partial_\mu \langle \bar{\psi}\gamma^\mu\gamma_5\psi(x) \rangle_A = -\frac{C(\mathbf{R})}{16\pi^2} F_{\mu\nu}^A \tilde{F}^{A\mu\nu}(x) = -2C(\mathbf{R})Q(x), \quad (3.14)$$

where $\text{tr}\{\mathbf{R}[T^A]\mathbf{R}[T^B]\} = C(\mathbf{R})\delta^{AB}$. If α is the angle of the axial rotation, the corresponding anomalous Ward identity is:

$$\frac{\partial}{\partial\alpha} \langle O \rangle = -2C(\mathbf{R}) \frac{\partial}{\partial\theta} \langle O \rangle. \quad (3.15)$$

sector, we conclude that the chiral symmetry maps the neutral sector into itself.

OrientiQCD If quarks in the fundamental representation are present, the chiral symmetry is

$$\begin{aligned} SU(n_f)_L \times SU(n_f)_R \times SU(n_f^{(F)})_L \times SU(n_f^{(F)})_R \times U(1)_V^2 \times U(1)_A \rightarrow \\ \rightarrow SU(n_f)_V \times U(1)_V^2 \times \mathbf{Z}_2, \end{aligned} \quad (3.17)$$

where $n_f^{(F)} = N_f - n_f$ is the number of fundamental flavours. The $U(1)_V^2$ term is generated by the number of antisymmetric and fundamental quarks separately. The axial non-anomalous symmetry is generated by the following combination of axial currents:

$$J_{5\mu} = n_f \sum_{i=1}^{N_f - n_f} \bar{\chi}_i \gamma_5 \gamma_\mu \chi_i - \frac{n_f^{(F)}}{N_c - 2} \sum_{i=1}^{n_f} \bar{\psi}_i \gamma_5 \gamma_\mu \psi_i, \quad (3.18)$$

where ψ_i are the antisymmetric quarks and χ_i are the fundamental quarks. Since the fundamental quarks do not belong to the neutral sector, in the large- N_c limit, the relevant symmetry subgroup is:

$$SU(n_f)_L \times SU(n_f)_R \times U(1)_V \times \mathbf{Z}_{2(N_c - 2)n_f} \rightarrow SU(n_f)_V \times U(1)_V \times \mathbf{Z}_2. \quad (3.19)$$

Unlike the AdjQCD, this symmetry does not map the neutral sector in itself. I want to identify the stabilizer of the neutral sector, that is the symmetry subgroup that leaves unchanged the neutral sector.

Let us focus first on the baryonic number $U(1)_V$. Its generator $\bar{\psi} \gamma_\mu \psi$ does not belong to the neutral sector, therefore the baryonic number does not belong to the stabilizer.

Let us come now to the chiral part. The key is to write the generators of $SU(n_f)$ as an orthonormal set of real symmetric traceless matrices S^a (with $a = 1, \dots, \frac{N^2 + N - 1}{2}$) and imaginary antisymmetric ones R^b (with

For n_f Majorana fermions in the adjoint representation ($C(R) = N_c$):

$$\frac{\partial}{\partial \alpha} \langle O \rangle = -2N_c n_f \frac{\partial}{\partial \theta} \langle O \rangle. \quad (3.16)$$

An axial rotation of angle $\alpha = 2\pi/(2N_c n_f)$ corresponds to a shift of 2π of the θ angle.

$b = 1, \dots, \frac{N^2-N}{2}$). The Noether currents associated to the $SU(n_f)_L \times SU(n_f)_R$ chiral symmetry are:

$$\bar{\psi}\gamma_\mu\gamma_5 S^a\psi, \quad i\bar{\psi}\gamma_\mu R^b\psi, \quad i\bar{\psi}\gamma_\mu\gamma_5 R^b\psi, \quad \bar{\psi}\gamma_\mu S^a\psi. \quad (3.20)$$

Only the first two belong to the neutral sector. By computing the commutators:

$$[\gamma_5 S^a, \gamma_5 S^{a'}] = [S^a, S^{a'}] = if_{SS}^{aa'} iR^b \quad (3.21a)$$

$$[\gamma_5 S^a, iR^b] = \gamma_5 [S^a, iR^b] = if_{SR}^{aba'} \gamma_5 S^{a'} \quad (3.21b)$$

$$[iR^b, iR^{b'}] = if_{RR}^{bb'b''} iR^{b''}, \quad (3.21c)$$

it is clear that these two neutral currents are a representation of an $SU(n_f)_T$ that mix the vectorial and axial components. The axial part is spontaneously broken and the remaining $i\bar{\psi}\gamma_\mu R^b\psi$ currents generate the subgroup $O(n_f)_T$. In conclusion, the symmetry pattern of the neutral sector:

$$SU(n_f)_T \rightarrow O(n_f)_T \quad (3.22)$$

exactly matches the continuum part of the symmetry pattern of AdjQCD.

Besides the chiral symmetry, the AdjQCD action is invariant under the action of the center \mathbf{Z}_{N_c} . The presence of this symmetry leads to the confinement of the non-abelian electric charges. In the large- N_c limit, the group symmetry becomes $U(1)$. Naively, one might say that, since the center symmetry acts multiplying the Polyakov loop by a complex phase, only a \mathbf{Z}_2 subgroup maps the neutral sector in itself. Thus, this symmetry should be recovered in the large- N_c limit of the OrientiQCD. Unfortunately, this argument is incorrect. Indeed, the center symmetry is not a symmetry of the Hamiltonian (a unitary operator on the Hilbert space cannot be defined), but just a symmetry of the action. This is connected to the fact that the Polyakov loop is not properly an observable, but simply the Lagrange multiplier for the Gauss constrain. Moreover as pointed in [30], a different full $U(1)$ symmetry is dynamically recovered in the sector generated by the Wilson loops with zero winding number around the temporal compact dimension. A more detailed analysis of the effective action for the Polyakov loop is required, and this will be done in chapter 5.

3.2 Relics of SUSY in QCD

Consider now the case of $n_f = 1$ flavours of massless antisymmetric quarks. In the large- N_c limit, OrientiQCD is equivalent to SYM. Thanks to supersym-

metry, some analytical results can be obtained in SYM; those can be transferred in QCD up to subleading corrections [3].

- The beta function is the exact NSVZ beta function:

$$\beta(\alpha) = -\frac{1}{2\pi} \frac{3N_c \alpha^2}{1 - (N_c \alpha)/(2\pi)} + \text{subleadings} . \quad (3.23)$$

- The degeneracy of even/odd parity bosonic states. For instance:

$$\frac{m_{\eta'}}{m_\sigma} = 1 + O\left(\frac{1}{N_c}\right) . \quad (3.24)$$

- The gluino condensate in SYM is exactly known:

$$\langle \lambda \lambda \rangle = \frac{i}{2} \langle \lambda^T \sigma_2 \lambda \rangle - \frac{i}{2} \langle \lambda^\dagger \sigma_2 \lambda^* \rangle = -\frac{6N_c^2}{\lambda} \Lambda_{SYM}^3 . \quad (3.25)$$

From the equality of the beta functions clearly $\Lambda_{SYM} = \Lambda_{OR}$, provided that the same renormalization scheme is used. This is not the case, because the above result in SYM was obtained through a Pauli-Villars scheme, while the quark condensate in QCD is usually defined through a DRED+ \overline{MS} scheme. However, the differences between these two schemes are subleading [7]. Therefore, the following prediction follows:

$$\langle \bar{\psi} \psi \rangle = -\frac{6N_c^2}{\lambda} \Lambda_{OR}^3 + \text{subleadings} . \quad (3.26)$$

This formula can be improved. Indeed, the quark condensate depends on the renormalization scale, and the same conclusion holds for the $1/N_c$ corrections. One can pull out the RG dependence and write the quark condensate as a function of a RG invariant function $\mathcal{K}(N_c) = 1 + O(1/N_c)$ [7]:

$$\langle \bar{\psi} \psi \rangle = -\frac{3}{2\pi} \mu^3 \lambda(\mu)^{-\frac{\gamma}{\beta_0} - \frac{3\beta_1}{\beta_0}} \exp\left(-\frac{9}{\beta_0 \lambda(\mu)}\right) \mathcal{K}(n_f^{(F)}, 1/N_c) . \quad (3.27)$$

3.3 The perturbative proof

The orientifold planar equivalence can be proved in the perturbative expansion [5]. Basically, after developing the technology to obtain graphs for theories

with fermions in the two-index representations, a map is established between the graphs of SYM and orientifold QCD in the planar limit.

Of course, the equivalence at each order of the perturbation expansion does not guarantee the full equivalence of the two theories. In fact, for two strong coupled theories the perturbation expansion gives us no information about the vacuum. Nevertheless all the perturbative results obtained in SYM can be used for orientifold QCD (for instance the beta function).

In this section, I will not report the proof. I want just to stress some crucial facts that will be useful in what follows.

- The Dirac fermion in the antisymmetric (AS) representation can be split in two left-handed Weyl fermions, one in the antisymmetric representation and the other in the conjugate of the antisymmetric representation ($\overline{\text{AS}}$). In order to perform a perturbation expansion, we need to fix the gauge. Since neither the gauge fixing term, nor the Fadeev-Popov term depend on the fermions (and thus are the same in SYM and in orientifold QCD), I will simply keep them implicit. The interaction terms in the Lagrangian of orientifold QCD are the following:

$$\mathcal{L}_{int} = gA_\mu^C (\bar{\chi}\sigma^\mu \text{AS}[T_C]\chi + \bar{\eta}\sigma^\mu \overline{\text{AS}}[T_C]\eta) . \quad (3.28)$$

Since the Lagrangian is quadratic in the fermionic fields, the fermionic propagators form closed oriented lines in graphs. Each χ -line linking k interaction vertex is proportional to

$$\text{tr} \{ \text{AS}[T_{A_1}] \text{AS}[T_{A_2}] \cdots \text{AS}[T_{A_k}] \} , \quad (3.29)$$

while the η -lines are proportional to:

$$\text{tr} \{ \overline{\text{AS}}[T_{A_1}] \overline{\text{AS}}[T_{A_2}] \cdots \overline{\text{AS}}[T_{A_k}] \} . \quad (3.30)$$

Now, we can group the graphs, in such a way that two graphs are in the same class if one is obtained from the other by simply replacing some χ -lines with η -lines or *viceversa*. These classes of graphs are proportional to:

$$\text{tr} \{ \text{AS}[T_{A_1}] \text{AS}[T_{A_2}] \cdots \text{AS}[T_{A_k}] \} + \text{tr} \{ \overline{\text{AS}}[T_{A_1}] \overline{\text{AS}}[T_{A_2}] \cdots \overline{\text{AS}}[T_{A_k}] \} . \quad (3.31)$$

- In the SYM is much easier, each fermionic line is proportional to:

$$\text{tr} \{ \text{Adj}[T_{A_1}] \text{Adj}[T_{A_2}] \cdots \text{Adj}[T_{A_k}] \} . \quad (3.32)$$

- If we label with \mathbf{N} the fundamental representation of $SU(N)$ and with $\bar{\mathbf{N}}$ the antifundamental one, the rules of the product of representations give the following results:

$$\mathbf{N} \times \bar{\mathbf{N}} = \text{Adj} + \mathbf{1} , \quad (3.33a)$$

$$\mathbf{N} \times \mathbf{N} = \text{AS} + \text{S} . \quad (3.33b)$$

In the planar limit the singlet is negligible and $\text{AS} \simeq \text{S}$. Thus, asymptotically:

$$\begin{aligned} \text{tr} \{ \text{Adj}[T_{A_1}] \text{Adj}[T_{A_2}] \cdots \text{Adj}[T_{A_k}] \} &\simeq \\ &\simeq \text{tr} \{ R_{\mathbf{N} \times \bar{\mathbf{N}}}[T_{A_1}] R_{\mathbf{N} \times \bar{\mathbf{N}}}[T_{A_2}] \cdots R_{\mathbf{N} \times \bar{\mathbf{N}}}[T_{A_k}] \} , \\ \text{tr} \{ \text{AS}[T_{A_1}] \text{AS}[T_{A_2}] \cdots \text{AS}[T_{A_k}] \} &\simeq \\ &\simeq \frac{1}{2} \text{tr} \{ R_{\mathbf{N} \times \mathbf{N}}[T_{A_1}] R_{\mathbf{N} \times \mathbf{N}}[T_{A_2}] \cdots R_{\mathbf{N} \times \mathbf{N}}[T_{A_k}] \} , \\ \text{tr} \{ \overline{\text{AS}}[T_{A_1}] \overline{\text{AS}}[T_{A_2}] \cdots \overline{\text{AS}}[T_{A_k}] \} &\simeq \\ &\simeq \frac{1}{2} \text{tr} \{ R_{\bar{\mathbf{N}} \times \bar{\mathbf{N}}}[T_{A_1}] R_{\bar{\mathbf{N}} \times \bar{\mathbf{N}}}[T_{A_2}] \cdots R_{\bar{\mathbf{N}} \times \bar{\mathbf{N}}}[T_{A_k}] \} . \end{aligned} \quad (3.34)$$

The $1/2$ factor in the previous relationships for the AS and $\overline{\text{AS}}$ representations balances the presence of two Weyl fermions in orientifold QCD, giving the same number of degrees of freedom like in SYM.

- The generators in the two-index representations are easily computed:

$$R_{\mathbf{N} \times \bar{\mathbf{N}}}[T_A] = T_A \otimes 1 + 1 \otimes \bar{T}_A , \quad (3.35a)$$

$$R_{\mathbf{N} \times \mathbf{N}}[T_A] = T_A \otimes 1 + 1 \otimes T_A , \quad (3.35b)$$

$$R_{\bar{\mathbf{N}} \times \bar{\mathbf{N}}}[T_A] = \bar{T}_A \otimes 1 + 1 \otimes \bar{T}_A , \quad (3.35c)$$

where $\bar{T}_A = -T_A^*$ is the generator in the antifundamental representation. Clearly the validity of the orientifold planar equivalence is based on the possibility of substituting somewhere $\bar{T}_A \leftrightarrow T_A$. This is not possible in general. However, in the large- N limit, just graphs that can be drawn on a sphere without self-intersections survive (the planar graphs). The fermionic lines split the sphere in disconnected pieces. Having chosen a fermionic line bounding a disconnected piece, the interaction vertices along that line are classified as internal and external to the piece (see figure 3.1).

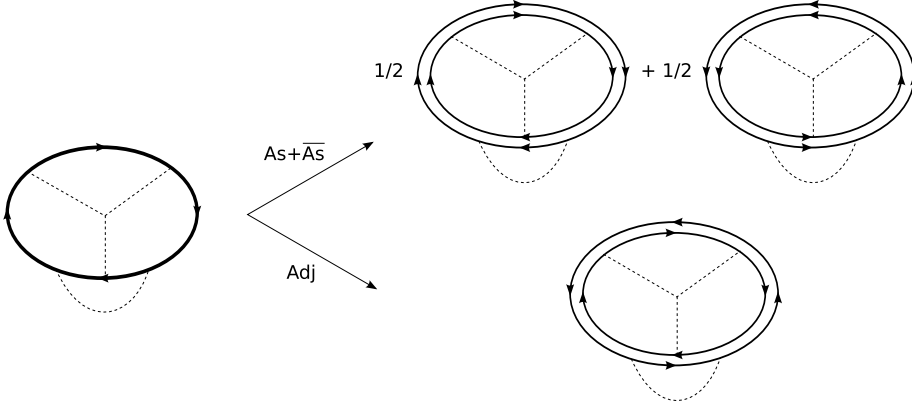


Figure 3.1: On the left side, a typical planar graph. The fermion may belong to an arbitrary representation. In the planar limit, the fermionic line factorize in two oriented lines (right side), representing traces of products of T 's (if the line is oriented in one side) and traces of products of \bar{T} 's (if the line is oriented in the opposite side). The antisymmetric representation has two contributions, corresponding to the two Majorana fermions in the action.

The colour traces in (3.34) factorize in an internal trace and an external one:

$$\begin{aligned}
 & \text{tr} \{ \text{Adj}[T_{A_1}] \text{Adj}[T_{A_2}] \cdots \text{Adj}[T_{A_k}] \} \simeq \\
 & \quad \simeq 2 \text{tr} \left\{ T_{A_{I_1}} \cdots T_{A_{I_p}} \right\} \text{tr} \left\{ \bar{T}_{A_{E_1}} \cdots \bar{T}_{A_{E_q}} \right\} , \\
 & \text{tr} \{ \text{AS}[T_{A_1}] \text{AS}[T_{A_2}] \cdots \text{AS}[T_{A_k}] \} \simeq \\
 & \quad \simeq \text{tr} \left\{ T_{A_{I_1}} \cdots T_{A_{I_p}} \right\} \text{tr} \left\{ T_{A_{E_1}} \cdots T_{A_{E_q}} \right\} , \\
 & \text{tr} \{ \overline{\text{AS}}[T_{A_1}] \overline{\text{AS}}[T_{A_2}] \cdots \overline{\text{AS}}[T_{A_k}] \} \simeq \\
 & \quad \simeq (-1)^p \text{tr} \left\{ \bar{T}_{A_{I_1}} \cdots \bar{T}_{A_{I_p}} \right\} \text{tr} \left\{ \bar{T}_{A_{E_1}} \cdots \bar{T}_{A_{E_q}} \right\} . \tag{3.36}
 \end{aligned}$$

- Each piece of a planar graph contains some traces of products of T 's alone or \bar{T} 's alone, whose colour indices are contracted with some f_{ABC} coming from the vertices of interaction. For instance, see the piece represented in

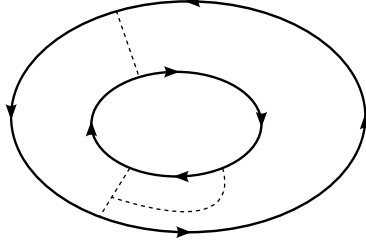


Figure 3.2: One piece of a planar graph.

figure 3.2; it is proportional to:

$$\text{tr} \{T_A T_B T_C\} \text{tr} \{\bar{T}_A \bar{T}_D\} f_{BCD} . \quad (3.37)$$

Since $[\bar{T}_B, \bar{T}_C] = i f_{BCD} \bar{T}_D$ and f_{BCD} is a completely skewsymmetric tensor, the following equalities hold:

$$\begin{aligned} \text{tr} \{T_A T_B T_C\} \text{tr} \{\bar{T}_A \bar{T}_D\} f_{BCD} &= \\ &= -\frac{i}{2} \text{tr} \{T_A [T_B, T_C]\} \text{tr} \{\bar{T}_A [\bar{T}_B, \bar{T}_C]\} = \\ &= f_{BCD} \text{tr} \{T_A T_D\} \text{tr} \{\bar{T}_A \bar{T}_B, \bar{T}_C\} , \end{aligned} \quad (3.38)$$

which is exactly the expression (3.37), after substituting $\bar{T}_A^* \leftrightarrow T_A$. This result has a general validity: in each connected piece of a planar graph we can invert the colour flux without change the value of the graph.

3.4 The nonperturbative proof on the lattice

A nonperturbative proof of the orientifold planar equivalence is presented in [23]. Unfortunately, it contains some hidden assumptions that I want to make explicit in this section. Moreover, in the cited paper, the authors keep implicit the regularization of the considered field theories. I will proceed in a different way in the section, by explicitly using the lattice regularization.

In order to avoid the complications related to the sign problem in the definition of the Majorana fermion (see section 4.1), I will discuss the planar equivalence of the following two theories:

2AdjQCD. Gauge theory with two Majorana fermions with mass m in the adjoint representation. Its effective action for the link variables is:

$$S_{2Adj}[U] = -\frac{2N_c^2}{\lambda} \sum_{p \in \mathcal{L}_\square} \Re W(p) - \log \text{Det}(aD_{Adj}[U]) . \quad (3.39)$$

2OrientiQCD. Gauge theory with two Dirac fermions with mass m in the antisymmetric two-index representation. Its effective action for the link variables is:

$$S_{2Or}[U] = -\frac{2N_c^2}{\lambda} \sum_{p \in \mathcal{L}_\square} \Re W(p) - 2 \log \text{Det}(aD_{AS}[U]) . \quad (3.40)$$

To keep the discussion as simple as possible, I will take a finite lattice. In this case, at fixed N_c the system has a finite number of degrees of freedom.

Let us consider a Wilson loop $W(\Gamma) = 1/N_c \text{tr} U(\Gamma)$. In order to prove the orientifold planar equivalence, one should prove the equality $\langle W(\Gamma) \rangle_{2Adj} = \langle W(\Gamma) \rangle_{2Or}$ in the planar limit. The idea is to write these expectation values in terms of expectation values over the vacuum of pure Yang-Mills $\langle \cdot \rangle_0$. For instance, for the 2Or:

$$\begin{aligned} \langle W(\Gamma) \rangle_{2Or} &= \frac{1}{Z_{2Or}} \int W(\Gamma) e^{-S_{YM}} \text{Det}(aD_{AS}[U])^2 dU = \\ &= \frac{\langle \text{Det}(aD_{AS}[U])^2 W(\Gamma) \rangle_0}{\langle \text{Det}(aD_{AS}[U])^2 \rangle_0} . \end{aligned} \quad (3.41)$$

Since in the planar limit the system has infinite degrees of freedom, it can develop spontaneous symmetry breaking. In this case, the expectation value of the Wilson loop can be computed only after having chosen one of the degenerate vacua (for instance, by restricting the domain of the functional integral). On the other side, the unrestricted $\lim_{N \rightarrow \infty} \langle W(\Gamma) \rangle$ gives the expectation value over a statistical ensemble of all the vacua. Let us make the following:

Assumption 1. The pure Yang-Mills (at zero temperature) has a non-degenerate vacuum in the planar limit.

This assumption seems in agreement with our knowledge of the pure Yang-Mills, but no proof of it exists. It will be crucial in what follows. For the moment, we need no assumptions about the vacua of 2Or and 2Adj. Thus, a priori

the expectation value (3.41) is computed over a statistical ensemble ρ_{AS} in the planar limit, and:

$$\text{tr}(\rho_{\text{AS}}W(\Gamma)) = \frac{\langle \text{Det}(aD_{\text{AS}}[U])^2 W(\Gamma) \rangle_0}{\langle \text{Det}(aD_{\text{AS}}[U])^2 \rangle_0}. \quad (3.42)$$

As we will see in section 4.2, the fermionic effective action can be expanded as:

$$\log \text{Det}(aD_{\text{R}}[U]) = \sum_{\alpha \in \mathcal{C}} \hat{m}^{-L(\alpha)} C(\alpha) N_c^2 W_{\text{R}}(\alpha), \quad (3.43)$$

where \mathcal{C} is the set of all the closed path linking nearest neighbours on the lattice, $L(\alpha)$ is the length of the path α , $C(\alpha)$ is a representation independent coefficient, $W_{\text{R}}(\alpha)$ is the Wilson loop along α in the representation R , and $\hat{m} = am + 4r$ for Wilson fermions. Notice that, for a two-index representation, $W_{\text{R}}(\alpha)$ is defined as $1/N_c^2 \text{tr} R[U(\alpha)]$. By substituting in the equation (3.42) and expanding the exponential, one is tempted to write in the planar limit:

$$\begin{aligned} \text{tr}(\rho_{\text{AS}}\mathcal{O}) &= \sum_n \sum_{\alpha_1, \dots, \alpha_n \in \mathcal{C}} \frac{m^{-\sum_i L(\alpha_i)}}{(n+1)!} C(\alpha_1) \cdots C(\alpha_n) \times \\ &\quad \times 2^n N_c^{2n} \langle W(\Gamma) W_{\text{AS}}(\alpha_1) \cdots W_{\text{AS}}(\alpha_n) \rangle_{0c}, \end{aligned} \quad (3.44)$$

where $\langle \cdot \rangle_{0c}$ is the connected expectation value on the vacuum of the pure Yang-Mills. This is possible only under the following:

Assumption 2. The large- \hat{m} expansion converges and commutes with the planar limit.

At this point, by using the assumption 1 and the factorization property, one can show that

$$\langle W(\Gamma) W_{\text{AS}}(\alpha_1) \cdots W_{\text{AS}}(\alpha_n) \rangle_{0c} = \frac{1}{2^n} \langle W(\Gamma) W_{\text{Adj}}(\alpha_1) \cdots W_{\text{Adj}}(\alpha_n) \rangle_{0c}, \quad (3.45)$$

in the planar limit. Let us see how this is possible in a simple case, if there are only two Wilson loops from the hopping expansion:

$$\langle W(\Gamma) W_{\text{AS}}(\alpha_1) W_{\text{AS}}(\alpha_2) \rangle_{0c} = \frac{1}{4} \langle W(\Gamma) W_{\text{Adj}}(\alpha_1) W_{\text{Adj}}(\alpha_2) \rangle_{0c}. \quad (3.46)$$

The Wilson loops in the two-index representations can be written in terms of the corresponding Wilson loops in the fundamental representation:

$$W_{\text{AS}}(\Gamma) = \frac{1}{2} \left\{ W(\Gamma)^2 - \frac{1}{N_c} W(\Gamma\Gamma) \right\} \quad (3.47a)$$

$$W_{\text{Adj}}(\Gamma) = |W(\Gamma)|^2 - \frac{1}{N_c^2}, \quad (3.47b)$$

in the planar limit. By using the formulae above and the factorization property of the planar limit (that holds only if the vacuum is a pure state), the connected expectation value for the antisymmetric representation is written as a sum of some contributes (for details, see [23]):

$$\begin{aligned} \langle W(\Gamma)W_{\text{As}}(\alpha_1)W_{\text{As}}(\alpha_2) \rangle_{0c} &= \\ &= \langle W(\Gamma)W(\alpha_1)W(\alpha_2) \rangle_0 \langle W(\alpha_1) \rangle_0 \langle W(\alpha_2) \rangle_0 + \\ &+ \langle W(\Gamma)W(\alpha_1) \rangle_0 \langle W(\alpha_1)W(\alpha_2) \rangle_0 \langle W(\alpha_2) \rangle_0 + \\ &+ \langle W(\Gamma)W(\alpha_2) \rangle_0 \langle W(\alpha_1)W(\alpha_2) \rangle_0 \langle W(\alpha_1) \rangle_0. \end{aligned} \quad (3.48)$$

Thanks to the assumption 1, the pure Yang-Mills vacuum is invariant under charge conjugation, and the expectation values are invariant under the substitution $U \rightarrow U^\dagger$. Thus, we can substitute

$$\langle W(\alpha_1) \rangle_0 \langle W(\alpha_2) \rangle_0 \rightarrow \langle W(\alpha_1)^\dagger \rangle_0 \langle W(\alpha_2)^\dagger \rangle_0$$

in the second line of the equation (3.48), and

$$\langle W(\alpha_1)W(\alpha_2) \rangle_0 \rightarrow \langle W(\alpha_1)^\dagger W(\alpha_2)^\dagger \rangle_0$$

in the last two. We obtain:

$$\begin{aligned} \langle W(\Gamma)W_{\text{AS}}(\alpha_1)W_{\text{AS}}(\alpha_2) \rangle_{0c} &= \\ &= \langle W(\Gamma)W(\alpha_1)W(\alpha_2) \rangle_0 \langle W(\alpha_1)^\dagger \rangle_0 \langle W(\alpha_2)^\dagger \rangle_0 + \\ &+ \langle W(\Gamma)W(\alpha_1) \rangle_0 \langle W(\alpha_1)^\dagger W(\alpha_2)^\dagger \rangle_0 \langle W(\alpha_2) \rangle_0 + \\ &+ \langle W(\Gamma)W(\alpha_2) \rangle_0 \langle W(\alpha_1)^\dagger W(\alpha_2)^\dagger \rangle_0 \langle W(\alpha_1) \rangle_0 = \\ &= 4 \langle W(\Gamma)W_{\text{Adj}}(\alpha_1)W_{\text{Adj}}(\alpha_2) \rangle_{0c}, \end{aligned} \quad (3.49)$$

as we want to prove.⁴

⁴In the general case, it is useful to introduce a diagrammatic representation of the connected

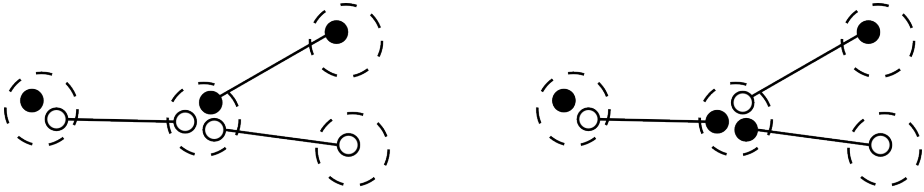


Figure 3.3: Two ASV diagrams contributing to $\langle W(\Gamma)W_R(\alpha_1)W_R(\alpha_1) \rangle_{0c}$. On the left, a graph of the OrientiQCD. On the right, a graph of the AdjQCD. Since each of these two graphs is obtain from the other one by inverting the colours of the central cluster, they have the same value.

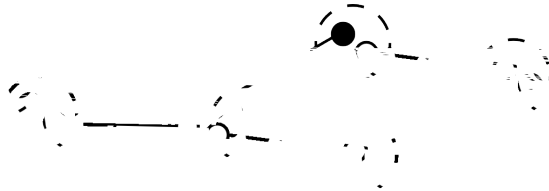


Figure 3.4: An ASV diagrams (for OrientiQCD) contributing to $\langle W(\Gamma_1)W(\Gamma_2)W_{AS}(\alpha_1)W_{AS}(\alpha_1) \rangle_{0c}$. The orientifold planar equivalence does not hold for this connected expectation value. Indeed, no corresponding graph exists in the AdjQCD.

Finally, if assumption 1 and 2 are fulfilled, in the planar limit:

$$\mathrm{tr}(\rho_{\mathrm{AS}} W(\Gamma)) = \mathrm{tr}(\rho_{\mathrm{Adj}} W(\Gamma)) . \quad (3.52)$$

I want to discuss now the assumption 2. At large enough mass of the fermions, the vacua of both the two theories 2Or and 2Adj are expected to be almost similar to the vacuum of pure Yang-Mills and the assumption 2 is expected to be fulfilled. We will see in section 4.2 that the hopping expansion (with Wilson fermions) is uniformly convergent if $\hat{m} > 32$. Here, the orientifold planar equivalence must be valid. As the mass decreases, some symmetry might break down and a phase transition might occur in one of the two theories with fermions. In such a case, the large- \hat{m} expansion (even if convergent) cannot

expectation values of the form:

$$N_c^{2L} \langle W(\Gamma_1) \cdots W(\Gamma_E) W_{\mathrm{R}}(\alpha_1) \cdots W_{\mathrm{R}}(\alpha_L) \rangle_{0c} . \quad (3.50)$$

This expression is represented by a sum of graphs (in what follows, ASV graphs), according

to [19] (see also [23, 31, 34, 38, 41, 42] for a review of the ASV graphs) and to [20] (see also [24, 25, 26, 27, 29, 30, 32, 33, 35, 36, 37, 39, 40, 43, 44, 45, 46, 47, 48, 49, 50, 51, 52, 53, 54, 55, 56, 57, 58, 59, 60, 61, 62, 63, 64, 65, 66, 67, 68, 69, 70, 71, 72, 73, 74, 75, 76, 77, 78, 79, 80, 81, 82, 83, 84, 85, 86, 87, 88, 89, 90, 91, 92, 93, 94, 95, 96, 97, 98, 99, 100] for a review of the ASV graphs).

give the right value for the expectation values and there is no reason for the orientifold planar equivalence to be still valid. On the other side, if no phase transition occurs, the large- \hat{m} expansion determines the expectation values at each value of the mass, by means of analytic continuation. Therefore, the orientifold planar equivalence is expected to hold in this case.

3.5 The role of the C-symmetry

From the discussion in the previous section, clearly if no phase transition occurs as the mass of the fermions decreases, then the orientifold planar equivalence holds. In the paper [26], a stronger result was found: it is sufficient to check that the charge-conjugation (\mathcal{C}) symmetry is not spontaneously broken.

This result was established by using the formalism of the coherent states for the planar limit [35]. I want to review here the main ideas of the proof; the reader should refer to [35, 26] for the details.

Let us start from an $SO(2N_c)$ gauge theory with fermions in the adjoint representation. The generators of $SO(2N_c)$ are the $2N_c \times 2N_c$ antisymmetric matrices. It is useful to write an explicit basis for the Lie algebra $\mathfrak{so}(2N_c)$. Let $\{S_a\}$ and $\{R_\alpha\}$ be two basis for respectively the real symmetric and antisymmetric $N_c \times N_c$ matrices, and define the matrix $J = i\sigma_2$. Then, the set with:

$$\mathbf{1} \otimes R_\alpha, \quad J \otimes S_a, \quad \sigma_1 \otimes R_\alpha, \quad \sigma_3 \otimes R_\alpha \quad (3.53)$$

is a basis for the real $2N_c \times 2N_c$ antisymmetric matrices. Since the set $\{R_\alpha, iS_a\}$ is a basis for the Lie algebra $\mathfrak{u}(N_c)$, the elements $\{\mathbf{1} \otimes R_\alpha, J \otimes S_a\}$ identify a subset $U(N_c) \subset SO(2N_c)$. Given a matrix $U \in U(N_c)$, its image in $SO(2N_c)$ is

$$\mathbf{R}_J[U] = \mathbf{1} \otimes \Re U + J \otimes \Im U. \quad (3.54)$$

The gluino field Λ belongs to the adjoint representation of $SO(2N_c)$. As a representation of the subgroup $U(N_c)$, it is instead reducible. Decompose the gluino field as:

$$\Lambda = \mathbf{R}_J[\lambda] + \sigma_+ \otimes \xi + \sigma_- \otimes \chi, \quad (3.55)$$

where $\lambda \in \mathfrak{u}(N_c)$, $\sigma_\pm = \frac{1}{\sqrt{2}}(\sigma_1 \pm \sigma_3)$, and ξ, χ are $N_c \times N_c$ antisymmetric matrices. Under a $U(N_c)$ gauge transformations, it is straightforward to prove that:

$$\mathbf{R}_J[U] \Lambda \mathbf{R}_J[U]^\dagger = \mathbf{R}_J[U \lambda U^\dagger] + \sigma_+ \otimes U^* \xi U^\dagger + \sigma_- \otimes U \chi U^T. \quad (3.56)$$

In words, the gluino Λ is decomposed in a Majorana fermion λ in the adjoint representation of $U(N_c)$, and in a Dirac fermion (quark+antiquark)

$$\psi = \begin{pmatrix} \chi \\ -i\sigma_2 \xi^\dagger \end{pmatrix} \quad (3.57)$$

in the antisymmetric representation of $U(N_c)$.

Similarly, one can decompose the gauge field:

$$W_\mu = \mathbf{R}_J[A_\mu] + \sigma_+ \otimes B_\mu + \sigma_- \otimes B_\mu^\dagger. \quad (3.58)$$

At this point, the game appears clearly. The $SO(N_c)$ gauge theory with Majorana fermions in the adjoint representation (parent theory) contains the degrees of freedom of both AdjQCD and OrientiQCD (daughter theories). One can kill the extra degrees of freedom with a projection, by imposing the constraints ($\hat{J} = J \otimes \mathbf{1}_{N_c}$):

- $\hat{J}W_\mu\hat{J}^\dagger = W_\mu$ in both cases;
- $\hat{J}\Lambda\hat{J}^\dagger = \Lambda$ for AdjQCD, or $\hat{J}\Lambda\hat{J}^\dagger = -\Lambda$ for OrientiQCD.

A map from the parent coherence algebra to the daughter ones is defined: choose an operator in the parent coherence algebra and change each field operator with the corresponding projected field. The coherence algebra of the parent theory is split into the bosonic and fermionic parts. Fermionic operators have a zero image in OrientiQCD (no fermionic operator can be built with fermions in the antisymmetric representation). Moreover, only some subalgebras of the daughter theories are reached by this map. To identify these subalgebras, it is useful to introduce the $SO(2N_c)$ gauge transformation $K = \sigma_3 \otimes \mathbf{1}_{N_c}$, which acts on the projected fields as:

$$KW_\mu K^\dagger = \sum_A A_\mu^A \mathbf{R}_J[T_A^*] \quad (3.59a)$$

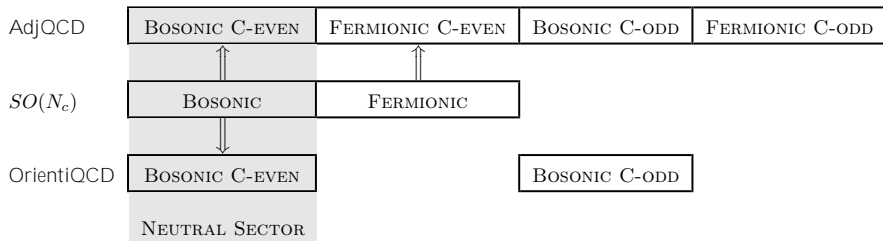
$$K\Lambda K^\dagger = \sum_A \lambda^A \mathbf{R}_J[T_A^*] - \sigma_+ \otimes \chi + \sigma_- \otimes \xi. \quad (3.59b)$$

The operator K is mapped into the charge conjugation symmetry in the daughter theories:

$$A_\mu^A T_A \rightarrow A_\mu^A T_A^* \quad (3.60a)$$

$$\lambda^A T_A \rightarrow \lambda^A T_A^*, \psi \rightarrow -i\gamma_2 \psi^*. \quad (3.60b)$$

Since K is a gauge transformation in the parent theory, the coherence algebra must be invariant under the action of K . This means that the image subalgebras in the daughter theories can contain only \mathcal{C} -even operators. In the following table the map between parent and daughter theories is represented. The neutral sector is the sector common to all the three theories. It is the set of the \mathcal{C} -even bosonic operators.



The isomorphisms between neutral sectors of coherence group, coherence algebra and coherent states do not imply yet the equality of the expectation values of the classical observables. Indeed one has to show that the degrees of freedom, that was killed by the projection, decouple from the neutral sector in the large- N_c limit. The details of this proof can be found in [36].

Finally, in order to prove the equivalence of the dynamics of the neutral sectors of the three theories, it is sufficient to show that the Hamiltonian of the daughter theories are obtained from the Hamiltonian of the parent theory, through the projection operation. This fact comes straightforward for the gauge part, and is a little bit more laborious for the fermionic part.

Summarising, expectation values inside the neutral sector are the same in parent and daughter theories; the neutral sector evolves into itself and the dynamics is the same in parent and daughter theories. This is not yet the orientifold planar equivalence: the equality of the vacuum expectation value of classical observables in the neutral sector should be proved. This is automatically guaranteed if the vacuum belongs to the neutral sector, that is if the vacuum is invariant under charge conjugation.

Therefore, the invariance of the vacuum under charge conjugation is a sufficient condition for the orientifold planar equivalence. But if we consider the one massless flavour case, we know that charge conjugation is not spontaneously broken in SYM, therefore the invariance of the OrientiQCD vacuum under charge conjugation becomes also a necessary condition.

Whether the \mathcal{C} -symmetry is spontaneously broken or not in the orientifold

QCD is not a trivial question. In [26, 40] it is shown that properly compactifying the spatial dimensions with periodic boundary conditions for the fermions the \mathcal{C} -symmetry is spontaneously broken only in the orientifold QCD and the orientifold planar equivalence does not hold. I will give some more details on this issue in chapter 6.

Chapter 4

The equivalence in the strong-coupling and large-mass phase on the lattice

In this chapter, I will give a proof of the orientifold planar equivalence at fixed lattice spacing and in the phase of strong coupling and large mass. I published the proof in [25]; it is based on the expansion in powers of $1/\lambda$ and $1/m$ of the functional integral. I will follow here a different (and more synthetic) strategy based on the formalism of the loop equations. All I need to assume is the factorization property of the large- N_c limit (this fact is proved in [25]).

Consider the following theories discretized on the lattice.

AdjQCD. Gauge theory with a Majorana fermion with mass m in the adjoint representation. Its effective action for the link variables is:

$$S_{Adj}[U] = -\frac{N_c^2}{\lambda} \sum_{p \in \mathcal{L}_\square} \Re W(p) - \frac{1}{2} \log \text{Det}(aD_{Adj}[U]) . \quad (4.1)$$

AsQCD. Gauge theory with a Dirac fermion with mass m in the antisymmetric

two-index representation. Its effective action for the link variables is:

$$S_{As}[U] = -\frac{N_c^2}{\lambda} \sum_{p \in \mathcal{L}_\square} \Re W(p) - \log \text{Det}(aD_{AS}[U]) . \quad (4.2)$$

In order to define the Majorana fermion, the Wilson discretization of the Dirac operator is suitable:

$$\begin{aligned} aD_{xy} = \hat{m}\delta_{xy} - K_{xy} = \hat{m}\delta_{xy} - \frac{1}{2} \sum_{\mu} \{ (r - \gamma_{\mu}) \mathbf{R}[U_{\mu}(x)]\delta_{y,x+a\hat{\mu}} + \\ + (r + \gamma_{\mu}) \mathbf{R}[U_{\mu}(x - a\hat{\mu})]^{\dagger}\delta_{y,x-a\hat{\mu}} \} , \end{aligned} \quad (4.3)$$

where $\hat{m} = (am + 4r)$ is the inverse of the hopping parameter¹. In the action of the AdjQCD, the square root of the fermionic determinant is used to describe the Majorana fermion. This is generally not allowed, because of a sign problem. Nevertheless, it is right in the large-mass phase. This issue will be discussed in section 4.1.

Once again, I want to discuss the meaning of the strong-coupling and large-mass expansion. The planar equivalence should be valid for any gauge-invariant observable, with a well defined vacuum expectation value in the planar limit. Assuming the factorization property, one can choose a single Wilson loop $W(\Gamma) = 1/N_c \text{tr} U(\Gamma)$ without losing generality. After fixing the number of colours and the lattice volume, the vacuum expectation value of $W(\Gamma)$ can be expanded in powers of λ^{-1} and \hat{m}^{-1} :

$$\langle W(\Gamma) \rangle(N, \lambda, \hat{m}) = \sum a_{i,j}(N) \lambda^{-i} \hat{m}^{-j} . \quad (4.5)$$

The planar limit $a_{i,j}(\infty) = \lim_{N \rightarrow \infty} a_{i,j}(N)$ is well-defined. In section 4.3, the loop equations will be generalised to the case of theories with fermions. By solving the loop equations (section 4.4), the coefficients $a_{i,j}(\infty)$ are computed, in both AsQCD and AdjQCD. We will finally conclude that $a_{i,j}^{AdjYM}(\infty) = a_{i,j}^{AsQCD}(\infty)$. However, in general the large- N_c limit cannot be exchanged with the strong-coupling and large-mass expansion. This fact is well known in pure gauge theories, where a bulk (non physical) transition appears as N_c becomes

¹In the current chapter space-time is Euclidean. The gamma matrices are

$$\gamma_0 = \begin{pmatrix} 0 & \mathbf{1}_2 \\ \mathbf{1}_2 & 0 \end{pmatrix}, \quad \gamma_i = \begin{pmatrix} 0 & i\sigma_i \\ -i\sigma_i & 0 \end{pmatrix}, \quad \gamma_5 = \begin{pmatrix} \mathbf{1}_2 & 0 \\ 0 & -\mathbf{1}_2 \end{pmatrix}. \quad (4.4)$$

infinite ([39] for the analytical computation in two dimensions, and [41] for numerical simulations in four dimensions), and it is connected with the discussion at the end of section 2.5. Although a solution of the loop equations has been found, it gives the expectation value of the Wilson loops with respect the vacuum (i.e. the *absolute* minimum of the Hamiltonian) only in the phase connected with the point $\lambda = \hat{m} = \infty$.

4.1 About the Majorana fermion

On the continuum, a Dirac fermion belonging to a real representation of the gauge group can be kinematically described as two Majorana fermions. It is possible [42] to follow the same procedure on the lattice. Let us consider Wilson discretization for fermions ψ and $\bar{\psi}$, and define

$$\lambda_1 = \frac{1}{\sqrt{2}} (\psi - C\bar{\psi}^T) \quad \lambda_2 = \frac{i}{\sqrt{2}} (\psi + C\bar{\psi}^T) , \quad (4.6)$$

where $C = i\gamma_0\gamma_2$ is the charge conjugation matrix. These are Majorana fermions, in the sense that they satisfy the condition:

$$\bar{\lambda}_j = \lambda_j^T C . \quad (4.7)$$

The fermionic action can be written in terms of the Majorana fermions:

$$\begin{aligned} a\bar{\psi}D_{\text{Adj}}[U]\psi &= \frac{a}{2} (\lambda_1^T + i\lambda_2^T) CD_{\text{Adj}}[U] (\lambda_1 - i\lambda_2) = \\ &= \frac{a}{2} \sum_{j=1,2} \lambda_j^T \tilde{D}_{\text{Adj}}[U] \lambda_j - \frac{i}{2} \lambda_1^T \tilde{D}_{\text{Adj}}[U] \lambda_2 + \frac{i}{2} \lambda_2^T \tilde{D}_{\text{Adj}}[U] \lambda_1 , \end{aligned} \quad (4.8)$$

where $\tilde{D}_{\text{Adj}} = CD_{\text{Adj}}$. Since the fermions belong to a real representation of the gauge group, by a straightforward computation, it is found that \tilde{D}_{Adj} is an antisymmetric matrix. Now, Grassmannian variables anticommute,

$$\lambda_2^T \tilde{D}_{\text{Adj}}[U] \lambda_1 = -\lambda_1^T \tilde{D}_{\text{Adj}}[U]^T \lambda_2 = \lambda_1^T \tilde{D}_{\text{Adj}}[U] \lambda_2 , \quad (4.9)$$

and the fermionic action in equation (4.8) reduces to:

$$a\bar{\psi}D_{\text{Adj}}\psi = \frac{a}{2} \sum_{j=1,2} \lambda_j^T \tilde{D}_{\text{Adj}}[U] \lambda_j . \quad (4.10)$$

Finally, the action for a Majorana fermion is obtained:

$$S_F = \frac{a}{2} \lambda^T \tilde{D}_{\text{Adj}}[U] \lambda. \quad (4.11)$$

The fermionic degrees of freedom can be integrated out. For Dirac fermions the determinant of the Dirac operator is originated; instead for Majorana fermions the Pfaffian of the matrix $a\tilde{D}_{\text{Adj}}$ comes out:

$$\int e^{\frac{1}{2} \lambda^T \tilde{D} \lambda} d\lambda = \text{Pf}(a\tilde{D}_{\text{Adj}}[U]). \quad (4.12)$$

If the dimension of the matrix A is $2n$, the Pfaffian is:

$$\text{Pf}(A) = \frac{1}{n! 2^n} \epsilon_{\alpha_1 \beta_1 \dots \alpha_n \beta_n} A_{\alpha_1 \beta_1} \dots A_{\alpha_n \beta_n}. \quad (4.13)$$

From equation (4.10), clearly $\text{Pf}(\tilde{D})^2 = \text{Det}(aD_{\text{Adj}})$, but in general nothing can be concluded about the sign of the Pfaffian. However I claim that the Pfaffian is positive in the large-mass phase and therefore $\text{Pf}(a\tilde{D}_{\text{Adj}}[U]) = \sqrt{\text{Det}(aD_{\text{Adj}}[U])}$. Let us see how to obtain this result.

Both the Pfaffian and the determinant are polynomial in the variable \hat{m} . If V is the number of points in the lattice, aD_{Adj} is a squared matrix with $4V(N^2-1)$ rows. Thus, the Pfaffian is a polynomial with degree $d = 2V(N^2-1)$. If δ_i are the (doubly degenerate) eigenvalues of the matrix K_{Adj} defined in the equation (4.3), the following formula holds:

$$\text{Pf}(a\tilde{D}_{\text{Adj}}[U]) = \prod_{i=1}^d (\hat{m} + \delta_i[U]). \quad (4.14)$$

As a function of \hat{m} , the Pfaffian is continuous and it can change its sign only when $-\hat{m}$ matches some of the eigenvalues $\delta_i[U]$. If $\bar{\delta}[U]$ is the highest eigenvalue in absolute value, the Pfaffian cannot change its sign for $\hat{m} > \bar{\delta}[U]$ and from its behaviour at $\hat{m} \rightarrow \infty$ we must conclude that it is positive.

Let us assume (but I will prove it in a moment) that $\bar{\delta}[U]$ is smaller than a constant M , independent of the gauge configuration, the volume of the lattice and the number of colours. In this case, for each mass with $\hat{m} > M$ the Pfaffian is positive and we can implement Majorana fermions by using the square root of $\text{Det}(aD_{\text{Adj}}[U])$.

At this point, I want to show that the eigenvalues of K_{R} are smaller than 32 . Let us consider the traces $\text{Tr} K_{\text{R}}^n$. By making explicit the dependence on

the site indexes:

$$\mathrm{Tr} K_{\mathbf{R}}^n = \sum_{x_1, \dots, x_n} \mathrm{tr} (K_{\mathbf{R}, x_1 x_2} K_{\mathbf{R}, x_2 x_3} \cdots K_{\mathbf{R}, x_n x_1}) . \quad (4.15)$$

Since the matrix $K_{\mathbf{R}}$ has non-zero elements only between nearest neighbours, contributions to the sum come only from n -ples (x_1, x_2, \dots, x_n) that make closed paths linking nearest neighbours on the lattice. Let us define \mathcal{C}_n as the set of such loops. Moreover, given ω in \mathcal{C}_n , I define $K_{\mathbf{R}}(\omega)$ as the ordered product of $K_{\mathbf{R}}$ on ω . Now, $K_{\mathbf{R}, xy}$ is a matrix with both spin and gauge indices; however, the spin part and the gauge one are factorizable. Actually, the gauge part is exactly the parallel transport along the link (x, y) , so one can write:

$$\mathrm{Tr} K_{\mathbf{R}}^n = \sum_{\omega \in \mathcal{C}_n} K_{\mathbf{R}}(\omega) = \sum_{\omega \in \mathcal{C}_n} c(\omega) \mathrm{tr} \mathbf{R}[U(\omega)] , \quad (4.16)$$

where $c(\omega)$ is a coefficient independent of the gauge configuration defined by:

$$c(\omega) = \frac{(-1)^{w(\omega)}}{2^n} \mathrm{tr} [(r - \gamma_{x_2 - x_1}) \cdots (r - \gamma_{x_1 - x_L})] , \quad (4.17)$$

with $\gamma_{\pm\hat{\mu}} = \pm\gamma_{\hat{\mu}}$ and $w(\omega)$ being the winding number of the path ω around the time direction (this $(-1)^{w(\omega)}$ factor takes into account the antiperiodic boundary conditions for the fermions).

I have kept these formulae with a generic representation, as they will be useful in what follows. At the moment, let us return to the adjoint representation. I want to obtain an upper bound for $\mathrm{Tr} K_{\mathbf{Adj}}^n$. By choosing $r \leq 1$, one sees that the elements of the matrices $r \pm \gamma_{\hat{\mu}}$ are less (in absolute value) than 1, thus $|c(\omega)| \leq 2^n$. Furthermore, the Wilson loops are traces of unitary matrices with $N_c^2 - 1$ rows, thus $\mathrm{tr} \mathbf{Adj}[U(\omega)] \leq N_c^2 - 1$. Finally, let us consider that the number of closed loops is less than $16^n V$. In fact, this is the number of all (both closed and open) paths, that is simply counted by fixing a starting point and by choosing a direction at each step.

Putting all together, one writes the following upper bound:

$$|\mathrm{Tr} K_{\mathbf{Adj}}^n[U]| = \left| \sum_{i=1}^{2d} \delta_i^n[U] \right| \leq 4V(N_c^2 - 1) \times 32^n . \quad (4.18)$$

As n grows, only the highest term gives a contribute to the previous sum, and the desired relationship $\bar{\delta}[U] \leq 32$ is finally found.

4.2 Hopping expansion

The fermionic effective action is:

$$S_F = -N_f \log \text{Det} (1 - \hat{m}^{-1} K_R[U]) , \quad (4.19)$$

up to an additive constant. The first step to obtain a large-mass expansion is the hopping expansion of S_F . It is obtained by expanding the logarithm of the Dirac operator as a power series in the hopping parameter \hat{m}^{-1} :

$$S_F = N_f \sum_{n=1}^{\infty} \frac{\hat{m}^{-n}}{n} \text{Tr} K_R^n = N_f \sum_{n=1}^{\infty} \sum_{\omega \in \mathcal{C}_n} \frac{\hat{m}^{-n}}{n} c(\omega) \text{tr} \mathbf{R}[U(\omega)] , \quad (4.20)$$

where I have used the decomposition (4.16). This gives the expansion in Wilson loops of the fermionic effective action. The coefficients $c(\omega)$ are real and representation independent. As I have shown in section 4.1, the eigenvalues of K_{Adj} are less (in absolute value) than some M , uniformly in the number of colours and of the lattice volume. Therefore the hopping expansion converges if $\hat{m} > M$.

4.3 Loop equations

For a generic two-index representation \mathbf{R} , remembering that $W_{\mathbf{R}}(\omega)$ is defined as $1/N_c^2 \text{tr} \mathbf{R}[U(\omega)]$ and using the hopping expansion, the total effective action is:

$$S[U] = -\frac{N_c^2}{\lambda} \sum_{p \in \mathcal{L}_{\square}} \Re W(p) - N_f N_c^2 \sum_{n=1}^{\infty} \sum_{\omega \in \mathcal{C}_n} \frac{\hat{m}^{-n}}{n} c(\omega) W_{\mathbf{R}}(\omega) , \quad (4.21)$$

where N_f must be chosen equal to 1 for the AsQCD and equal to 1/2 for the AdjQCD. The loop equations for these theories are obtained following the same procedure as in section 2.5, and can be written synthetically as:

$$\int d_{\alpha}^A \left[e^{-S(U)} d_{\alpha}^A W(\Gamma) \right] dU = 0 , \quad (4.22)$$

or substituting the action, equivalently as:

$$\begin{aligned} & \frac{1}{N_c} \langle d_{\alpha}^A d_{\alpha}^A W(\Gamma) \rangle + \frac{N_c}{\lambda} \sum_{p \in \mathcal{L}_{\square}} \langle d_{\alpha}^A W(\Gamma) d_{\alpha}^A W(p) \rangle + \\ & + N_f N_c \sum_{n=1}^{\infty} \sum_{\omega \in \mathcal{C}_n} \frac{\hat{m}^{-n}}{n} c(\omega) \langle d_{\alpha}^A W(\Gamma) d_{\alpha}^A W_{\mathbf{R}}(\omega) \rangle = 0 . \end{aligned} \quad (4.23)$$

From the relationships (3.47), the Lie derivatives $d_\alpha^A W_R(\omega)$ can be computed:

$$d_\alpha^A W_{\text{AS}}(\omega) = W(\omega) d_\alpha^A W(\omega) - \frac{1}{2N_c} d_\alpha^A W(\omega\omega) , \quad (4.24a)$$

$$d_\alpha^A W_{\text{Adj}}(\omega) = W(\omega) d_\alpha^A W(\bar{\omega}) + W(\bar{\omega}) d_\alpha^A W(\omega) . \quad (4.24b)$$

Substituting in the case of AsQCD, neglecting the subleading term in the formula (4.24a) and using the factorization property, the loop equations in the large- N_c limit become:

$$\begin{aligned} & \frac{1}{N_c} \langle d_\alpha^A d_\alpha^A W(\Gamma) \rangle + \frac{N_c}{\lambda} \sum_{p \in \mathcal{L}_\square} \langle d_\alpha^A W(\Gamma) d_\alpha^A W(p) \rangle + \\ & + N_c \sum_{n=1}^{\infty} \sum_{\omega \in \mathcal{C}_n} \frac{\hat{m}^{-n}}{n} c(\omega) \langle W(\omega) \rangle \langle d_\alpha^A W(\Gamma) d_\alpha^A W(\omega) \rangle \stackrel{N_c \rightarrow \infty}{\equiv} 0 . \end{aligned} \quad (4.25)$$

I want to point out that the terms like

$$1/N_c \langle d_\alpha^A d_\alpha^A W(\Gamma) \rangle \quad \text{and} \quad N_c \langle d_\alpha^A W(\Gamma_1) d_\alpha^A W(\Gamma_2) \rangle$$

are of order 1 in the large- N_c , as already seen by explicit computation in section 2.5.

Instead, the loop equations in the large- N_c limit for AdjQCD are:

$$\begin{aligned} & \frac{1}{N_c} \langle d_\alpha^A d_\alpha^A W(\Gamma) \rangle + \frac{N_c}{\lambda} \sum_{p \in \mathcal{L}_\square} \langle d_\alpha^A W(\Gamma) d_\alpha^A W(p) \rangle + \\ & + \frac{N_c}{2} \sum_{n=1}^{\infty} \sum_{\omega \in \mathcal{C}_n} \frac{\hat{m}^{-n}}{n} c(\omega) \langle W(\bar{\omega}) \rangle \langle d_\alpha^A W(\Gamma) d_\alpha^A W(\omega) \rangle + \\ & + \frac{N_c}{2} \sum_{n=1}^{\infty} \sum_{\omega \in \mathcal{C}_n} \frac{\hat{m}^{-n}}{n} c(\omega) \langle W(\omega) \rangle \langle d_\alpha^A W(\Gamma) d_\alpha^A W(\bar{\omega}) \rangle \stackrel{N_c \rightarrow \infty}{\equiv} 0 . \end{aligned} \quad (4.26)$$

Since for each path $\omega \in \mathcal{C}_n$ the reversed one $\bar{\omega}$ also belongs to \mathcal{C}_n , and since $c(\omega) = c(\bar{\omega})$, the last two terms in the l.h.s. of the equation above are equals. Moreover, if the \mathcal{C} -symmetry is not spontaneously broken (and so it is in the

strong-coupling phase), then $\langle W(\bar{\omega}) \rangle = \langle W(\omega) \rangle$:

$$\begin{aligned}
 & \frac{N_c}{2} \sum_{n=1}^{\infty} \sum_{\omega \in \mathcal{C}_n} \frac{\hat{m}^{-n}}{n} c(\omega) \langle W(\bar{\omega}) \rangle \langle d_\alpha^A W(\Gamma) d_\alpha^A W(\omega) \rangle + \\
 & + \frac{N_c}{2} \sum_{n=1}^{\infty} \sum_{\omega \in \mathcal{C}_n} \frac{\hat{m}^{-n}}{n} c(\omega) \langle W(\omega) \rangle \langle d_\alpha^A W(\Gamma) d_\alpha^A W(\bar{\omega}) \rangle = \\
 & = N_c \sum_{n=1}^{\infty} \sum_{\omega \in \mathcal{C}_n} \frac{\hat{m}^{-n}}{n} c(\omega) \langle W(\omega) \rangle \langle d_\alpha^A W(\Gamma) d_\alpha^A W(\omega) \rangle . \quad (4.27)
 \end{aligned}$$

Therefore, the loop equations for the AdjQCD are completely equivalent to the loop equations (4.25) for the AsQCD in the large- N_c limit, in a phase that does not break the charge conjugation. It is useful to remember that this result is based on a large-mass expansion.

For sake of completeness, I will write the loop equations after having explicitly computed all the Lie-derivatives, as done in the equation (2.47):

$$\begin{aligned}
 & |\Gamma| \langle W(\Gamma) \rangle + \left\{ \sum_{\substack{\text{self-intersections} \\ \text{with parallel link}}} - \sum_{\substack{\text{self-intersections} \\ \text{with opposite link}}} \langle W(\Gamma_1) \rangle \langle W(\Gamma_2) \rangle \right\} = \\
 & = -\frac{1}{\lambda} \left\{ \sum_{\substack{\Gamma \text{ and } p \in \mathcal{L}_\square \text{ join} \\ \text{with parallel link}}} - \sum_{\substack{\Gamma \text{ and } p \in \mathcal{L}_\square \text{ join} \\ \text{with opposite link}}} \langle W(\Gamma p) \rangle \right\} + \\
 & - \sum_{n=1}^{\infty} \frac{\hat{m}^{-n}}{n} \left\{ \sum_{\substack{\Gamma \text{ and } \omega \in \mathcal{C}_n \text{ join} \\ \text{with parallel link}}} - \sum_{\substack{\Gamma \text{ and } \omega \in \mathcal{C}_n \text{ join} \\ \text{with opposite link}}} c(\omega) \langle W(\omega) \rangle \langle W(\Gamma \omega) \rangle \right\} . \quad (4.28)
 \end{aligned}$$

4.4 Solution of the loop equations and planar equivalence

Even if the loop equations are the same in the two theories in the large- N_c limit and in the large-mass phase, this does not imply the equality of the solution because the solution of a non-linear infinite system of equations is in general

not unique, as already discussed in section 2.5. However, if one considers only solutions which can be expanded as a series of powers of both $1/\lambda$ and $1/\hat{m}$, the solution is actually found to be unique. Therefore, in the strong-coupling and large-mass phase, the expectation values of the Wilson loops coincide in AsQCD and AdjQCD.

Let us see how to prove the uniqueness of the solution. Since we are interested in a power expansion of the solution, the equations (4.28) is solved iteratively, by truncating each time at an higher order.

We inductively search the solution at the order $\lambda^{-i}\hat{m}^{-j}$ for some fixed pair (i, j) , by assuming that the solution at all the lower orders exists and is unique. In the equations (4.28), the highest order (i, j) clearly appears only in the l.h.s., while the r.h.s. is completely known. Consider now a closed path Γ without self-intersections. The loop equations become:

$$|\Gamma|\langle W(\Gamma) \rangle = \text{something depending only on the lower orders} .$$

The solution for this equation exists and is unique. For a generic closed path Γ with k self-intersections:

$$|\Gamma|\langle W(\Gamma) \rangle + \left\{ \sum_{\substack{\text{self-intersections} \\ \text{with parallel link}}} - \sum_{\substack{\text{self-intersections} \\ \text{with opposite link}}} \langle W(\Gamma_1) \rangle \langle W(\Gamma_2) \rangle \right\} = \\ = \text{something depending only on the lower orders} .$$

In the second term of the l.h.s. only loops with at most $k - 1$ self-intersections appear. Thus, by induction the solution truncated at the order (i, j) exists and is unique for each closed path Γ .

In the case of $i = j = 0$ since 'something depending only on the lower orders' is zero, the unique solution for a non-trivial path Γ is $\langle W(\Gamma) \rangle = 0$. Again by induction, one concludes that the solution exists and is unique at each order (i, j) . And this is precisely what we wanted to prove.

Chapter 5

The center symmetry in the planar limit

Where center symmetry is present, it implies the confinement of the colour. Its spontaneous breaking leads to the deconfinement transition. For a gauge theory discretized on the lattice, the action of the center is defined as:

$$U_0(x_0 = 0, \mathbf{x}) \rightarrow uU_0(x_0 = 0, \mathbf{x}) , \quad (5.1)$$

where x_0 is the coordinate along the time direction, and u is an element of the center. The center transformation counts the winding number of Wilson loops around the time direction. If the loop Γ wraps w times around the time direction, the transformation rule is:

$$W(\Gamma) \rightarrow u^w W(\Gamma) . \quad (5.2)$$

Since the action for pure gauge is given by the sum of plaquettes, that have zero winding number, it is invariant under the action of the center.

The generic representation \mathbf{R} of the gauge group induces a representation of the center subgroup, that can be labelled by an integer $N_{\mathbf{R}}$ (with $0 \leq N_{\mathbf{R}} < N_c$), the N -ality of the representation:

$$\mathbf{R}[u] = u^{N_{\mathbf{R}}} , \quad \mathbf{R}[uU] = u^{N_{\mathbf{R}}} \mathbf{R}[U] . \quad (5.3)$$

Clearly, if matter in a representation with zero N -ality is present, the theory is still invariant under the action of the center. Otherwise, invariance under some

CHAPTER 5. THE CENTER SYMMETRY IN THE PLANAR LIMIT

subgroup could survive. In the following table the theories relevant for this work are summarized.

5.1 Potentials for the Polyakov loop

In this section, I will define some useful functions of the Polyakov loop on the lattice discretized theory. The fermionic representation will be kept generic, unless explicitly specified. In what follows, it is useful to distinguish the temporal from the spatial coordinates $\mathbf{x} = (x_0, \mathbf{x})$, and the temporal link variable $U_0(x_0, \mathbf{x})$ from the spatial ones $U_\mu(x_0, \mathbf{x})$.

Define the parallel transport Ω around the temporal dimension and the Polyakov loop P :

$$\Omega(\mathbf{x}) = U_0(0, \mathbf{x})U_0(1, \mathbf{x}) \cdots U_0(T-1, \mathbf{x}) , \quad (5.4)$$

$$P(\mathbf{x}) = \text{tr } \Omega(\mathbf{x}) . \quad (5.5)$$

One can use the gauge invariance and fix the temporal gauge:

$$U_0(x_0, \mathbf{x}) = \begin{cases} \mathbf{1} & \text{if } x_0 = 0, \dots, T-2 \\ \Omega(\mathbf{x}) & \text{if } x_0 = T-1 \end{cases} . \quad (5.6)$$

The action $S(\Omega, U_\mu)$ (the fermions have been integrated out) is invariant under time-independent gauge transformations. The Fadeev-Popov determinant for this gauge fixing is one, thus the measure of the functional integral is simply:

$$\exp \{-S(\Omega, U_\mu)\} \prod_{\mu, x_0, \mathbf{x}} dU_\mu(x_0, \mathbf{x}) \prod_{\mathbf{x}} d\Omega(\mathbf{x}) . \quad (5.7)$$

At this point, the following functionals can be defined.

Probability distribution of $\Omega(\mathbf{0})$. It is obtained by integrating out all the degrees of freedom, except $\Omega(\mathbf{0}) = \hat{\Omega}$:

$$e^{-S(\hat{\Omega})} = \frac{1}{Z} \int e^{-S(\Omega, U_\mu)} \Big|_{\Omega(\mathbf{0})=\hat{\Omega}} \prod_{\mu, x_0, \mathbf{x}} dU_\mu(x_0, \mathbf{x}) \prod_{\mathbf{x} \neq \mathbf{0}} d\Omega(\mathbf{x}) . \quad (5.8)$$

If $f(\hat{\Omega})$ is a function of Ω in a single point, its expectation value is given by:

$$\langle f(\hat{\Omega}) \rangle = \int f(\hat{\Omega}) e^{-S(\hat{\Omega})} d\hat{\Omega} . \quad (5.9)$$

Probability distribution of the Polyakov loop. It is defined as the expectation value of the delta function of the Polyakov loop:

$$e^{-N_c^2 V(z)} = \langle \delta \left(z - \frac{1}{N_c} \text{tr } \hat{\Omega} \right) \rangle = \int \delta \left(z - \frac{1}{N_c} \text{tr } \hat{\Omega} \right) e^{-S(\hat{\Omega})} d\hat{\Omega} . \quad (5.10)$$

The function $V(z)$ is often referred as effective potential of the Polyakov loop. But in this chapter I will adopt a different definition, which will be given below.

Generator of connected expectation values. It is obtained by coupling the Polyakov loop to a complex external source:

$$W(\alpha, \bar{\alpha}) = -\frac{1}{N_c^2} \log \left\langle \exp \left\{ -N_c \frac{\bar{\alpha} \operatorname{tr} \hat{\Omega} + \alpha \operatorname{tr} \hat{\Omega}^\dagger}{2} \right\} \right\rangle. \quad (5.11)$$

Expanding as a power series of the source:

$$\begin{aligned} W(\alpha, \bar{\alpha}) &= -\frac{1}{N_c^2} \log \left\langle \exp \left\{ -N_c \frac{\bar{\alpha} \operatorname{tr} \hat{\Omega} + \alpha \operatorname{tr} \hat{\Omega}^\dagger}{2} \right\} \right\rangle = \\ &= -\sum_{n=1}^{\infty} \frac{(-1)^n}{n!} \frac{\left\langle \left(\frac{\bar{\alpha} \operatorname{tr} \hat{\Omega} + \alpha \operatorname{tr} \hat{\Omega}^\dagger}{2} \right)^n \right\rangle_c}{N_c^{2-n}} = \\ &= 1 - \sum_{p,q=0}^{\infty} \left(-\frac{1}{2} \right)^{p+q} \frac{1}{p!q!} \bar{\alpha}^p \alpha^q \frac{\left\langle (\operatorname{tr} \hat{\Omega})^p (\operatorname{tr} \hat{\Omega}^\dagger)^q \right\rangle_c}{N_c^{2-p-q}}. \end{aligned} \quad (5.12)$$

Since the connected expectation value of N_c loops is at most of order N_c^{2-n} , each term of the previous expansion keeps finite in the large- N_c limit.

Generator of one-particle irreducible graphs. It is the Legendre transform of the generator of connected expectation values:

$$z(\alpha, \bar{\alpha}) = 2\bar{\partial}_\alpha W(\alpha, \bar{\alpha}) = \frac{\left\langle \operatorname{tr} \hat{\Omega} \exp \left\{ -N_c \frac{\bar{\alpha} \operatorname{tr} \hat{\Omega} + \alpha \operatorname{tr} \hat{\Omega}^\dagger}{2} \right\} \right\rangle}{N_c \left\langle \exp \left\{ -N_c \frac{\bar{\alpha} \operatorname{tr} \hat{\Omega} + \alpha \operatorname{tr} \hat{\Omega}^\dagger}{2} \right\} \right\rangle}, \quad (5.13)$$

$$\Gamma(z, \bar{z}) = W(\alpha, \bar{\alpha}) - \frac{\bar{\alpha}z + \alpha\bar{z}}{2}. \quad (5.14)$$

The definition above works only if the map $(\alpha, \bar{\alpha}) \leftrightarrow (z, \bar{z})$ is invertible. This is true in the strong-coupling phase, and is assumed true if no symmetry is spontaneously broken, as at low temperature. I will refer to the function $\Gamma(z, \bar{z})$ as the effective potential of the Polyakov loop. In general, it is different by the function $V(z)$; but it can be shown that the two function coincide in the limit of infinite spatial volume.

The center action is a symmetry if and only if the effective potential $\Gamma(z, \bar{z})$ is invariant². Because of the Legendre transform, the effective potential is not so easy to compute. Since $z(u\alpha, \bar{u}\bar{\alpha}) = uz(\alpha, \bar{\alpha})$,

$$\Gamma(uz, \bar{u}\bar{z}) = W(u\alpha, \bar{u}\bar{\alpha}) - \frac{\bar{\alpha}z(\alpha, \bar{\alpha}) + \alpha\bar{z}(\alpha, \bar{\alpha})}{2}, \quad (5.15)$$

and the following implications hold:

$$\text{center is a symmetry} \Leftrightarrow \Gamma(uz, \bar{u}\bar{z}) = \Gamma(z, \bar{z}) \Leftrightarrow W(u\alpha, \bar{u}\bar{\alpha}) = W(\alpha, \bar{\alpha}). \quad (5.16)$$

Therefore, the functional $W(\alpha, \bar{\alpha})$ encodes full information about the center symmetry. The terms of the expansion in equation (5.12) are classified in table 5.1 according to their symmetry properties.

| Term in W | Symmetry |
|-----------------|--------------------|
| $p = q \pmod 2$ | \mathbf{Z}_2 |
| $p = q \pmod N$ | \mathbf{Z}_{N_c} |
| $p = q$ | $U(1)$ |

Table 5.1: Symmetry properties of the Polyakov connected correlators $\langle (P)^p (P^\dagger)^q \rangle_c$. We say that G is a symmetry group for the Polyakov connected correlator if it is invariant under the transformation $\Omega(\mathbf{x}) \rightarrow u\Omega(\mathbf{x})$ with $u \in G$. Note that G is not necessarily a subgroup of the center.

5.2 The connected graphs in the large-mass expansion

The formalism of the large-mass expansion has already been developed in section 3.4. I want to briefly review some formulae. The fermionic effective action can be written as a sum of Wilson loops in the appropriate representation:

$$S_f(\Omega, U_\mu) = \sum_{\omega \in \mathcal{C}} c(\omega) \text{tr} \mathbf{R}[U(\omega)], \quad (5.17)$$

²In principle, one should consider the effective potential of a generic loop arbitrarily wrapping along the time direction. This can be done using the same formalism that I will develop in the current chapter. However I will assume that the Polyakov loop completely characterise the center symmetry.

where $\mathbf{R}[U]$ is the matrix representing U in the representation \mathbf{R} , and ω indicates a generic closed path on the lattice with length $L(\omega)$. The coefficients $c(\omega)$ depend on the spin structure of the chosen discretization of the Dirac operator and are independent of the colour structure. They are of order of $m^{-L(\omega)}$, where m is the bare fermion mass. It will be convenient to split the set \mathcal{C} of all the closed paths into the union of the sets $\mathcal{C}(w)$ of the closed paths with winding number w around the thermal dimension.

The generic connected expectation value of Polyakov loops can be formally thought as a function of the coefficients $c(\omega)$. In the large-mass phase, it can be expanded as a power series around $c(\omega) = 0$:

$$\begin{aligned} & \frac{1}{N_c^{2-p-q}} \langle (\text{tr } \hat{\Omega})^p (\text{tr } \hat{\Omega}^\dagger)^q \rangle_c = \\ & = \sum_{n=0}^{\infty} \frac{1}{n!} \sum_{\omega_1 \dots \omega_n} \frac{c(\omega_1) \cdots c(\omega_n)}{N_c^{2-p-q}} \left. \frac{d^n \langle (\text{tr } \hat{\Omega})^p (\text{tr } \hat{\Omega}^\dagger)^q \rangle_c}{dc(\omega_1) \cdots dc(\omega_n)} \right|_{S_f=0}. \end{aligned} \quad (5.18)$$

The derivative in $c(\omega)$ corresponds to the insertion of a vertex $\text{tr } \mathbf{R}[U(\omega)]$ in the expectation value. Since the derivative must be computed at $S_f = 0$, each term in the expansion above can be written as combinations of the connected expectation values in the pure Yang-Mills, as shown in some explicit examples later on. Therefore the asymptotic behaviour of the connected expectation values in the theory with dynamical fermions can be reconstructed from the asymptotic behaviour of the connected expectation values in the pure Yang-Mills one.

5.2.1 Pure gauge

Let $\omega_1, \dots, \omega_n$ be some closed paths and w_1, \dots, w_n be their respective winding numbers around the thermal direction. Consider the generic normalized connected expectation value in the pure Yang-Mills theory:

$$\frac{\langle \prod_i \text{tr } U(\omega_i) \rangle_{c,\text{YM}}}{N_c^{2-n}}. \quad (5.19)$$

As already seen in chapter 2, this quantity is always finite in the large- N_c limit (it could be also 0 and in this case I will say that the leading order is not saturated). The following cases are given.

- $\sum_i w_i \neq 0 \pmod{N_c}$. The expression in (5.19) transforms with a multiplicative constant under center transformations. Since the center symmetry is not broken in the confined phase, the expression is exactly zero for every value of N_c .
- $\sum_i w_i = 0 \pmod{N_c}$ but $\sum_i w_i \neq 0$ (see figure 5.2, 5.3). The expression in (5.19) is invariant under \mathbf{Z}_{N_c} but not $U(1)$. By the strong-coupling expansion (see section 5.5) it is possible to prove that it vanishes in the large- N_c limit. This result can be extended beyond the strong-coupling phase, under the commonly accepted assumption that the $U(N_c)$ and $SU(N_c)$ Yang-Mills theories differ in the large- N_c limit only for subleading contributions. If the gauge group were $U(N_c)$, the expression in (5.19) would be exactly zero for every value of N_c . Since we are interested in the $SU(N_c)$ gauge group, it must be zero in the large- N_c limit.
- The loops with winding number different from zero appear in pairs of loops with opposite winding number (see figure 5.1). In particular $\sum_i w_i = 0$. From the strong-coupling expansion (see section 5.5) the expression in (5.19) in this case is different from zero in the large- N_c limit. It is natural to assume that this result extends beyond the strong-coupling phase.
- $\sum_i w_i = 0$ but some of the loops with winding number $w \neq 0$ cannot be paired with a loop with winding number $-w$. Although the expression in (5.19) is invariant under the center (both \mathbf{Z}_{N_c} and $U(1)$), in the strong-coupling phase (see section 5.5) it vanishes because of the topology of the torus. I cannot say if this result extends beyond the strong-coupling expansion, but anyway I will not use it in this work.

5.2.2 Adjoint fermions

For fermions in the adjoint representation, the full theory is still invariant under the center group \mathbf{Z}_N and the large- N_c behaviour of the connected correlators is expected to be the same as for the pure gauge theory.

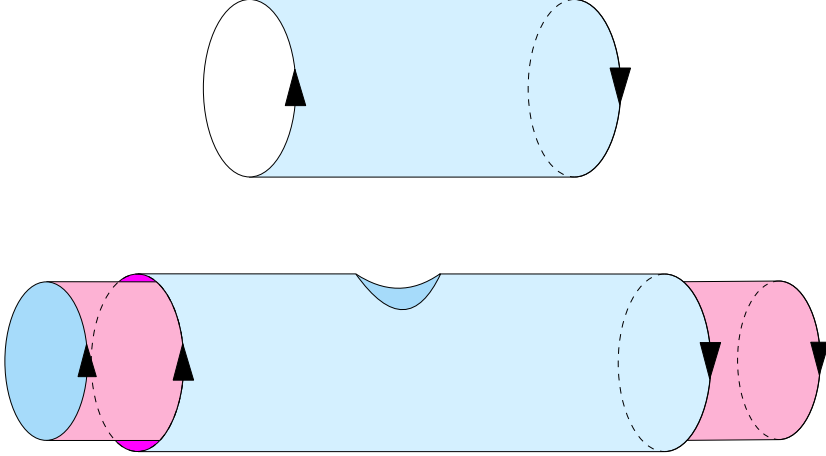


Figure 5.1: Representations of some connected expectation values of products of loops with net winding number equal to zero, in pure Yang-Mills. The first one is $\langle \text{tr } \Omega \text{ tr } \Omega^\dagger \rangle_{c, \text{YM}}$; the Polyakov loops are connected by an oriented surface that wraps around the thermal dimension. In the strong-coupling expansion, the surface is tiled by plaquettes coming from the Wilson action; two (or more) products of group elements associated to each link of the lattice are integrated with respect to the Haar measure. This graph yields a contribution $O(N_c^0)$. The second graph represents $\langle (\text{tr } \Omega \text{ tr } \Omega^\dagger)^2 \rangle_{c, \text{YM}}$; the two tubes are glued together through an hole. This graph is $O(N_c^{-2})$.

5.2.3 Fundamental fermions

When fermions in the fundamental representation are considered, the generic term of the r.h.s. of the equation (5.18) is:

$$\frac{1}{N_c^{2-p-q}} \frac{d^n \langle (\text{tr } \hat{\Omega})^p (\text{tr } \hat{\Omega}^\dagger)^q \rangle_{c, \text{F}}}{dc(\omega_1) \cdots dc(\omega_n)} \Big|_{S_f=0} = \frac{\langle (\text{tr } \hat{\Omega})^p (\text{tr } \hat{\Omega}^\dagger)^q \text{tr } U(\omega_1) \cdots \text{tr } U(\omega_n) \rangle_{c, \text{YM}}}{N_c^{2-p-q}}. \quad (5.20)$$

The expectation value that appears in the numerator of the r.h.s. of (5.20) is at most of order $N_c^{2-p-q-n}$, since it contains $p + q + n$ loops. Thus for $n \neq 0$, the whole term is at most of order N_c^{-1} . If $p = q$ the Yang-Mills contribution

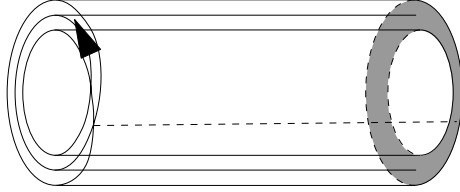


Figure 5.2: Graphical representation of $\langle \text{tr}(\Omega_c^N) \rangle_{c, \text{YM}}$ for $N_c = 3$. The surface wraps N_c times around the thermal direction and ends in the gray area, that represents the integration of the product of N_c group elements, all oriented in the same direction. This integration yields a non-zero value, because the product of N_c fundamental representations of $SU(N_c)$ contains a singlet, given by the contraction with the completely skew-symmetric tensor. This graph yields a contribution $O(N_c^0)$.

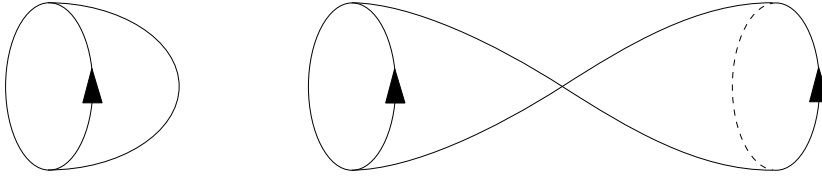


Figure 5.3: These graphs are the would-be leading contributions of respectively $\langle \text{tr} \Omega \rangle_{\text{YM}}$ and $\langle (\text{tr} \Omega)^2 \rangle_{c, \text{YM}}$. They are forbidden by the topology of the thermal dimension.

($n = 0$) dominates the sum. Otherwise, the leading contribution is at most of order N_c^{-1} :

$$\begin{aligned} \frac{\langle (\text{tr} \hat{\Omega})^p (\text{tr} \hat{\Omega}^\dagger)^q \rangle_{c, \text{F}}}{N_c^{2-p-q}} &\simeq \frac{\langle (\text{tr} \hat{\Omega})^p (\text{tr} \hat{\Omega}^\dagger)^q \rangle_{c, \text{YM}}}{N_c^{2-p-q}}, & \text{if } p = q, \\ \frac{\langle (\text{tr} \hat{\Omega})^p (\text{tr} \hat{\Omega}^\dagger)^q \rangle_{c, \text{F}}}{N_c^{2-p-q}} &= O\left(\frac{1}{N_c}\right), & \text{if } p \neq q. \end{aligned} \quad (5.21)$$

For $p \neq q$, the $1/N_c$ scaling is only an upper limit for the asymptotic behaviour. However in the case of the expectation value of the Polyakov loop, the

$O(N_c^{-1})$ is saturated by the contribution:

$$\begin{aligned} \frac{\langle \text{tr } \hat{\Omega} \rangle}{N_c} &= \sum_{n=0}^{\infty} \frac{1}{n!} \sum_{\omega_1 \dots \omega_n} \frac{c(\omega_1) \cdots c(\omega_n)}{N_c^{2-p-q}} \frac{d^n \langle \text{tr } \hat{\Omega} \rangle_c}{dc(\omega_1) \cdots dc(\omega_n)} \Big|_{S_f=0} = \\ &= \frac{1}{N_c} \sum_{\omega \in \mathcal{C}(-1)} c(\omega) \langle \text{tr } \hat{\Omega} \text{ tr } U(\omega) \rangle_{c, \text{YM}} + O\left(\frac{1}{N_c^2}\right). \end{aligned} \quad (5.22)$$

Recall that $\mathcal{C}(-1)$ is the set of the closed paths on the lattice which winding number equal to -1 around the thermal dimension.

From the large- N_c behaviour of the coefficients of the Taylor expansion, we see that, in the large- N_c limit, the functional W is the same for Yang-Mills and for the theory with fundamental quarks:

$$\begin{aligned} \lim_{N_c \rightarrow \infty} W_F(\alpha, \bar{\alpha}) &= \lim_{N_c \rightarrow \infty} W_{\text{YM}}(\alpha, \bar{\alpha}) = \\ &= 1 - \sum_{p=0}^{\infty} \frac{|\alpha|^{2p}}{(p!2^p)^2} \lim_{N_c \rightarrow \infty} \frac{\left\langle \left| \text{tr } \hat{\Omega} \right|^{2p} \right\rangle_{c, \text{YM}}}{N_c^{2-2p}} \end{aligned} \quad (5.23)$$

This is the manifestation in this particular sector of the theory of the usual subleading contribution from the fermion determinant when fermions are in the fundamental representation.

5.2.4 S/AS fermions

Again, in the generic term of the r.h.s. of the equation (5.18):

$$\frac{1}{N_c^{2-p-q}} \frac{d^n \langle (\text{tr } \hat{\Omega})^p (\text{tr } \hat{\Omega}^\dagger)^q \rangle_{c, \text{S/AS}}}{dc(\omega_1) \cdots dc(\omega_n)} \Big|_{S_f=0}, \quad (5.24)$$

each derivative in $c(\omega)$ produces the insertion of a vertex $\text{tr } \mathbf{R}[U(\omega)]$. When the fermions are in the (anti)symmetric representation, we can use the algebraic relationships:

$$\text{tr S/AS}[U] = \frac{(\text{tr } U)^2 \pm \text{tr}(U^2)}{2}. \quad (5.25)$$

In general, the insertion of some terms of the form $(\text{tr } U)^2/2$ will disconnect the expectation value $\langle (\text{tr } \hat{\Omega})^p (\text{tr } \hat{\Omega}^\dagger)^q \rangle_{c, \text{S/AS}}$. In order to gain some confidence with these computations, I report in the following subsections the explicit computation of the leading orders of $\langle (\text{tr } \hat{\Omega})^2 \rangle_{c, \text{S/AS}}$, $\langle \text{tr } \hat{\Omega} \text{ tr } \hat{\Omega}^\dagger \rangle_{c, \text{S/AS}}$ and

$\langle \text{tr } \hat{\Omega} \rangle_{c,S/AS}$. The end of the section is devoted to a discussion of the general case.

Before entering into the details of the computations, I summarize here the results:

$$\begin{aligned}
 \frac{\langle (\text{tr } \hat{\Omega})^p (\text{tr } \hat{\Omega}^\dagger)^q \rangle_{c,S/AS}}{N_c^{2-p-q}} &= O(1), & \text{if } p - q \text{ even} \\
 \frac{\langle (\text{tr } \hat{\Omega})^p (\text{tr } \hat{\Omega}^\dagger)^q \rangle_{c,S/AS}}{N_c^{2-p-q}} &= O\left(\frac{1}{N_c}\right), & \text{if } p - q \text{ odd and } N_c \text{ odd} \\
 \frac{\langle (\text{tr } \hat{\Omega})^p (\text{tr } \hat{\Omega}^\dagger)^q \rangle_{c,S/AS}}{N_c^{2-p-q}} &= 0, & \text{if } p - q \text{ odd and } N_c \text{ even}
 \end{aligned} \tag{5.26}$$

Hence the large- N_c limit for the functional W yields:

$$\begin{aligned}
 \lim_{N_c \rightarrow \infty} W_{S/AS}(\alpha, \bar{\alpha}) &= \\
 &= 1 - \sum_{\substack{p,q=0 \\ p-q \text{ even}}}^{\infty} \frac{1}{p!q!} \bar{\alpha}^p \alpha^q \lim_{N_c \rightarrow \infty} \frac{\langle (\text{tr } \hat{\Omega})^p (\text{tr } \hat{\Omega}^\dagger)^q \rangle_{c,S/AS}}{N_c^{2-p-q}}.
 \end{aligned} \tag{5.27}$$

Since all the terms with $p - q$ even contribute to the sum, we get $W_{S/AS}(\alpha, \bar{\alpha}) = W_{S/AS}(u\alpha, \bar{u}\bar{\alpha})$ in the planar limit if and only if $u = \pm 1$. Therefore a \mathbf{Z}_2 symmetry is recovered in the large- N_c limit.

Computation of $\langle \text{tr } \hat{\Omega} \rangle_{S/AS}$

Let us start with the single-derivative term in the expansion (5.18):

$$\begin{aligned}
 \frac{1}{N_c} \frac{d\langle \text{tr } \hat{\Omega} \rangle_{S/AS}}{dc(\omega)} \Big|_{S_f=0} &= \\
 &= \frac{1}{N_c} \left\{ \langle \text{tr } \hat{\Omega} \text{ tr } \mathbf{R}[U(\omega)] \rangle_{\text{YM}} - \langle \text{tr } \hat{\Omega} \rangle_{\text{YM}} \langle \text{tr } \mathbf{R}[U(\omega)] \rangle_{\text{YM}} \right\} = \\
 &= \frac{1}{2N_c} \left\{ \langle \text{tr } \hat{\Omega} [\text{tr } U(\omega)]^2 \rangle_{\text{YM}} \pm \langle \text{tr } \hat{\Omega} \text{ tr}[U(\omega)^2] \rangle_{\text{YM}} \right\} = \\
 &= \frac{1}{2N_c} \left\{ \langle \text{tr } \hat{\Omega} [\text{tr } U(\omega)]^2 \rangle_{c,\text{YM}} + 2\langle \text{tr } \hat{\Omega} \text{ tr } U(\omega) \rangle_{c,\text{YM}} \langle \text{tr } U(\omega) \rangle_{c,\text{YM}} \right. \\
 &\quad \left. \pm \langle \text{tr } \hat{\Omega} \text{ tr}[U(\omega)^2] \rangle_{c,\text{YM}} \right\}.
 \end{aligned} \tag{5.28}$$

Let w be the winding number around the thermal dimension of the closed path ω . I shall analyse each term in turn. The term $\langle \text{tr} \hat{\Omega} [\text{tr} U(\omega)]^2 \rangle_{c, \text{YM}}$ saturates its N_c^{-1} behaviour only if $1 + 2w = 0$, that corresponds to the invariance under the action of $U(1)$. But this equation has no integer solution, therefore the highest order is never saturated. The only non zero contribution come from loops that satisfies $1 + 2w = kN_c$ (both k and N_c must be odd). In this case, the first term goes like N_c^{-2} .

The second term $\langle \text{tr} \hat{\Omega} \text{tr} U(\omega) \rangle_{c, \text{YM}} \langle \text{tr} U(\omega) \rangle_{c, \text{YM}}$ saturates its N_c asymptotic behaviour only if each factor is separately invariant under the action of $U(1)$. This corresponds to the equations $1 + w = 0$ and $w = 0$. For the discussion in the general case, these equations imply again the condition $1 + 2w = 0$, that corresponds to the over all invariance of the product under the action of $U(1)$. Again, this equation admits no solution and the leading order is not saturated. We can look for subleading contributions. Since we want $\langle \text{tr} U(\omega) \rangle_{c, \text{YM}}$ not vanishing, it must be $w = kN_c$. Requiring that $\langle \text{tr} \hat{\Omega} \text{tr} U(\omega) \rangle_{c, \text{YM}}$ is not vanishing, we get $1 + w = 1 + kN_c = k'N_c$ that means $(k' - k)N_c = 1$. Again, this equation has no solution, therefore the second term is always zero.

The necessary condition for the last term $\langle \text{tr} \hat{\Omega} \text{tr}[U(\omega)^2] \rangle_{c, \text{YM}}$ to saturate its N_c^0 behaviour is again $1 + 2w = 0$. Looking for subleading contributions, we have to request $1 + 2w = kN_c$. This equation admits a solution if both k and N_c are odd, as for the first term. But unlike the first term, the last one goes like N_c^{-1} .

Putting all together, the single-derivative in equation (5.18) is of order N_c^{-2} and this behaviour is summarized by the formula:

$$\frac{1}{N_c} \left. \frac{d \langle \text{tr} \hat{\Omega} \rangle_{S/AS}}{dc(\omega)} \right|_{S_f=0} = \pm \frac{1}{2N_c} \langle \text{tr} \hat{\Omega} \text{tr}[U(\omega)^2] \rangle_{c, \text{YM}} + O\left(\frac{1}{N_c^3}\right). \quad (5.29)$$

Consider now the generic term in the expansion (5.18). I will not write the explicit expression, but it should be clear that it can be written as a sum of products of connected expectation values in the pure Yang-Mills theory. Let w_i be the winding number of the path ω_i . If we require that some of these products saturates the leading contribution, then this product must be invariant under the action of $U(1)$. In a formula, the sum of all the winding numbers must vanish:

$$1 + 2 \sum_i w_i = 0. \quad (5.30)$$

The factor 2 is due to the two-index representation. For each closed path ω_i with winding number w_i , a loop $\text{tr} \mathbf{R}[U(\omega)]$ with N -ality equal to $2w_i$ is inserted.

The equation above has no solution, therefore the leading order for $\langle \text{tr } \hat{\Omega} \rangle_{c,S/AS}$ is not saturated. This argument lets us to conclude that:

$$\lim_{N_c \rightarrow \infty} \frac{\langle \text{tr } \hat{\Omega} \rangle_{S/AS}}{N_c} = 0, \quad (5.31)$$

but we still cannot say if it is a $O(1/N_c)$ or rather a $O(1/N_c^2)$ as the single-derivative term suggests. Since this is not essential to the main discussion of the center symmetry, I state simply the result as:

$$\begin{aligned} \frac{\langle \text{tr } \hat{\Omega} \rangle}{N_c} = & \pm \frac{1}{N_c} \sum_{n=0}^{\infty} \frac{1}{n!} \sum_{k \text{ odd}} \sum_{\bar{\omega} \in \mathcal{C}(\frac{kN_c-1}{2})} \sum_{\omega_1 \dots \omega_n} \\ & c(\bar{\omega})c(\omega_1) \cdots c(\omega_n) \left. \frac{d^n \langle \text{tr } \hat{\Omega} \text{tr}[U(\bar{\omega})^2] \rangle_c}{dc(\omega_1) \cdots dc(\omega_n)} \right|_{S_f=0} + \dots \end{aligned} \quad (5.32)$$

Computation of $\langle (\text{tr } \hat{\Omega})^2 \rangle_{c,S/AS}$

I want to check here that the leading term of $\langle (\text{tr } \hat{\Omega})^2 \rangle_{c,S/AS}$, which is expected to be N_c^0 , is actually different from zero. This can be easily shown by computing the single-derivative term in the expansion (5.18). Starting from the definition of the connected correlator: $\langle (\text{tr } \hat{\Omega})^2 \rangle_{c,S/AS} = \langle (\text{tr } \hat{\Omega})^2 \rangle_{S/AS} - \langle \text{tr } \hat{\Omega} \rangle_{S/AS}^2$, and assuming that ω is a generic closed path with winding number -1 around the thermal dimension, we can rewrite the single-derivative coefficient of the expansion of $\langle (\text{tr } \hat{\Omega})^2 \rangle_{c,S/AS}$ as:

$$\begin{aligned} \left. \frac{d \langle (\text{tr } \hat{\Omega})^2 \rangle_{c,S/AS}}{dc(\omega)} \right|_{S_f=0} &= \langle (\text{tr } \hat{\Omega})^2 \mathbf{R}[U(\omega)] \rangle_{\text{YM}} - \langle (\text{tr } \hat{\Omega})^2 \rangle_{\text{YM}} \langle \mathbf{R}[U(\omega)] \rangle_{\text{YM}} = \\ &= \frac{1}{2} \langle (\text{tr } \hat{\Omega})^2 [\text{tr } U(\omega)]^2 \rangle_{\text{YM}} = \\ &= \frac{1}{2} \left\{ \langle (\text{tr } \hat{\Omega})^2 [\text{tr } U(\omega)]^2 \rangle_{c,\text{YM}} + 2 \langle \text{tr } \hat{\Omega} \text{tr } U(\omega) \rangle_{c,\text{YM}} \langle \text{tr } \hat{\Omega} \text{tr } U(\omega) \rangle_{c,\text{YM}} \right\} = \\ &= \langle \text{tr } \hat{\Omega} \text{tr } U(\omega) \rangle_{c,\text{YM}} \langle \text{tr } \hat{\Omega} \text{tr } U(\omega) \rangle_{c,\text{YM}} + O\left(\frac{1}{N_c^2}\right); \end{aligned} \quad (5.33)$$

(as illustrated in figure 5.4). This is exactly a $O(N_c^0)$ term.

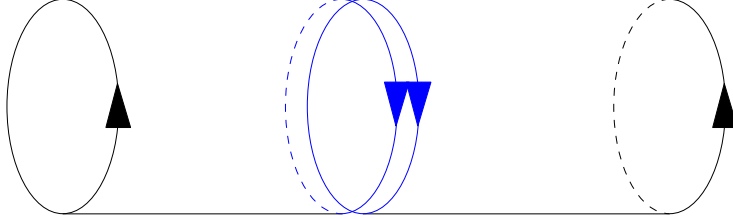


Figure 5.4: This graph is a leading contribution of $\langle (\text{tr } \hat{\Omega})^2 \rangle_{c,S/AS}$. The pair of blue loops represent the insertion of a vertex $\text{tr } \mathbf{R}[U(\omega)]$, due to the derivative with respect to $c(\omega)$.

Computation of $\langle \text{tr } \hat{\Omega} \text{tr } \hat{\Omega}^\dagger \rangle_{c,S/AS}$

This is the easiest example: since $\text{tr } \hat{\Omega} \text{tr } \hat{\Omega}^\dagger$ is invariant under the action of $U(1)$ by itself, the zero-derivative term $\langle \text{tr } \hat{\Omega} \text{tr } \hat{\Omega}^\dagger \rangle_{c,YM}$ in the expansion (5.18) trivially saturates the N_c^0 behaviour of $\langle \text{tr } \hat{\Omega} \text{tr } \hat{\Omega}^\dagger \rangle_{c,S/AS}$.

The generic $\langle \text{tr } \hat{\Omega}^p (\text{tr } \hat{\Omega}^\dagger)^q \rangle_{c,S/AS}$

As already discussed in the case of $\langle \text{tr } \hat{\Omega} \rangle_{c,S/AS}$, each term in the expansion (5.18) of the generic connected expectation value can be written as a sum of products of connected expectation values with respect to the YM vacuum. Each of these connected expectation values contains some $\text{tr } \hat{\Omega}$'s and $\text{tr } \hat{\Omega}^\dagger$'s from the original expectation value, and some $\text{tr } U(\omega)$ from the derivatives with respect to the coefficient $c(\omega)$. When the derivative with respect to $c(\omega_i)$ is computed, a $[\text{tr } U(\omega_i)]^2$ or a $\text{tr}[U(\omega_i)^2]$ is inserted. In both cases, if w_i is the winding number of the path ω_i , a parallel transport with $2w_i$ winding number is inserted. A necessary condition for the leading order to be saturated is that the overall winding number, that is the sum of all the winding numbers of the operators involved, must be zero (this corresponds to the invariance under action of $U(1)$). In a formula:

$$p - q + 2 \sum_i w_i = 0. \quad (5.34)$$

This argument implies that $p - q$ must be even. If it is odd, the leading behaviour cannot be saturated.

Now I want to show that this is also a sufficient condition, by explicitly constructing a term that saturates the leading behaviour. The $p = q$ case is

trivial since the leading behaviour is saturated by the pure YM term:

$$\frac{\langle (\text{tr } \hat{\Omega})^p (\text{tr } \hat{\Omega}^\dagger)^p \rangle_{c, \text{S/AS}}}{N_c^{2-2p}} = \frac{\langle (\text{tr } \hat{\Omega})^p (\text{tr } \hat{\Omega}^\dagger)^p \rangle_{c, \text{YM}}}{N_c^{2-2p}} + \dots \quad (5.35)$$

Consider now the $p > q$ case (the opposite can be obtained by charge-conjugation). If ω is a path with winding number -1 , a leading contribution comes for instance from (see figure 5.5):

$$\begin{aligned} & \frac{1}{N_c^{2-p-q}} \left. \frac{d^n \langle (\text{tr } \hat{\Omega})^p (\text{tr } \hat{\Omega}^\dagger)^q \rangle_c}{dc(\omega)^n} \right|_{S_f=0} = \\ & = \frac{p!(p-q)!}{\left(\frac{p+q}{2}\right)! \left[\left(\frac{p-q}{2}\right)!\right]^2} \frac{\langle (\text{tr } \hat{\Omega})^{\frac{p+q}{2}} [\text{tr } U(\omega)]^{\frac{p-q}{2}} (\text{tr } \hat{\Omega}^\dagger)^q \rangle_{c, \text{YM}}}{N_c^{2-p-q}} \times \\ & \quad \times \langle (\text{tr } \hat{\Omega} \text{ tr } U(\omega)) \rangle_{c, \text{YM}}^{\frac{p-q}{2}} + \dots \end{aligned} \quad (5.36)$$

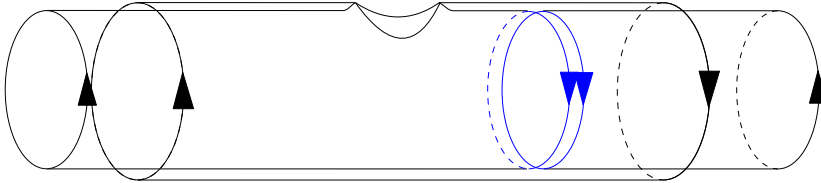


Figure 5.5: This graph is a leading contribution of $\langle (\text{tr } \Omega)^3 \text{tr } \Omega^\dagger \rangle_{c, \text{S/AS}}$. The pair of blue loops represent the insertion of a vertex $\text{tr } \mathbf{R}[U(\omega)]$, due to the derivative with respect to $c(\omega)$.

5.3 The effective potentials in the large-mass expansion

The analysis of the connected graphs in the previous section exhausts the issue of the center symmetry. However, I want to compare my results with the prediction in [24] about the effective potential of the Polyakov loop. Sannino gives general formulae for the effective potential $\Gamma(z, \bar{z})$ for small z , keeping only the lowest terms relevant to determine the correct symmetry group.

Pure gauge or adjoint fermions.

$$\Gamma(z, \bar{z}) = a_2 z \bar{z} + a_4 (z \bar{z})^2 + a_{N_c} (z^{N_c} + \bar{z}^{N_c}) \quad (5.37)$$

Fundamental fermions.

$$\Gamma(z, \bar{z}) = b_1 (z + \bar{z}) + a_2 z \bar{z} + a_4 (z \bar{z})^2 + a_{N_c} (z^{N_c} + \bar{z}^{N_c}) \quad (5.38)$$

S/AS fermions with N_c even.

$$\Gamma(z, \bar{z}) = b_2 (z^2 + \bar{z}^2) + a_2 z \bar{z} + a_4 (z \bar{z})^2 + a_{N_c} (z^{N_c} + \bar{z}^{N_c}) \quad (5.39)$$

S/AS fermions with N_c odd.

$$\Gamma(z, \bar{z}) = b_1 (z + \bar{z}) + b_2 (z^2 + \bar{z}^2) + a_2 z \bar{z} + a_4 (z \bar{z})^2 + a_{N_c} (z^{N_c} + \bar{z}^{N_c}) \quad (5.40)$$

In the large- N_c limit not all the coefficients survive. In particular:

$$\lim_{N_c \rightarrow \infty} a_{N_c}(N_c) = 0, \quad (5.41)$$

for all the theories; moreover, in the case of fundamental fermions:

$$\lim_{N_c \rightarrow \infty} b_1(N_c) = \lim_{N_c \rightarrow \infty} b_2(N_c) = 0, \quad (5.42)$$

while in the case of S/AS fermions:

$$\lim_{N_c \rightarrow \infty} b_1(N_c) = 0 \quad \lim_{N_c \rightarrow \infty} b_2(N_c) \neq 0, \quad (5.43)$$

I stress that this behaviour is constrained by the symmetry properties derived in the previous section. Nevertheless, I want now to check explicitly the last two equations.

5.3.1 The b_1 coefficient

Since $\alpha(z, \bar{z}) = -2\bar{\partial}_z \Gamma(z, \bar{z})$, from Taylor expansion of the effective potential:

$$b_1 = \partial_z \Gamma(0, 0) = -\frac{1}{2} \alpha_0, \quad (5.44)$$

where α_0 is the real source, defined by the condition $z(\alpha_0, \alpha_0) = \bar{z}(\alpha_0, \alpha_0) = 0$, that is the same as:

$$(\partial_\alpha + \bar{\partial}_\alpha) W(\alpha_0, \alpha_0) = 0. \quad (5.45)$$

Using the series expansion of $W(\alpha, \bar{\alpha})$, the above condition becomes:

$$\frac{\langle \text{tr } \hat{\Omega} \rangle}{N_c} - \alpha_0 \sum_{n=0}^{\infty} \frac{(-\alpha_0)^n}{(n+1)!} \frac{\langle (\Re \text{tr } \hat{\Omega})^{n+2} \rangle_c}{N_c^{-n}} = 0. \quad (5.46)$$

Since $\frac{\langle \text{tr } \hat{\Omega} \rangle}{N_c}$ vanishes in the large- N_c limit, the equation can be solved iteratively. At the leading order:

$$\alpha_0 = \frac{\langle \text{tr } \hat{\Omega} \rangle}{N_c \langle (\Re \text{tr } \hat{\Omega})^2 \rangle_c} + \text{subleadings}. \quad (5.47)$$

Expanding the denominator, the b_1 coefficient is:

$$b_1 = - \frac{\langle \text{tr } \hat{\Omega} \rangle}{N_c \left\{ \langle |\text{tr } \hat{\Omega}|^2 \rangle_c + \langle (\text{tr } \hat{\Omega})^2 \rangle_c \right\}} + \text{subleadings}, \quad (5.48)$$

and it vanishes in the large- N_c limit, with both fundamental and S/AS fermions.

5.3.2 The b_2 coefficient

The second order in the Taylor expansion of the effective potential is obtained by inverting the Hessian matrix of the functional W :

$$\begin{pmatrix} 2b_2 & a_2 \\ a_2 & 2b_2 \end{pmatrix} (0) = -\frac{1}{4} \begin{pmatrix} \bar{\partial}_\alpha^2 W & \partial_\alpha \bar{\partial}_\alpha W \\ \partial_\alpha \bar{\partial}_\alpha W & \partial_\alpha^2 W \end{pmatrix}^{-1} (\alpha_0). \quad (5.49)$$

The entries of the Hessian matrix in the large- N_c limit are:

$$\begin{aligned} \partial_\alpha^2 W(\alpha_0) &= -\frac{1}{4} \frac{\langle (\text{tr } \hat{\Omega})^2 \exp \left\{ -N_c \alpha_0 \Re \text{tr } \hat{\Omega} \right\} \rangle}{\langle \exp \left\{ -N_c \alpha_0 \Re \text{tr } \hat{\Omega} \right\} \rangle} + \\ &\quad + \frac{1}{4} \left(\frac{\langle \text{tr } \hat{\Omega} \exp \left\{ -N_c \alpha_0 \Re \text{tr } \hat{\Omega} \right\} \rangle}{\langle \exp \left\{ -N_c \alpha_0 \Re \text{tr } \hat{\Omega} \right\} \rangle} \right)^2 = \\ &= -\frac{1}{4} \langle (\text{tr } \hat{\Omega})^2 \rangle_c + \dots \end{aligned} \quad (5.50)$$

$$\begin{aligned}
 \partial_\alpha \bar{\partial}_\alpha W(\alpha_0) &= -\frac{1}{4} \frac{\langle |\text{tr } \hat{\Omega}|^2 \exp \left\{ -N_c \alpha_0 \Re \text{tr } \hat{\Omega} \right\} \rangle}{\langle \exp \left\{ -N_c \alpha_0 \Re \text{tr } \hat{\Omega} \right\} \rangle} + \\
 &\quad + \frac{1}{4} \left| \frac{\langle \text{tr } \hat{\Omega} \exp \left\{ -N_c \alpha_0 \Re \text{tr } \hat{\Omega} \right\} \rangle}{\langle \exp \left\{ -N_c \alpha_0 \Re \text{tr } \hat{\Omega} \right\} \rangle} \right|^2 = \\
 &= -\frac{1}{4} \langle |\text{tr } \hat{\Omega}|^2 \rangle_c + \dots
 \end{aligned} \tag{5.51}$$

Computing the inverse of the Hessian and putting altogether, one obtains:

$$a_2 = -\frac{\langle |\text{tr } \hat{\Omega}|^2 \rangle_c}{\langle (\text{tr } \hat{\Omega})^2 \rangle_c^2 - \langle |\text{tr } \hat{\Omega}|^2 \rangle_c^2} \tag{5.52}$$

$$b_2 = \frac{\langle (\text{tr } \hat{\Omega})^2 \rangle_c}{2 \left\{ \langle (\text{tr } \hat{\Omega})^2 \rangle_c^2 - \langle |\text{tr } \hat{\Omega}|^2 \rangle_c^2 \right\}}. \tag{5.53}$$

In particular, the a_2 coefficient is always of order 1; the b_2 coefficient is of order N_c^{-1} for fundamental fermions, while it is of order 1 for S/AS fermions.

5.4 The center symmetry in the Hamiltonian formalism

I want to obtain the same results of the previous sections, using the Hamiltonian and coherent states formalism. I believe that this approach allows to have a deeper picture of the center symmetry, and its remnants in the large- N_c limit.

The center symmetry is not a symmetry of the Hamiltonian. Indeed the center acts only on the temporal component of the gauge field, which is not a real degree of freedom of the theory: it is the Lagrange multiplier for the Gauss constraint. I want to review here this issue.

If H is the Hamiltonian of the gauge theory on the lattice (notations are the same as in section 3.5), the partition function is given by:

$$Z = \text{Tr}(e^{-\beta H} \mathbb{P}), \tag{5.54}$$

where \mathbb{P} is the projector on the gauge-invariant states. If g is an element of the gauge group, let $\mathcal{G}_{\mathbf{x}}[g]$ denote the unitary operator, which acts on the Hilbert

space by producing the gauge transformation g in the point \mathbf{x} . Thanks to the invariance of the Haar measure, the projector \mathbb{P} and the partition function can be written as:

$$\mathbb{P} = \int \prod_{\mathbf{x}} \{ \mathcal{G}_{\mathbf{x}}[\Omega(\mathbf{x})] d\Omega(\mathbf{x}) \} \quad (5.55)$$

$$\mathcal{Z}(\beta) = \int \text{Tr} \left(e^{-\beta H} \prod_{\mathbf{x}} \mathcal{G}_{\mathbf{x}}[\Omega(\mathbf{x})] \right) \prod_{\mathbf{x}} d\Omega(\mathbf{x}) . \quad (5.56)$$

If $\{\psi_n\}$ is a basis for the Hilbert space, the trace in the integral can be written as:

$$\text{Tr} \left(e^{-\beta H} \prod_{\mathbf{x}} \mathcal{G}_{\mathbf{x}}[\Omega(\mathbf{x})] \right) = \sum_n \langle \psi_n | e^{-\beta H} | \psi_n^{(\Omega)} \rangle , \quad (5.57)$$

where $\psi_n^{(\Omega)}$ is obtained by applying the gauge transformation Ω to the state ψ_n . From the equation above, $\Omega(\mathbf{x})$ is the $SU(N_c)$ phase that the state ψ_n acquires after a translation around the temporal direction. By writing the element matrix of $e^{-\beta H}$ as a functional integral, one sees that $\Omega(\mathbf{x})$ is the parallel transport around the time direction and $\frac{1}{N_c} \text{tr} \Omega(\mathbf{x})$ is the Polyakov loop.

All the potentials of section 5.3 can be written using the Hamiltonian formalism. For instance, the probability distribution of $\Omega(\mathbf{0})$ is:

$$e^{-S(\hat{\Omega})} = \frac{1}{Z} \int \text{Tr} \left\{ e^{-\beta H} \prod_{\mathbf{x}} \mathcal{G}_{\mathbf{x}}[\Omega(\mathbf{x})] \right\}_{\Omega(\mathbf{0})=\hat{\Omega}} \prod_{\mathbf{x} \neq \mathbf{0}} d\Omega(\mathbf{x}) . \quad (5.58)$$

If u is an element of the center, a center transformation is defined as $\Omega(\mathbf{x}) \rightarrow u\Omega(\mathbf{x})$. It does not affect the degrees of freedom in the Hamiltonian, but only the Gauss constrain.

$$e^{-S(u\hat{\Omega})} = \frac{1}{Z} \int \text{Tr} \left\{ e^{-\beta H} \prod_{\mathbf{x}} \mathcal{G}_{\mathbf{x}}[u\Omega(\mathbf{x})] \right\}_{\Omega(\mathbf{0})=\hat{\Omega}} \prod_{\mathbf{x} \neq \mathbf{0}} d\Omega(\mathbf{x}) . \quad (5.59)$$

When a center symmetry is present, it is not a symmetry for the quantum system in a proper sense: it is not implemented by a unitary operator on the Hilbert space. It is a symmetry only of the potential $S(\hat{\Omega})$.

This fact implies that an analysis of the center symmetry in the large- N_c via the coherent states formalism cannot be developed in a straightforward way, like for the chiral symmetries (see section 3.1). Indeed, in the coherent

state formalism, the Gauss constrain is completely solved by taking only gauge-invariant observables as degrees of freedom. Thus, no analog of the Polyakov loop exists.

One can use a trick to go round this problem. Indeed, it is possible to rotate the system (in the Euclidean space-time) and interpret the gauge theory on an infinite space and at finite temperature, as the same theory at zero temperature and on a space $S_1 \times \mathbf{R}^2$ with antiperiodic boundary conditions for the fermions. After the rotation, the Polyakov loop becomes the parallel transport around the spatial compact dimension, and the center acts now on the physical degrees of freedom of the theory. If Σ is a plane orthogonal to the compact dimension, and $\mathcal{L}_\pm^\pm(\Sigma)$ is the set of all the positive links departing from sites of Σ and orthogonal to it, the center acts as:

$$U_\ell \rightarrow u U_\ell \quad \text{if } \ell \in \mathcal{L}_\pm^+(\Sigma) . \quad (5.60)$$

Consider a Wilson loop $W(\Gamma)$ in the space lattice. The center symmetry counts the winding number $w(\Gamma)$ of the Wilson loop:

$$W(\Gamma) \rightarrow u^{w(\Gamma)} W(\Gamma) . \quad (5.61)$$

It is clear that, unless $u \in \mathbf{Z}_2$, the center mixes the real and imaginary parts of the Wilson loops, therefore it does not commute with the charge conjugation symmetry.

Let us come back to the orientifold planar equivalence. The $SO(N_c)$ parent theory has a \mathbf{Z}_2 symmetry in the large- N_c limit. This symmetry is mapped through the orientifold projection in the \mathbf{Z}_2 symmetry of the OrientiQCD in the large- N_c limit. Instead, the AdjQCD has a $U(1)$ symmetry in the large- N_c limit, but only the \mathbf{Z}_2 subgroup maps the neutral sector into itself. At this point, the matching of the symmetries is complete.

5.5 Appendix: The planar limit in pure gauge on the lattice

In this work I am interested in computing connected expectation values of products of closed loops in pure Yang-Mills theories. The Boltzmann weight e^{-S} in the path integral can be expanded in a series in $1/\lambda$. The expansion of the Wilson gauge action produces a series of monomials of elementary plaquettes. The expectation values are computed by integrating each link variable over the group manifold, and non-vanishing results are obtained only when the plaquettes

from the expansion of the action produce a tiling of a surface whose boundary is given by the closed loops. Each plaquette in this expansion appears with a factor of N_c . The rules for the $SU(N_c)$ group integration are known in detail; I will use here the following integrals:

$$\int dUU_{i_1 j_1} U_{l_1 m_1}^\dagger = \frac{1}{N_c} \delta_{i_1, m_1} \delta_{j_1, l_1} , \quad (5.62a)$$

$$\begin{aligned} \int dUU_{i_1 j_1} U_{i_2 j_2} U_{l_1 m_1}^\dagger U_{l_2 m_2}^\dagger &= \\ &= \frac{1}{N_c^2 - 1} (\delta_{i_1, m_1} \delta_{j_1, l_1} \delta_{i_2, m_2} \delta_{j_2, l_2} + \delta_{i_1, m_2} \delta_{j_1, l_2} \delta_{i_2, m_1} \delta_{j_2, l_1}) \\ &\quad - \frac{1}{N_c(N_c^2 - 1)} (\delta_{i_1, m_1} \delta_{j_2, l_2} \delta_{i_2, m_2} \delta_{j_1, l_1} + \delta_{i_1, m_2} \delta_{j_2, l_1} \delta_{i_2, m_1} \delta_{j_1, l_2}) , \end{aligned} \quad (5.62b)$$

$$\int dUU_{i_1 j_1} \cdots U_{i_{N_c} j_{N_c}} = \frac{1}{N_c!} \epsilon_{i_1 \dots i_{N_c}} \epsilon_{j_1 \dots j_{N_c}} . \quad (5.62c)$$

Each trace over color indices (i, j, l, m) contributes a factor of N_c . Collecting all contributions one obtains that each diagram is proportional to N_c^χ , where χ is the Euler characteristics of the surface spanned by the tiling, see e.g. Ref. [43].

For the diagram considered in this work:

$$\chi = 2 - 2H - 2B , \quad (5.63)$$

where H is the number of handles, and B the number of boundaries of the surface. The number of boundaries is given by the number of closed loops. One can readily see that the planar limit is obtained by considering surfaces with $H = 0$.

Let us now describe in detail the computations that appear in the derivation of the results in section 5.3.

Consider the connected expectation values:

$$\left\langle \prod_{i=1}^n \text{tr} U(\omega_i) \right\rangle_{c, \text{YM}} . \quad (5.64)$$

I will prove that the leading N_c^{2-n} behaviour is saturated if loops with winding number different from zero exist in pairs of opposite winding numbers.

The easiest case is

$$\langle \text{tr} U(\omega_1) \text{tr} U(\omega_2) \rangle_{\text{YM}, c}$$

with $w_1 = -w_2$. In this case the surface connecting the two loops is a cylinder, wrapping $|w_1|$ times around the thermal dimension (see figure 5.1). Notice that it is essential that the loops have opposite directions, since the cylinder cannot be twisted because of the topology of the torus. Since the surface is planar, this diagram saturates the leading behaviour of the connected expectation value:

$$\langle \text{tr} U(\omega_1) \text{tr} U(\omega_2) \rangle_{YM,c} = O(N_c^0) \quad \text{with } w_1 = -w_2 . \quad (5.65)$$

Consider now the more complex case of

$$\langle \text{tr} U(\omega_1) \text{tr} U(\omega_2) \text{tr} U(\omega_3) \text{tr} U(\omega_4) \rangle_{YM,c}$$

with $w_1 = -w_2$ and $w_3 = -w_4$. The planar surface is built by connecting each pair of loops with a cylinder with an hole, and then gluing the two cylinders through the boundary of the holes (see figure 5.1). The Euler characteristic of this surface is $\chi = -2$ therefore the corresponding diagram behaves like N_c^{-2} .

The above procedure can be iteratively generalized to the case of an arbitrary number of pairs of loops. Moreover an arbitrary number of loops with zero winding number can be included simply adding holes to the surface. The resulting surface is always planar.

Consider again the generic connected expectation value in equation (5.64). If some loop ω_i with winding number w_i different from zero is not paired to a loop with winding number $-w_i$ then the leading behaviour cannot be saturated. Since this fact is not crucial for the present work, I will illustrate it in some simple cases.

For $n = 3$ and $w_1 = w_2 = 1$, $w_3 = -2$, the connected expectation value

$$\langle \text{tr} U(\omega_1) \text{tr} U(\omega_2) \text{tr} U(\omega_3) \rangle_{YM,c}$$

still have zero net winding number. Anyway it is not possible to build a surface connecting this three loops because of the topology of the torus. One can ask if it is possible to use the four-link measure to get a leading contribution. I want to convince the reader that this is not the case. I will proceed by small steps. First of all, one can deform each loop by taking a contiguous plaquette from the expansion of the Boltzmann weight and integrating the common link, as depicted in figure 5.6. If $\text{tr}(AU)$ is schematically the loop and $N_c \lambda^{-1} \text{tr}(U^\dagger B)$ is the relevant term of the action:

$$N_c \lambda^{-1} \int dU \text{tr}(AU) \text{tr}(U^\dagger B) = \lambda^{-1} \text{tr}(AB) . \quad (5.66)$$

In this way, the loop is replaced by the deformed one times a factor $1/\lambda$. One can use iteratively this procedure for each loop until the glued plaquettes shape three cylinders that end in three loops in the same spatial point (figure 5.7). Now let us start to integrate one of the links of these three loops, by using the four-link formula in (5.62b). If we want to integrate the link U , we can write the three loops schematically as $\text{tr}(AU)$, $\text{tr}(AU)$, $\text{tr}(U^\dagger A^\dagger U^\dagger A^\dagger)$ (remember that they all are coincident). The result of the integration is:

$$\begin{aligned} \int dU \text{tr}(AU) \text{tr}(AU) \text{tr}(U^\dagger A^\dagger U^\dagger A^\dagger) &= \\ &= \frac{2}{N_c^2 - 1} \text{tr}(AA^\dagger AA^\dagger) - \frac{2}{N_c(N_c^2 - 1)} [\text{tr}(AA^\dagger)]^2 = \\ &= \frac{2N_c}{N_c^2 - 1} - \frac{2N_c^2}{N_c(N_c^2 - 1)} = 0. \end{aligned} \quad (5.67)$$

In the last line I used the fact that A is the product of all the links but U and therefore it is a unitary matrix. We can conclude that this kind of diagrams does not contribute to the connected expectation value.

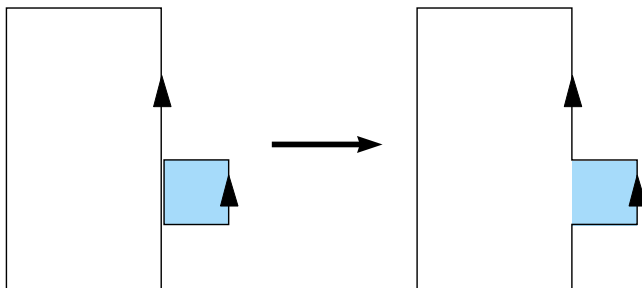


Figure 5.6: The equation (5.66) is represented. In the left side, the big loop $\text{tr}(AU)$ and the plaquette $\text{tr}(U^\dagger B)$; in the right side, the deformed loop $\text{tr}(AB)$.

The last non-trivial case I want to illustrate is $n = 1$ and $w_1 = N_c$. In this case the connected expectation value $\langle \text{tr} U(\omega_1) \rangle_{YM,c}$ is invariant under the center \mathbf{Z}_{N_c} , but not $U(1)$. Therefore a non-zero contribution can be constructed only using the N_c -link integration formula for $SU(N_c)$ in equation (5.62c). By using the same construction as above, the loop $\text{tr} U(\omega_1)$ can be deformed (without introducing extra N_c factors) into a loop wrapping straight in the thermal direction (see figure 5.2), that can be written schematically as $\text{tr}[(AU)^{N_c}]$. In-

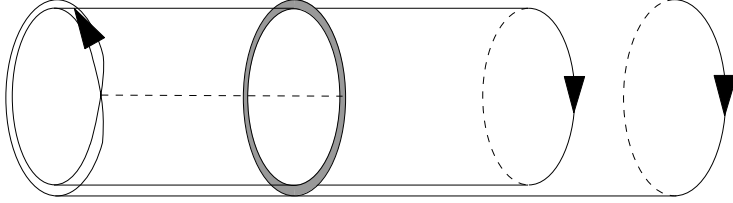


Figure 5.7: The connected expectation value $\langle \text{tr} U(\omega_1) \text{tr} U(\omega_2) \text{tr} U(\omega_3) \rangle_{YM,c}$ with $w_1 = w_2 = 1$, $w_3 = -2$. The four-link integration in the gray area makes vanish this contribution, as explained in equation (5.67).

tegrating the link U :

$$\begin{aligned} \int dU \text{tr}[(UA)^{N_c}] &= \frac{1}{N_c!} \epsilon_{i_1 \dots i_{N_c}} A_{i_1 j_1} \cdots A_{j_1 j_{N_c}} \epsilon_{j_1 \dots j_{N_c}} = \\ &= \det A = 1 . \end{aligned} \tag{5.68}$$

This is a subleading contribution since the leading term of the expectation value of a single loop is expected to be proportional to N_c .

Chapter 6

Breaking of the charge conjugation symmetry

The role of the charge conjugation symmetry in the proof of the orientifold planar equivalence was widely discussed in chapter 3. Briefly, the equivalence was proved first in [23]; in this proof it was implicitly used that the \mathcal{C} -symmetry is not spontaneously broken. An alternative proof may be found in [26]; it has the merit of clarifying that the invariance of the vacuum under charge conjugation is both a necessary and sufficient condition for the validity of the orientifold planar equivalence.

While the invariance under spatial parity has been rigorously proved [44] for vectorial gauge theories on the \mathbf{R}^4 space-time (Lorentz invariance is essential), no analogous result exists for the charge conjugation.

It is well known [45] that, in a space with some sufficiently small compact dimension (with non-trivial cycles) and with periodic boundary conditions for the fermions, the charge conjugation, spatial parity, time reversal and \mathcal{CPT} symmetries are spontaneously broken in QCD. This result can be extended to the $SU(N_c)$ gauge theory with fermions in the antisymmetric representation (OrientiQCD). Therefore, when some small compact spatial dimensions and periodic boundary conditions for the fermions are considered, the orientifold planar equivalence does not hold [26, 46, 40].

The dependence of the symmetry breaking on the boundary conditions, the breaking of \mathcal{P} , the breaking of \mathcal{CPT} give convincing evidence that all the discrete symmetries are restored at large enough size of the compact dimensions.

In our work [47], we¹ have investigated the physical consequences of the breaking of the discrete symmetries, that is what local observables can be used to detect it. Since \mathcal{CP} (as well as \mathcal{PT} and \mathcal{CT}) remains unbroken, we can easily say which observables cannot be used: the masses of particles and antiparticles are still degenerate, the baryon number is still conserved. We will show that the breaking induces the generation of baryon currents, propagating along the compact dimensions. It is worth noticing that a non-zero expectation value for a current breaks the Lorentz symmetry, and therefore it must be zero in the limit of infinite volume.

This current is similar to the supercurrent observed in superconductors. However, there is a fundamental difference: unlike the case of superconductors, in QCD in a compact not simply connected space the current is still conserved, since the $U(1)$ baryon symmetry (which in the case of QCD is a global symmetry) remains unbroken. The persistent flow is induced by the spontaneous breaking of discrete symmetries. In this case, pairs of quarks and antiquarks condense in the vacuum, while the total baryonic number is zero. The quark and the antiquark move with opposite momenta along the compact dimensions. The total momentum is zero, but there is a net baryonic current.

The breaking of the charge conjugation symmetry and its restoration at large volume have been investigated by means of lattice simulations also in [27, 48].

6.1 Breaking of discrete symmetries

Consider a gauge theory with gauge group $SU(N_c)$ and N_f flavours of fundamental (F) or antisymmetric (AS) Dirac fermions. The manifold on which the theory is defined is $\mathbf{R}^d \times T_n$, where $d + n = 4$ and T_n is a spatial n -dimensional torus. For simplicity, the torus has the same extension R in all the compact dimensions. Moreover, spatial directions are closed with periodic boundary conditions for both fermions and bosons.

In what follows, $(x_a)_{a=1,\dots,d}$ are the coordinates on \mathbf{R}^d , while $(z_\alpha)_{\alpha=1,\dots,n}$ are the coordinates of the compact dimensions.

The relevant quantities are the eigenvalues of the parallel transports around the compact dimensions:

$$\text{diag Pexp} \left(i \int_0^R A_\alpha(x, z) dz_\alpha \right) = \left(e^{iv_{1\alpha}^{(A)}(x,z)}, \dots, e^{iv_{N_c\alpha}^{(A)}(x,z)} \right). \quad (6.1)$$

¹This work is done in collaboration with Biagio Lucini (Swansea) and Claudio Pica (BNL).

The effective potential for those eigenvalues is defined as²:

$$e^{iV_d V(v_1, \dots, v_{N_c})} = \int e^{iS} \prod_k \delta \left(v_k - \frac{1}{V_d R^n} \int v_k^{(A)}(\mathbf{x}) dx dz \right) \mathcal{D}A \mathcal{D}\bar{\psi} \mathcal{D}\psi. \quad (6.2)$$

The absolute minima of $V(v_1, \dots, v_{N_c})$ give the expectation values for the set of the eigenvalues. If the \mathcal{C} -symmetry is broken, the set of eigenvalues is not invariant under the substitution $v \rightarrow -v$. In the one-loop approximation, the effective potentials respectively with fundamental and antisymmetric fermions are given by [49]:

$$V_F(\vec{v}_1, \dots, \vec{v}_{N_c}) = \sum_{i,j=1}^{N_c} f(0, \vec{v}_i - \vec{v}_j) - 2N_f \sum_{i=1}^{N_c} f(m, \vec{v}_i), \quad (6.3a)$$

$$V_{AS}(\vec{v}_1, \dots, \vec{v}_{N_c}) = \sum_{i,j=1}^{N_c} f(0, \vec{v}_i - \vec{v}_j) - 2N_f \sum_{i < j=1}^{N_c} f(m, \vec{v}_i + \vec{v}_j), \quad (6.3b)$$

$$\text{with } f(m, \vec{v}) = \frac{1}{R^d} \left(\frac{mR}{\pi} \right)^2 \sum_{\vec{k} \neq 0} \frac{K_2(mRk)}{k^2} \sin^2 \left(\frac{1}{2} \vec{k} \cdot \vec{v} \right),$$

where K_2 is the modified Bessel function of the second kind of order 2 and the sum runs over n -index integer vectors \vec{k} . For $m \gg L^{-1}$, $K_2(mLk) \approx e^{-mLk} \sqrt{\pi/(2mLk)}$ and the sum in f is dominated by terms with $k = 1$. This is true also in general, the higher frequencies in the sum being quickly oscillating with amplitude suppressed at least as $1/k^4$. The first term of equations (6.3a) and (6.3b) gives rise to an attraction between the eigenvalues. The second term produces an unconstrained absolute minimum at $v_i = \pi$ for the fundamental fermions and $v_i = \pi/2$ for the antisymmetric fermions. When the $SU(N_c)$ constraint is taken into account, the minima respectively for fundamental and antisymmetric fermion are:

$$v_{(F)1}^* = \dots = v_{(F)N_c}^* = \begin{cases} \pm \frac{N_c-1}{N_c} \pi & \text{for } N_c \text{ odd} \\ \pi & \text{for } N_c \text{ even} \end{cases} \quad (6.4a)$$

$$v_{(AS)1}^* = \dots = v_{(AS)N_c}^* = \begin{cases} \pm \frac{N_c+1}{2N_c} \pi & \text{for } N_c \text{ odd} \\ \frac{\pi}{2} & \text{for } N_c = 0 \pmod{4} \\ \pm \frac{N_c \pm 1}{2N_c} & \text{for } N_c = 2 \pmod{4} \end{cases}. \quad (6.4b)$$

²We drop the subscript α where this does not lead to ambiguities.

The spontaneous symmetry breaking shows up as a non-zero imaginary part of the Wilson line. Hence, with fundamental fermions and N_c even, there is no symmetry breaking. Otherwise \mathcal{P} , \mathcal{C} , \mathcal{T} , \mathcal{CPT} are broken. This result is due to the spacial periodic boundary conditions for the fermions. The validity of the calculation in the non-perturbative regime has been checked on the lattice in [50], and the discrete symmetries are shown to be broken for R below the fermi scale.

6.2 Baryon currents

The Wilson line wrapping around a compact dimension is an order parameter for the symmetry breaking. However, if the theory is not invariant under \mathcal{P} , \mathcal{C} , \mathcal{T} , we expect this to be reflected by some local observable. This observable must be odd under the broken symmetries, but even under the combined action of two of them. The spatial components of the baryon current $j_\alpha = \langle \sum_{i=1}^{N_f} \bar{\psi}_i \gamma_\alpha \psi_i \rangle$ satisfy this property.

Why should we expect a non-zero baryon current? A non trivial vacuum expectation value of the Wilson line means a non-zero value of the gauge field in that direction. Since the system is translationally invariant along the compact direction, the value of the gauge field must be constant (note that in the presence of toroidal topology a constant field cannot be gauged away). The background gauge field acts as a non-trivial source for the baryon current. Hence, we expect this current to be different from zero.

Let us focus on fermions in the fundamental representation. In order to compute the expectation value of the baryonic current, we define the partition function of the system in presence of a generalised "chemical potential" μ_α :

$$Z(\mu) = \int \mathcal{D}A \mathcal{D}\bar{\psi} \mathcal{D}\psi \exp \left\{ iS_G + i \sum_{f=1}^{N_f} \int \bar{\psi}_f(x) (i\hat{\mathcal{D}} - \mathcal{A} - \mu_\alpha \gamma_\alpha - m) \psi_f(x) d^4x \right\}. \quad (6.5)$$

Since the insertion of the μ -term has the same effect as shifting $A_\alpha(\mathbf{x}, x_\alpha) \rightarrow A_\alpha(\mathbf{x}, x_\alpha) + \mu_\alpha \mathbf{1}_{N_c}$ (the gauge action is not affected by this shift), or as shifting the phases of the eigenvalues of the Wilson lines $v_{\alpha k}(\mathbf{x}) \rightarrow v_{\alpha k}(\mathbf{x}) + R\mu_\alpha$, the partition function can be obtained as:

$$Z(\mu) = e^{iV_d V(v_1^* + R\mu, \dots, v_{N_c}^* + R\mu)} \quad (6.6)$$

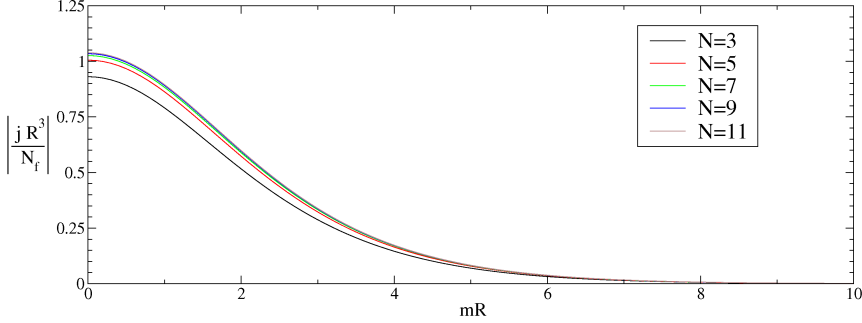


Figure 6.1: The baryon current (one-loop approximation) vs. mR at different values of N_c .

On the other side, as the chemical potential in (6.5) acts like a source for the current, which is obtained by deriving the partition function with respect to μ_α :

$$j_\alpha = \frac{i}{V_d R^n} \frac{d \log Z}{d \mu_\alpha}(0) = -\frac{1}{R^{n-1}} \sum_k \frac{\partial V}{\partial v_k}(v_1^*, \dots, v_{N_c}^*). \quad (6.7)$$

Using the one-loop expression for the effective potentials in (6.3a) and (6.3b), we obtain for the baryon current:

$$\langle j_\alpha \rangle = -\frac{N_f N_c (mR)^2}{R^3 \pi^2} \sum_{\vec{k} \neq 0} \frac{K_2(mkR) k_\alpha \sin(\vec{k} \vec{v}^*)}{k^2}. \quad (6.8)$$

$\langle j_\alpha \rangle$ is zero when $v_\alpha^* = 0$ or $v_\alpha^* = \pi$ (i.e. when the symmetry breaking does not occur in direction α), is odd under $v_\alpha^* \rightarrow -v_\alpha^*$, goes to zero when $m \rightarrow \infty$ (figure 6.1).

For fermions in the antisymmetric representation, the right relationship is:

$$\begin{aligned} \langle j_\alpha \rangle &= -\frac{1}{2R^{n-1}} \sum_k \frac{\partial V}{\partial v_k}(v_1^*, \dots, v_{N_c}^*) = \\ &= -\frac{N_f N_c (mR)^2}{2R^3 \pi^2} \sum_{\vec{k} \neq 0} \frac{K_2(mkR) k_\alpha \sin(2\vec{k} \vec{v}^*)}{k^2}. \end{aligned} \quad (6.9)$$

$\langle j_\alpha \rangle$ is zero when v_α^* is a multiple of $\pi/2$, in particular when N_c is a multiple of 4 even though the \mathcal{C} -symmetry is broken; while it is different from zero in the other cases.

6.3 The lattice calculation

In order to get a better handle on the properties of the baryonic current in the broken phase beyond perturbation theory, we have performed a lattice simulation using four flavours of staggered quarks coupled to an $SU(3)$ gauge field (the two considered representations are equivalent in this case). The number of flavours has been fixed as the minimal one for which the staggered action has an undoubtedly well defined continuum limit. For the pure gauge action we have used the standard Wilson form $S_G = \beta \sum_P (1 - \frac{1}{3} \text{tr} U_P)$, where $\beta = 2N_c/g_0^2$ is the coupling of the theory, U_P is the path-ordered product of link variables around the elementary plaquette P and the sum runs over all plaquettes P . For the fermionic part we have used the simple staggered action

$$S_F = \sum_{x,\mu} \eta_\mu(x) \frac{1}{2} (\bar{\chi}(x) U_\mu(x) \chi(x + \hat{\mu}) - c.c.) + am \sum_x \bar{\chi}(x) \chi(x), \quad (6.10)$$

with $\eta_\mu(x) = (-1)^{\sum_{\nu=0}^{\mu-1} x_\nu}$ ($\eta_0(x) = 1$), χ a complex three-vector, am the mass in lattice units (a is the lattice spacing) and c.c. stands for the complex conjugate term to the first one in parentheses. More complicated formulations of the action or choice of another discretized form for the fermionic fields would have added extra complication with very little payoff for the problem at hand.

Using as a base the publicly available MILC code ³, we have performed a simulation for $\beta = 5.5$ and $am = 0.1$. The physical scale has been determined by measuring the Sommer parameter r_0 [51] on a 24×16^3 lattice, where the three equal spatial directions N_s have been closed with periodic boundary conditions and the temporal direction N_t with antiperiodic boundary conditions for the fermions, while the gauge fields are periodic in all directions. We find $ar_0 = 4.0(1)$; since the Sommer scale is $\simeq 0.5$ fm, the lattice spacing is $a \simeq 0.125$ fm, which means that $L_s = aN_s \simeq 2$ fm and $L_t = aN_t \simeq 3$ fm. Hence, in physical units the lattice is large enough for the calculation to be reliable and the spatial volume is such that C, P and T are not broken.

We then studied the system with the same β and m on a 24×4^3 lattice, with the same boundary conditions as above. The spatial geometry is a three-

³See <http://www.physics.utah.edu/~detar/milc>.

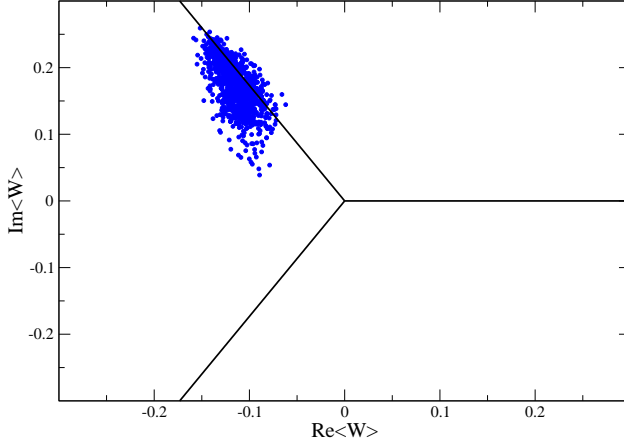


Figure 6.2: Scatter plot for 1000 measurements of the Wilson line in one compact direction on a 24×4^3 lattice at $\beta = 5.5$ and $am = 0.1$. The directions corresponding to the three cubic roots of the unity are indicated by the black solid lines.

torus, while the size of the temporal direction is large enough for the system to be confined. In this setup, $L_s \simeq 0.5$ fm. A quick check of the v_{ev} of the spatial Wilson loops shows that the system is in the broken symmetry phase. An example of the obtained distribution for $\langle W \rangle$ is displayed in figure 6.2, which shows $\langle W \rangle$ clustering around $e^{i\frac{2}{3}\pi}$.

The discretized version of the baryonic current can be obtained like in the continuous case, by relating the physical fermionic degrees of freedom to the staggered ones. Defining the massless Dirac operator as

$$D^{x,y} = \sum_{\mu} \eta_{\mu}(x) (U_{\mu}(x)\delta_{y,x+\hat{\mu}} - U_{\mu}^{\dagger}(x-\hat{\mu})\delta_{y,x-\hat{\mu}}) \quad (6.11)$$

and the four matrices

$$K_{\mu}^{x,y} = \eta_{\mu}(x) (U_{\mu}(x)\delta_{y,x+\hat{\mu}} + U_{\mu}^{\dagger}(x-\hat{\mu})\delta_{y,x-\hat{\mu}}) \quad (6.12)$$

the current reads

$$\langle \vec{j} \rangle = \frac{1}{TL^3} \text{Tr} \left((D + m)^{-1} \vec{K} \right) . \quad (6.13)$$

In order to evaluate the current on a given configuration, we have taken 100 stochastic estimates. Since the current is an antihermitian operator in the

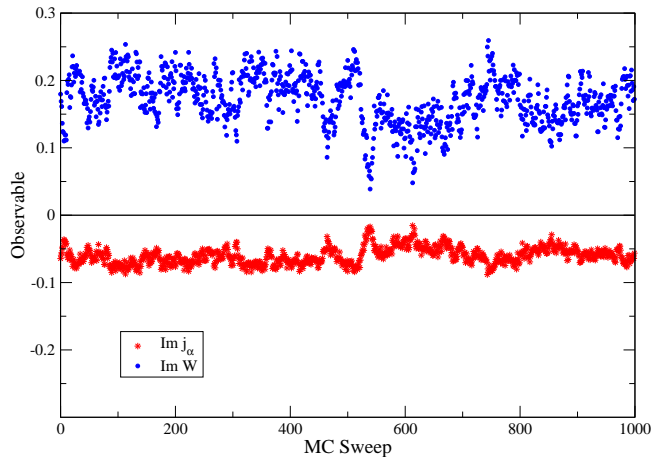


Figure 6.3: The imaginary part of the current and the imaginary part of the Polyakov loop in one compact direction as a function of the Monte Carlo sweeps.

Euclidean space, we expect its imaginary part to develop a *vev*, while the real part should average to zero. In figure 6.3 we show the behaviour of the imaginary part of the baryonic current in a compact direction as a function of the Monte Carlo sweeps, and we contrast such behaviour with that of the imaginary part of the Wilson line in the same direction. Not only does the plot show that the baryonic current is different from zero, but it also strongly suggests that there is a correlation between the value of the current and the value of the Wilson line. In particular, the modulus of the imaginary part of the current grows when the modulus of the imaginary part of the Wilson line grows, the sign being opposite between the two. This is better shown by figure 6.4, which displays the behaviour of the current in another compact direction. In this case, the system makes a transition between the vacuum identified by the phase of the Wilson line being $\frac{2}{3}\pi$ to the other vacuum and then back. Noticeably, the current changes sign exactly at the points in which the imaginary part of the Wilson line changes sign, with its magnitude always tracking closely the magnitude of the phase of $\langle W \rangle$. The sum of the terms with $|\vec{k}| = 1$ in the current (6.8) is proportional to $\langle W \rangle$. The strong correlation between the two quantities suggests that the non-leading terms in (6.8) do not affect significantly the behaviour of j_α .

Transitions between the different vacua like those shown in figure 6.4 are

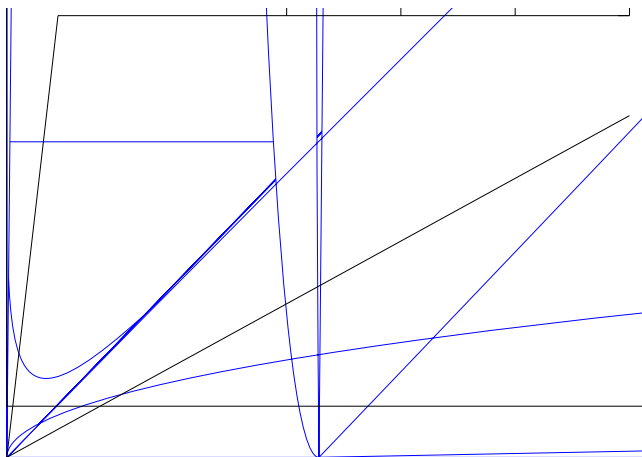


Figure 6.4: As in figure 6.3, but in another compact direction. The system shows a transition between two vacua. The transition probability is finite, due to the finite lattice extension.

possible because of the finite spatial size of the system. We have verified that increasing β at fixed lattice extensions N_s and N_t , which corresponds to decreasing the physical volume, the frequency of the transitions increases. Likewise, decreasing β decreases the likelihood of a transition taking place.

Since the baryonic current is zero for symmetry reasons in the symmetric phase, its behaviour in the broken symmetry phase makes it legitimate to use that current as an order parameter for the symmetry breaking. For consistency, we have also checked that the real part of the current in the compact directions and the zero component are zero also in the broken symmetry phase.

In order to evaluate the magnitude of the current, we averaged over directions for which no tunneling between the two vacua took place. We find

$$|\Im \langle j_\alpha \rangle| = 0.060 \pm 0.002 . \quad (6.14)$$

It is instructive to compare this number with the one loop expression (equation (6.8)), which gives $\langle j_\alpha \rangle \simeq 0.037473(4)$, where the error is a conservative estimate for the truncation of the sum. Hence, quite remarkably the one loop calculation pins down the correct order of magnitude even for a compact dimension with size of the order of $1/\Lambda_{QCD}$. Non-perturbative effects could explain the discrepancy between the perturbative formula and the measured value. Be-

sides, our calculation being at one single lattice spacing, we do not have any handle on the size of discretization errors. For this reason, a careful comparison between the perturbative expression and the lattice result should be the subject of a more detailed study, which is beyond the scope of this paper. Our preliminary Monte Carlo results for the current closer to the continuum limit show substantial agreement between the measured value and the perturbative formula.

Chapter 7

Some results in the quenched theory

In this chapter, I will present some results that my collaborators and I have obtained by using the HiRep code that we have developed (for details, see chapter 8).

The first result¹ I want to discuss (section 7.2) is the computation of the condensate of fermions in the adjoint and antisymmetric representations, in the quenched theory and in the large- N_c limit [52]. It is worth to stress that the large- N_c limit of the gauge theory with dynamical fermions in a two-index representation is not quenched, because the fermionic action is of order $O(N_c^2)$, just like the gluonic one. Thus, I am considering now a simpler (trivial, for some aspects) case than the hypothesis of the orientifold planar equivalence. As we will see in section 7.2, the orientifold planar equivalence is expected to hold also in the quenched case for the mesonic observables. Therefore, the aim of the computation of the fermionic condensate in the quenched theory is three-fold:

- to test the HiRep code, by comparing our results with the existing ones for $N_c = 2, 3$;
- to check the orientifold planar equivalence in a simpler case;
- to understand how large the $1/N_c$ corrections are.

¹This work is done in collaboration with Adi Armoni (Swansea), Biagio Lucini (Swansea) and Claudio Pica (BNL).

The condensate is computed at fixed lattice spacing ($a \simeq 0.145$ fm). The main results can be summarized in the chiral limit by the formulae:

$$\frac{1}{N_c^2} \langle \bar{\psi}\psi \rangle_{\text{S,qu.}} (m=0) = 0.2269(26) + \frac{0.449(17)}{N_c} - \frac{0.550(55)}{N_c^2} + \dots, \quad (7.1a)$$

$$\frac{1}{N_c^2} \langle \bar{\psi}\psi \rangle_{\text{AS,qu.}} (m=0) = 0.2269(26) - \frac{0.449(17)}{N_c} - \frac{0.550(55)}{N_c^2} + \dots, \quad (7.1b)$$

$$\frac{1}{N_c^2} \langle \lambda\lambda \rangle_{\text{Adj,qu.}} (m=0) = 0.2290(20) - \frac{0.301(39)}{N_c^2} + \dots. \quad (7.1c)$$

The first two corrections are found to describe very well the data up to $N_c = 3$. The orientifold planar equivalence is proved to work in this simple case within the statistical errors of the computation:

$$\lim_{N_c \rightarrow \infty} \frac{\langle \bar{\psi}\psi \rangle_{\text{AS}} - \langle \lambda\lambda \rangle_{\text{Adj}}}{\sqrt{\sigma_{\text{AS}} + \sigma_{\text{Adj}}}} = 0.64. \quad (7.2)$$

The second result² I want to discuss (section 7.3) is the computation of the mesonic spectrum in the large- N_c limit, in the quenched theory with quarks in the fundamental representation [53]. Of course, this computation is not related to the orientifold planar equivalence. However, the computation of the mesonic spectra in the full theories with fermions in the two-index representations in the large- N_c limit is one of the main goal in the long-term project of checking the orientifold planar equivalence. Since no results about mesons in the large- N_c limit existed until the Lattice 2007 conference³, it was natural to begin from the simplest case.

In our work, we computed the masses of the pion and the rho, and the PCAC quark mass at $N_c = 2, 3, 4, 6$ as functions of the hopping parameter of the Wilson fermions. The chiral and large- N_c extrapolations are performed. We find that the $1/N_c^2$ corrections are always manageable and small. The two central results are summarized by the parametrisation:

$$am_\pi(N_c) = \left(1.262(8) - \frac{0.82(6)}{N_c^2} \right) \left(\frac{1}{\kappa} - 5.945(4) + \frac{0.0398(6)}{N_c^2} \right)^{1/2}, \quad (7.3)$$

²This work is done in collaboration with Luigi Del Debbio (Edinburgh), Biagio Lucini (Swansea), Claudio Pica (BNL).

³In an earlier work, Narayanan and Neuberger [54] computed the pion mass on small lattices by using the hypothesis of the volume-independence in the large- N_c limit.

and

$$am_\rho(N_c) = \left(0.539(3) - \frac{0.62(3)}{N_c^2}\right) + \left(0.5224(8) + \frac{1.10(1)}{N_c^2}\right) a^2 m_\pi^2(N_c). \quad (7.4)$$

An analogous computation was simultaneously and independently performed by Bali and Bursa [55]. The agreement of the results (see section 7.3.4 for a discussion) is a remarkable cross-check of the HiRep code.

7.1 Setting the scale in the quenched theory

Several strategies can be used to tune the physical scale as N_c grows. It was already pointed out that, in order to have a well-defined large- N_c limit, the 't Hooft bare coupling $\lambda = g^2 N_c$ should be kept constant. Thus, one can think to fix the coupling g at $N_c = 3$ by fixing for instance the string tension, and then to change N_c while the 't Hooft coupling λ is constant.

This is not the best method when one wants to perform numerical simulations indeed. The value of the string tension (in units of the lattice size) at $N_c = 3$ should be chosen not too small in order to avoid finite-volume effects and not too large in order to avoid discretization effects. Typically, one has a reasonable window for the string tension. As N_c grows, the string tension changes and approaches some finite limit, that is not known a priori. In particular, it might exit from the window in which both the finite-volume and discretization errors are under control.

A possible way out is to force the value of the string tension in units of the lattice spacing to be the same as N_c grows. In this case, the 't Hooft coupling is not constant and approaches a finite limit at large- N_c . Any other physical observable with a finite large- N_c could be used to fix the scale. When all the other observables are expressed in physical units, the large- N_c limit is independent of the criterion used to fix the scale. This is not true for the subleading corrections.

For the simulations described in the following sections, the values of $\beta = 2N_c/g^2$ have been chosen in such a way that the deconfinement phase transition occurs at the critical temperature $T_c = (5a)^{-1}$. Using the value $T_c = 270$ MeV, for the lattice spacing a we get $a \simeq 0.145$ fm. The values of β were measured in [18] for $N_c = 2, 3, 4, 6, 8$, and are summarized in the following table:

| N_c | β |
|-------|---------|
| 2 | 2.3715 |
| 3 | 5.8000 |
| 4 | 10.6370 |
| 6 | 24.5140 |
| 8 | 44.0000 |

7.2 The fermionic condensate at large- N_c

7.2.1 Analytical equivalence

In the quenched theory the condensate of Dirac fermions is equal to the condensate of Majorana fermions in the adjoint representation, in the large- N_c limit. More precisely:

$$\begin{aligned} \lim_{N_c \rightarrow \infty} \frac{1}{N_c^2} \langle \bar{\psi} \psi \rangle_{\text{As, quenched}} &= \lim_{N_c \rightarrow \infty} \frac{1}{N_c^2} \langle \lambda \lambda \rangle_{\text{Adj, quenched}} = \\ &= \lim_{N_c \rightarrow \infty} \frac{1}{2N_c^2} \langle \bar{\psi} \psi \rangle_{\text{Adj, quenched}} , \end{aligned} \quad (7.5)$$

where ψ is a Dirac spinor, while λ is a Majorana spinor.

Here, I want to prove a more general proposition. The eigenvalues distribution (normalized to 1) of the Dirac operator for fermions in the generic representation R is defined as:

$$\rho(\lambda) = \frac{1}{N_{\text{ev}}} \sum_{\alpha=1}^{N_{\text{ev}}} \langle \delta(\lambda - \lambda_{\alpha}[U]) \rangle_{YM} , \quad (7.6)$$

where $\lambda_{\alpha}[U]$ are the eigenvalues of the Dirac operator at fixed gauge background, and N_{ev} is the number of eigenvalues. Since in the adjoint representation a Dirac fermion can be always split into two identical non-interacting Majorana fermions, the eigenvalues distribution (normalized to 1) of the Majorana operator is exactly the same as the Dirac operator. In what follows, all the eigenvalues distributions are to be intended as normalized to 1.

I will show now that in the quenched theory the eigenvalues distribution of the Dirac operator for the antisymmetric representation is equal to the eigenvalues distribution of the Dirac operator for the adjoint representation, in the large- N_c .

In practice, I will consider the staggered discretization of the Dirac operator in the generic representation R :

$$\begin{aligned} D_{xy} &= m\delta_{xy} + K_{xy} = \\ &= m\delta_{xy} - \frac{1}{2} \sum_{\mu} \eta_{\mu}(x) \{ R[U_{\mu}(x)]\delta_{x,y+\hat{\mu}} - R[U_{\mu}(x-\hat{\mu})]^{\dagger}\delta_{x,y-\hat{\mu}} \} . \end{aligned} \quad (7.7)$$

The eigenvalues of the staggered Dirac operator are of the form $m + i\lambda_{\alpha}$, where λ_{α} is real, and they are present in pairs of complex conjugates. The operator $H = D^{\dagger}D = m^2 - K^2$ has doubly-degenerate eigenvalues of the form $m^2 + \lambda_{\alpha}^2$; in particular, it is positive definite. Clearly, assigning the spectrum of D is completely equivalent to assign the spectrum of H , once that the mass is fixed. Since it is more convenient to deal with real positive eigenvalues, in what follows I will refer to the eigenvalues of H , rather than D .

In this case, the eigenvalues distribution is defined as:

$$\rho(\tau) = \frac{1}{d_R V} \sum_{\alpha} \langle \delta(\tau - m^2 - \lambda_{\alpha}^2[U]) \rangle_{YM} , \quad (7.8)$$

where d_R is the dimension of the representation. It is also useful to consider the Laplace transform of the probability distribution:

$$\hat{\rho}(z) = \int \rho(\lambda) e^{z\lambda} d\lambda = \frac{1}{d_R V} \sum_{\alpha} \langle e^{z(m^2 + \lambda_{\alpha}^2[U])} \rangle_{YM} = \frac{1}{d_R V} \langle \text{Tr} e^{zH} \rangle_{YM} . \quad (7.9)$$

This function can be expanded in loops, by expanding the exponential:

$$\begin{aligned} \hat{\rho}(z) &= \frac{e^{zm^2}}{d_R V} \langle \text{Tr} e^{-zK^2} \rangle_{YM} = \\ &= \frac{e^{zm^2}}{d_R V} \sum_{n=0}^{\infty} \frac{(-z)^n}{n!} \langle \text{Tr} K^{2n} \rangle_{YM} = \\ &= \frac{e^{zm^2}}{d_R V} \sum_{n=0}^{\infty} \frac{(-z)^n}{n!} \sum_{\omega \in \mathcal{C}_{2n}} c(\omega) \langle \text{tr} R[U(\omega)] \rangle_{YM} \end{aligned} \quad (7.10)$$

Since the spectrum of K is bounded, the series converges and its radius of convergence is infinite. Thus, $\hat{\rho}(z)$ is an analytical function on the whole complex plane.

Consider now fermions in the adjoint representation. Since the upper bound of the K operator is uniform in the number of colours (for Wilson fermions, I

showed that in section 4.1; for staggered fermions, it works in an similar way), the large- N_c limit commutes with the infinite sum:

$$\lim_{N_c \rightarrow \infty} \hat{\rho}_{\text{As}}(z) = \frac{e^{zm^2}}{V} \sum_{n=0}^{\infty} \frac{(-z)^n}{n!} \sum_{\omega \in \mathcal{C}_{2n}} c(\omega) \lim_{N_c \rightarrow \infty} \frac{\langle [\text{tr} U(\omega)]^2 \rangle_{YM}}{N_c(N_c - 1)}. \quad (7.11)$$

This function is still analytical on the whole complex plane. Since in the large- N_c limit, using the charge conjugation invariance of the pure Yang-Mills:

$$\lim_{N_c \rightarrow \infty} \frac{\langle [\text{tr} U(\omega)]^2 \rangle_{YM}}{N_c(N_c - 1)} = \lim_{N_c \rightarrow \infty} \frac{\langle |\text{tr} U(\omega)|^2 \rangle_{YM}}{N_c^2 - 1}, \quad (7.12)$$

one can obtain:

$$\begin{aligned} \lim_{N_c \rightarrow \infty} \hat{\rho}_{\text{As}}(z) &= \frac{e^{zm^2}}{V} \sum_{n=0}^{\infty} \frac{(-z)^n}{n!} \sum_{\omega \in \mathcal{C}_{2n}} c(\omega) \lim_{N_c \rightarrow \infty} \frac{\langle |\text{tr} U(\omega)|^2 \rangle_{YM}}{N_c^2 - 1} = \\ &= \lim_{N_c \rightarrow \infty} \hat{\rho}_{\text{Adj}}(z). \end{aligned} \quad (7.13)$$

The equality of the Laplace transform immediately implies the equality of the eigenvalues distributions. The relationship between the condensates can be obtained by integrating the eigenvalues distribution:

$$\begin{aligned} \langle \bar{\psi}\psi \rangle_{\text{quenched}} &= \frac{1}{V} \langle \text{Tr} D^{-1} \rangle_{YM} = \frac{m}{V} \langle \text{Tr} H^{-1} \rangle_{YM} = \\ &= \frac{m}{V} \int_0^{\infty} \text{Tr} e^{-tH} dt = md_R \int_0^{\infty} \hat{\rho}(-t) dt. \end{aligned} \quad (7.14)$$

The second equality comes observing that $D^{-1} = (m-K)/(m^2-K^2) = mH^{-1} - KH^{-1}$ and the trace of the second term vanishes, since the eigenvalues of K are present in couples of opposites. By taking the large- N_c limit:

$$\begin{aligned} \lim_{N_c \rightarrow \infty} \frac{2}{N_c^2} \langle \bar{\psi}\psi \rangle_{\text{As, quenched}} &= m \int_0^{\infty} \lim_{N_c \rightarrow \infty} \hat{\rho}_{\text{As}}(-t) dt = \\ &= m \int_0^{\infty} \lim_{N_c \rightarrow \infty} \hat{\rho}_{\text{Adj}}(-t) dt = \lim_{N_c \rightarrow \infty} \frac{1}{N_c^2} \langle \bar{\psi}\psi \rangle_{\text{Adj, quenched}}. \end{aligned} \quad (7.15)$$

The large- N_c limit and the integral can be exchanged because the Laplace transform is controlled by the lowest eigenvalue in the range $t \in [0, \infty)$, i.e. $|\hat{\rho}(-t)| \leq e^{-tm^2}$.

7.2.2 Separating the $1/N_c$ corrections

The fermionic condensate in the (anti)symmetric representation contains corrections of order $1/N_c$ to the planar limit. In the quenched approximations, some analytical relationships allow to separate the even corrections from the odd ones.

The fermionic condensate in the quenched approximation is analytical for each positive mass⁴, and it is uniquely identified by its series expansion (although the series could have a finite range of convergence):

$$\langle \bar{\psi}\psi \rangle_{\text{quenched}} = \frac{m}{V} \sum_{n=0}^{\infty} \frac{1}{m^{2(n+1)}} \sum_{\omega \in \mathcal{C}_{2n}} c(\omega) \langle \text{tr } R[U(\omega)] \rangle_{YM} . \quad (7.18)$$

Consider now the antisymmetric and symmetric representations. By using the formulae:

$$\text{tr AS}[U] = \frac{1}{2} [(\text{tr } U)^2 - \text{tr}(U^2)] , \quad (7.19a)$$

$$\text{tr S}[U] = \frac{1}{2} [(\text{tr } U)^2 + \text{tr}(U^2)] , \quad (7.19b)$$

⁴The Laplace transform of the eigenvalues distribution is clearly analytical as a function of the mass. I will explicitly write the dependence on the mass:

$$\hat{\rho}(-t, m) = \frac{e^{-tm^2}}{d_R V} \left\langle \text{Tr } e^{tK^2} \right\rangle_{YM} . \quad (7.16)$$

In order to investigate the analyticity close to the positive real axis, it is useful to consider complex values of the mass of the form $m = |m|e^{i\epsilon}$ with $0 < m_{\min} < |m| < m_{\max}$ and $\epsilon < \epsilon_{\max} < 1$. The absolute value of $\hat{\rho}(-t, m)$ and its complex derivative can be bounded from above, uniformly in the mass, with a function that is integrable in $t \in (0, \infty)$:

$$|\hat{\rho}(-t, m)| < e^{-tm_{\min}^2 \cos(2\epsilon_{\max})} , \quad (7.17a)$$

$$\left| \frac{d\hat{\rho}}{dm}(-t, m) \right| = \left| -2tm \frac{e^{-tm^2}}{d_R V} \left\langle \text{Tr } e^{tK^2} \right\rangle_{YM} \right| < 2tm_{\max} e^{-tm_{\min}^2 \cos(2\epsilon_{\max})} . \quad (7.17b)$$

For the dominated convergence theorems for the Lebesgue integrals, this is enough to conclude that the integral $\int_0^{\infty} \hat{\rho}(-t, m) dt$ has a complex derivative with respect to m . Thus, it is analytical.

the condensates are written as:

$$\begin{aligned} \langle \bar{\psi}\psi \rangle_{S/AS, \text{qu.}} = & N_c^2 \left\{ \frac{m}{V} \sum_{n=0}^{\infty} \frac{1}{m^{2(n+1)}} \sum_{\omega \in \mathcal{C}_{2n}} c(\omega) \frac{\langle [\text{tr} U(\omega)]^2 \rangle_{YM}}{2N_c^2} \right\} \pm \\ & \pm N_c \left\{ \frac{m}{V} \sum_{n=0}^{\infty} \frac{1}{m^{2(n+1)}} \sum_{\omega \in \mathcal{C}_{2n}} c(\omega) \frac{\langle \text{tr}[U(\omega)^2] \rangle_{YM}}{2N_c} \right\}. \end{aligned} \quad (7.20)$$

Both the expressions in the curly brackets are finite in the large- N_c limit. Moreover, since they are expectation values of gluonic operators, they contain only powers of $1/N_c^2$. I will write schematically:

$$\frac{1}{N_c^2} \langle \bar{\psi}\psi \rangle_{S, \text{qu.}} = f\left(\frac{1}{N_c^2}, m\right) + \frac{1}{N_c} g\left(\frac{1}{N_c^2}, m\right), \quad (7.21a)$$

$$\frac{1}{N_c^2} \langle \bar{\psi}\psi \rangle_{AS, \text{qu.}} = f\left(\frac{1}{N_c^2}, m\right) - \frac{1}{N_c} g\left(\frac{1}{N_c^2}, m\right). \quad (7.21b)$$

The functions f and g describe respectively the even and odd corrections to the planar limit of the fermionic condensate in the (anti)symmetric representation. They can be computed by inverting the equations above.

The condensate in the adjoint representation gets only even contributions in $1/N_c$. By using the formula:

$$\text{tr Adj}[U] = |\text{tr} U|^2 - 1, \quad (7.22)$$

the condensate is written as:

$$\begin{aligned} \langle \bar{\psi}\psi \rangle_{\text{Adj, qu.}} = & N_c^2 \left\{ \frac{m}{V} \sum_{n=0}^{\infty} \frac{1}{m^{2(n+1)}} \sum_{\omega \in \mathcal{C}_{2n}} c(\omega) \frac{\langle |\text{tr} U(\omega)|^2 \rangle_{YM}}{N_c^2} \right\} - \\ & - \left\{ \frac{m}{V} \sum_{n=0}^{\infty} \frac{1}{m^{2(n+1)}} \sum_{\omega \in \mathcal{C}_{2n}} c(\omega) \right\}. \end{aligned} \quad (7.23)$$

I will write schematically:

$$\frac{1}{2N_c^2} \langle \bar{\psi}\psi \rangle_{\text{Adj, quenched}} = \tilde{f}\left(\frac{1}{N_c^2}, m\right) - \frac{1}{2N_c^2} \langle \bar{\psi}\psi \rangle_{\text{free}}, \quad (7.24)$$

where $\langle \bar{\psi}\psi \rangle_{\text{free}}$ is the condensate of free fermions. The functions f and \tilde{f} are unrelated at generic N_c . However, at large- N_c the orientifold planar equivalence holds; while at $N_c = 2$ the symmetric and the adjoint are the same representation, and the antisymmetric is the trivial representation. Therefore:

$$f(0, m) = \tilde{f}(0, m), \quad f(1/4, m) = \tilde{f}(1/4, m). \quad (7.25)$$

| N_c | β | m |
|-------|---------|----------------------------------------------------------------------------------------------------------------|
| 2 | 2.3715 | .012, .013, .014, .015, .016, .017, .018, .019, .02, .04, .06, .08, .1, .2, .4, .6, .8, 1, 2, 4, 6, 8 |
| 3 | 5.8000 | |
| 4 | 10.6370 | |
| 6 | 24.5140 | |
| 8 | 44.0000 | |

Table 7.1: Bare parameters used the simulations of the fermionic condensate.

7.2.3 Details of the simulations

A Monte Carlo ensemble of gauge fields is generated using the Wilson action. The link variables are updated using a Cabibbo-Marinari algorithm [56], where each $SU(2)$ subgroup of $SU(N_c)$ is updated in turn. Microcanonical and heat-bath steps have been alternated in a ratio 4:1. I will call *sweep* the sequence of four microcanonical and one heat-bath update.

We chose the staggered discretization of the Dirac operator:

$$\begin{aligned}
 D_{xy} &= m\delta_{xy} + K_{xy} = \\
 &= m\delta_{xy} - \frac{1}{2} \sum_{\mu} \eta_{\mu}(x) \{ R[U_{\mu}(x)]\delta_{x,y+\hat{\mu}} - R[U_{\mu}(x-\hat{\mu})]^{\dagger}\delta_{x,y-\hat{\mu}} \} . \quad (7.26)
 \end{aligned}$$

The complete set of bare parameters used in our simulations is summarized in table 7.1. For this work, we run simulations for $N_c = 2, 3, 4, 6, 8$ and for the symmetric, antisymmetric, adjoint representations. We used a $N_s^3 \times N_t$ lattice with the size $N_s = N_t = 14$ (which corresponds to about 2.0 fm). For the fermion fields we used periodic boundary conditions in the spatial directions and antiperiodic boundary conditions in the temporal direction. For the gauge field we used periodic boundary conditions in all directions.

The fermionic condensate is computed from the formula (7.14), that I rewrite here for convenience:

$$\langle \bar{\psi}\psi \rangle = \frac{m}{V} \langle \text{Tr}(m^2 - K^2)^{-1} \rangle_{YM} , \quad (7.27)$$

where the trace is estimated stochastically with one noisy vector per configuration. In general, this noisy sources are complex. However in the case of the adjoint representation, the staggered Dirac operator is real and the noisy vector can be taken also real. In this way, we are simulating four (since the fermions

are staggered) flavours of Dirac fermions in the (anti)symmetric representation or four flavours of Majorana fermions in the adjoint representation.

The values of the masses have been chosen in an interesting window for the condensate. As the quark mass changes, the condensate goes through three different regimes (see the figure 7.1). Since the lattice volume is finite, no chiral symmetry breaking is expected, therefore in the limit of zero mass the condensate vanishes. This fact is well-known for the staggered fermions [57, 58]. Let us write the condensate in terms of the eigenvalues of the massless staggered Dirac operator K :

$$\langle \bar{\psi}\psi \rangle = \frac{1}{V} \sum_{\alpha} \left\langle \frac{m}{m^2 + \lambda_{\alpha}^2} \right\rangle_{YM} . \quad (7.28)$$

The staggered Dirac operator has an average gap in the eigenvalues. For much lower masses than the gap the condensate is proportional to the mass (*region I*). If the volume increases, the gap shrinks and the condensate becomes different from zero in the chiral limit. The same behaviour is expected as N_c increases, since in the planar limit the condensate is independent of the volume [20, 59]. However at fixed number of colours, as the mass increases the value of the condensate is less sensitive to the lowest eigenvalues, and it becomes approximately independent of the volume (figure 7.2). Practically, a sudden change in the slope of the condensate occurs. The condensate still increases with the mass (*region II*). At some value of the mass, the condensate starts to decrease and the $1/m$ asymptotic behaviour at large mass is recovered (*region III*). The region I is not interesting, since here the condensate is heavily affected by the finite volume effects. Thus, the masses are chosen in order to explore the regions II and III.

The algorithm used for the inversion required in (7.27) is a multishift CG. This enables us to compute all the condensates corresponding to different masses simultaneously. For all the inversions we required a relative precision of 10^{-9} . We found that the average number of applications of the Dirac matrix required is about 2500 for masses greater than 1.2×10^{-2} .

7.2.4 Numerical results

The condensates for the antisymmetric, symmetric, adjoint representation are reported respectively in tables 7.2, 7.3, 7.4. The data for $N_c = 2$ with the antisymmetric representation are obtained by computing exactly (no random noise) the condensate for the free fermion, and the result were conventionally truncated to the third digit.

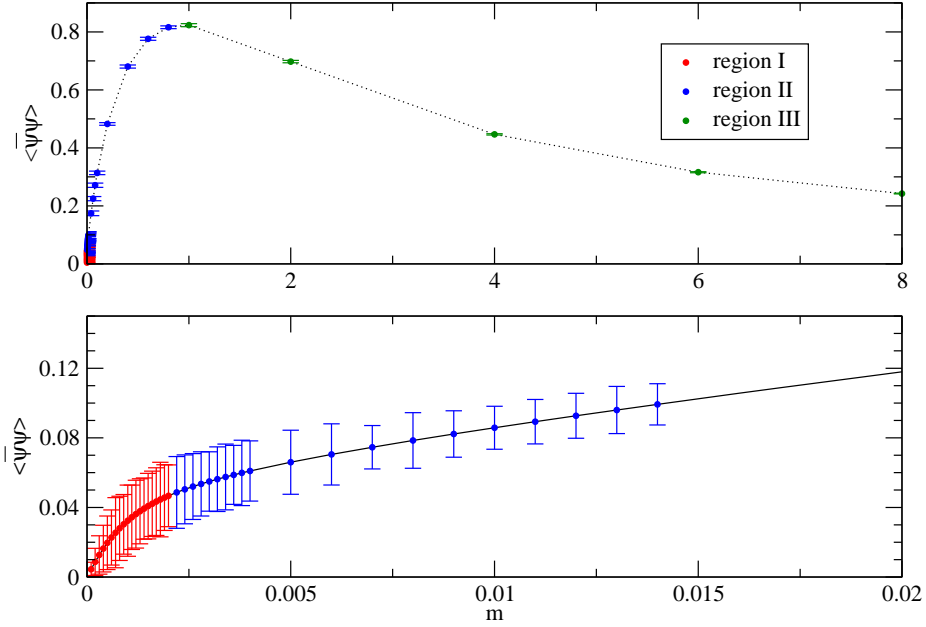


Figure 7.1: The condensate of staggered fermions in the fundamental representation on a 14^4 lattice, at $\beta = 2.3715$, $N_c = 2$ (in two different scales).

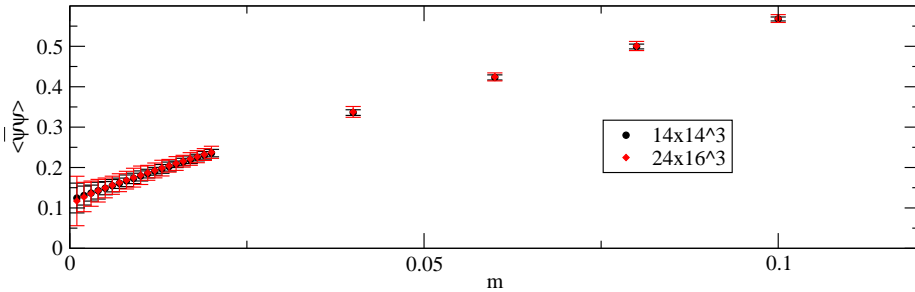


Figure 7.2: The condensate of staggered fermions in the antisymmetric representation at $\beta = 5.8$, $N_c = 3$ for two different lattices. The condensate is independent of the volume (inside the error bars) in these region of masses.

| m | $N_c = 2$ | $N_c = 3$ | $N_c = 4$ | $N_c = 6$ | $N_c = 8$ |
|-------|-----------|------------|------------|------------|------------|
| 0.012 | 0.00746 | 0.193(18) | 1.128(51) | 4.99(10) | 10.62(16) |
| 0.013 | 0.00808 | 0.199(19) | 1.140(47) | 5.00(10) | 10.64(13) |
| 0.014 | 0.00870 | 0.204(16) | 1.153(50) | 5.015(95) | 10.66(14) |
| 0.015 | 0.00932 | 0.210(17) | 1.165(48) | 5.03(11) | 10.68(13) |
| 0.016 | 0.00995 | 0.216(15) | 1.177(49) | 5.04(10) | 10.70(12) |
| 0.017 | 0.0106 | 0.221(16) | 1.188(44) | 5.058(94) | 10.72(13) |
| 0.018 | 0.0112 | 0.227(15) | 1.200(52) | 5.072(83) | 10.74(14) |
| 0.019 | 0.0118 | 0.232(15) | 1.211(45) | 5.087(99) | 10.76(11) |
| 0.02 | 0.0124 | 0.238(15) | 1.222(43) | 5.101(77) | 10.78(11) |
| 0.04 | 0.0248 | 0.338(13) | 1.416(29) | 5.354(58) | 11.132(88) |
| 0.06 | 0.0371 | 0.4244(99) | 1.570(26) | 5.567(52) | 11.432(72) |
| 0.08 | 0.0493 | 0.501(11) | 1.698(21) | 5.750(48) | 11.691(62) |
| 0.1 | 0.0614 | 0.5688(98) | 1.808(21) | 5.909(45) | 11.918(56) |
| 0.2 | 0.119 | 0.8222(86) | 2.187(14) | 6.468(31) | 12.715(44) |
| 0.4 | 0.216 | 1.0948(79) | 2.544(13) | 6.957(21) | 13.368(32) |
| 0.6 | 0.286 | 1.2156(58) | 2.667(10) | 7.050(18) | 13.403(27) |
| 0.8 | 0.331 | 1.2589(57) | 2.6778(95) | 6.946(14) | 13.129(25) |
| 1 | 0.355 | 1.2589(53) | 2.6277(81) | 6.739(14) | 12.688(18) |
| 2 | 0.338 | 1.0502(47) | 2.1218(69) | 5.333(10) | 9.974(15) |
| 4 | 0.223 | 0.6699(25) | 1.3427(32) | 3.3575(48) | 6.2684(98) |
| 6 | 0.158 | 0.4740(16) | 0.9492(29) | 2.3724(39) | 4.4283(72) |
| 8 | 0.121 | 0.3636(14) | 0.7280(22) | 1.8192(31) | 3.3957(51) |

Table 7.2: Results for the condensate of antisymmetric Dirac fermions.

| m | $N_c = 2$ | $N_c = 3$ | $N_c = 4$ | $N_c = 6$ | $N_c = 8$ |
|-------|------------|------------|------------|------------|-----------|
| 0.012 | 1.309(43) | 2.896(77) | 4.93(11) | 10.34(15) | 17.5702 |
| 0.013 | 1.310(46) | 2.898(70) | 4.93(11) | 10.34(13) | 17.5804 |
| 0.014 | 1.311(45) | 2.900(68) | 4.932(92) | 10.35(13) | 17.5902 |
| 0.015 | 1.312(46) | 2.902(74) | 4.933(04) | 10.36(12) | 17.5996 |
| 0.016 | 1.313(40) | 2.903(67) | 4.93(10) | 10.36(11) | 17.6088 |
| 0.017 | 1.314(34) | 2.905(65) | 4.937(89) | 10.37(10) | 17.6177 |
| 0.018 | 1.315(45) | 2.907(67) | 4.938(86) | 10.37(11) | 17.6264 |
| 0.019 | 1.316(37) | 2.908(71) | 4.940(80) | 10.38(10) | 17.6349 |
| 0.02 | 1.317(43) | 2.910(62) | 4.942(91) | 10.38(11) | 17.6433 |
| 0.04 | 1.336(30) | 2.937(50) | 4.975(66) | 10.463(80) | 17.7926 |
| 0.06 | 1.355(25) | 2.960(37) | 5.007(47) | 10.532(60) | 17.9212 |
| 0.08 | 1.372(23) | 2.980(30) | 5.035(40) | 10.593(51) | 18.0325 |
| 0.1 | 1.387(18) | 2.997(26) | 5.060(39) | 10.645(48) | 18.1285 |
| 0.2 | 1.441(15) | 3.053(18) | 5.137(26) | 10.806(35) | 18.4295 |
| 0.4 | 1.4783(94) | 3.065(14) | 5.138(22) | 10.801(29) | 18.4569 |
| 0.6 | 1.4650(85) | 3.002(11) | 5.022(17) | 10.554(23) | 18.0558 |
| 0.8 | 1.4254(81) | 2.901(10) | 4.845(13) | 10.182(20) | 17.4306 |
| 1 | 1.3720(63) | 2.7789(85) | 4.638(12) | 9.746(17) | 16.6922 |
| 2 | 1.0704(47) | 2.1488(67) | 3.5808(86) | 7.523(12) | 12.8961 |
| 4 | 0.6715(27) | 1.3444(40) | 2.2395(55) | 4.7048(67) | 8.06711 |
| 6 | 0.4743(19) | 0.9493(33) | 1.5812(32) | 3.3219(42) | 5.69596 |
| 8 | 0.3636(17) | 0.7278(21) | 1.2123(29) | 2.5469(37) | 4.36723 |

Table 7.3: Results for the condensate of symmetric Dirac fermions.

| m | $N_c = 2$ | $N_c = 3$ | $N_c = 4$ | $N_c = 6$ | $N_c = 8$ |
|-------|------------|------------|------------|------------|-----------|
| 0.012 | 0.657(43) | 1.774(64) | 3.373(75) | 7.99(13) | 14.3679 |
| 0.013 | 0.658(37) | 1.776(47) | 3.375(72) | 8.00(14) | 14.382 |
| 0.014 | 0.658(39) | 1.777(58) | 3.377(74) | 8.00(12) | 14.3959 |
| 0.015 | 0.659(36) | 1.778(53) | 3.380(71) | 8.01(12) | 14.4095 |
| 0.016 | 0.659(33) | 1.779(47) | 3.382(73) | 8.01(13) | 14.4228 |
| 0.017 | 0.660(34) | 1.781(43) | 3.384(70) | 8.02(10) | 14.4359 |
| 0.018 | 0.660(38) | 1.782(42) | 3.387(72) | 8.02(12) | 14.4488 |
| 0.019 | 0.661(34) | 1.783(52) | 3.389(65) | 8.03(14) | 14.4614 |
| 0.02 | 0.661(33) | 1.785(48) | 3.392(63) | 8.04(13) | 14.4737 |
| 0.04 | 0.671(20) | 1.811(35) | 3.440(48) | 8.14(80) | 14.6855 |
| 0.06 | 0.680(19) | 1.835(27) | 3.483(39) | 8.233(71) | 14.856 |
| 0.08 | 0.688(16) | 1.856(23) | 3.520(37) | 8.314(59) | 15.002 |
| 0.1 | 0.695(13) | 1.875(23) | 3.553(32) | 8.386(52) | 15.1293 |
| 0.2 | 0.7215(82) | 1.942(14) | 3.668(25) | 8.632(42) | 15.5642 |
| 0.4 | 0.7397(74) | 1.985(11) | 3.738(17) | 8.767(25) | 15.7986 |
| 0.6 | 0.7329(61) | 1.9630(97) | 3.691(17) | 8.642(22) | 15.5681 |
| 0.8 | 0.7131(52) | 1.9076(85) | 3.583(11) | 8.381(17) | 15.0956 |
| 1 | 0.6864(42) | 1.8346(85) | 3.444(11) | 8.051(15) | 14.4977 |
| 2 | 0.5355(30) | 1.4289(57) | 2.6795(76) | 6.256(12) | 11.262 |
| 4 | 0.3359(21) | 0.8959(36) | 1.6794(47) | 3.9199(56) | 7.0556 |
| 6 | 0.2373(15) | 0.6327(23) | 1.1860(29) | 2.7682(45) | 4.98261 |
| 8 | 0.1819(10) | 0.4851(18) | 0.9094(23) | 2.1226(40) | 3.82042 |

Table 7.4: Results for the condensate of adjoint Majorana fermions.

7.2.5 Extrapolation to $SU(\infty)$

Using the data at finite N_c we have computed the functions f , g , \tilde{f} defined in section 7.2.2, and that I report here for convenience:

$$\frac{1}{N_c^2} \langle \bar{\psi}\psi \rangle_{\text{S,quenched}} = f\left(\frac{1}{N_c^2}, m\right) + \frac{1}{N_c} g\left(\frac{1}{N_c^2}, m\right), \quad (7.29a)$$

$$\frac{1}{N_c^2} \langle \bar{\psi}\psi \rangle_{\text{AS,quenched}} = f\left(\frac{1}{N_c^2}, m\right) - \frac{1}{N_c} g\left(\frac{1}{N_c^2}, m\right), \quad (7.29b)$$

$$\frac{1}{N_c^2} \langle \lambda\lambda \rangle_{\text{Adj,quenched}} = \tilde{f}\left(\frac{1}{N_c^2}, m\right) - \frac{1}{2N_c^2} \langle \bar{\psi}\psi \rangle_{\text{free}}. \quad (7.29c)$$

At fixed mass, the large- N_c limit of this functions has been computed by fitting the data for $N_c = 3, 4, 6, 8$ with the function $a + b/N_c^2$. The fit has been checked to be stable if a $1/N_c^4$ term is added. The reduced χ^2 are all less than 1.1. The value of the parameters a , b and of the reduced χ^2 are reported in tables 7.5, 7.6, 7.7. The f , g , \tilde{f} functions for $N_c = 2, 3, 4, 6, 8, \infty$ are displayed in the plots 7.3.

The orientifold planar equivalence requires that $f(0, m) = \tilde{f}(0, m)$. This relationship is verified with an accuracy of 1σ for each value of the mass. The difference $f(0, m) - \tilde{f}(0, m)$ is plotted in 7.4.

7.2.6 Chiral limit

The chiral limit of the condensates is obtained by fitting each coefficient $a(f)$, $b(f)$, $a(g)$, $b(g)$, $a(\tilde{f})$, $b(\tilde{f})$ in the range of masses (.012, .1) with a linear polynomial $c_0 + c_1 m$. The result of the fits are reported in the table 7.8.

In the chiral limit, these results can be summarized in the following formulae for the bare condensates:

$$\frac{1}{N_c^2} \langle \bar{\psi}\psi \rangle_{\text{S,qu.}} (m=0) = 0.2269(26) + \frac{0.449(17)}{N_c} - \frac{0.550(55)}{N_c^2} + \dots, \quad (7.30a)$$

$$\frac{1}{N_c^2} \langle \bar{\psi}\psi \rangle_{\text{AS,qu.}} (m=0) = 0.2269(26) - \frac{0.449(17)}{N_c} - \frac{0.550(55)}{N_c^2} + \dots, \quad (7.30b)$$

$$\frac{1}{N_c^2} \langle \lambda\lambda \rangle_{\text{Adj,qu.}} (m=0) = 0.2290(20) - \frac{0.301(39)}{N_c^2} + \dots. \quad (7.30c)$$

| m | $a(f)$ | $b(f)$ | χ^2/dof |
|-------|--------------|-------------|---------------------|
| 0.012 | 0.2281(26) | -0.537(57) | 0.83 |
| 0.013 | 0.2282(27) | -0.530(55) | 0.79 |
| 0.014 | 0.2283(26) | -0.528(53) | 0.94 |
| 0.015 | 0.2287(25) | -0.532(55) | 0.88 |
| 0.016 | 0.2288(25) | -0.522(51) | 0.84 |
| 0.017 | 0.2288(25) | -0.522(50) | 0.96 |
| 0.018 | 0.2292(24) | -0.521(50) | 0.88 |
| 0.019 | 0.2296(23) | -0.526(51) | 0.97 |
| 0.02 | 0.2296(22) | -0.516(47) | 0.89 |
| 0.04 | 0.2334(15) | -0.485(36) | 0.93 |
| 0.06 | 0.2361(13) | -0.448(28) | 0.90 |
| 0.08 | 0.2386(11) | -0.420(25) | 0.74 |
| 0.1 | 0.24082(97) | -0.393(22) | 0.51 |
| 0.2 | 0.24801(74) | -0.297(16) | 0.14 |
| 0.4 | 0.25160(57) | -0.184(13) | 0.04 |
| 0.6 | 0.24772(49) | -0.120(10) | 0.04 |
| 0.8 | 0.24002(41) | -0.0796(92) | 0.04 |
| 1 | 0.23040(38) | -0.0541(82) | 0.03 |
| 2 | 0.17879(27) | -0.0095(64) | 0.005 |
| 4 | 0.11199(16) | -0.0006(37) | 0.003 |
| 6 | 0.07908(11) | 0.0000(27) | 0.003 |
| 8 | 0.060635(87) | 0.0000(20) | 0.003 |

Table 7.5: The function f was fitted with $a + b/N_c^2$ for each value of the mass. In the table, the results of the fit and the reduced χ^2 .

| m | $a(g)$ | $b(g)$ | χ^2/dof |
|-------|-------------|------------|---------------------|
| 0.012 | 0.444(17) | 0.13(24) | 0.97 |
| 0.013 | 0.443(17) | 0.12(23) | 0.90 |
| 0.014 | 0.444(17) | 0.11(22) | 1.05 |
| 0.015 | 0.441(16) | 0.13(23) | 1.01 |
| 0.016 | 0.441(16) | 0.12(21) | 0.94 |
| 0.017 | 0.442(16) | 0.11(21) | 1.05 |
| 0.018 | 0.439(15) | 0.12(20) | 0.97 |
| 0.019 | 0.438(15) | 0.14(21) | 1.09 |
| 0.02 | 0.437(14) | 0.13(19) | 0.98 |
| 0.04 | 0.4202(97) | 0.17(14) | 1.04 |
| 0.06 | 0.4092(81) | 0.15(11) | 0.99 |
| 0.08 | 0.3993(73) | 0.15(10) | 0.85 |
| 0.1 | 0.3895(63) | 0.158(88) | 0.66 |
| 0.2 | 0.3570(48) | 0.144(66) | 0.27 |
| 0.4 | 0.3169(36) | 0.106(52) | 0.04 |
| 0.6 | 0.2897(31) | 0.074(42) | 0.01 |
| 0.8 | 0.2679(26) | 0.051(38) | 0.01 |
| 1 | 0.2493(24) | 0.035(34) | 0.01 |
| 2 | 0.1822(17) | 0.008(26) | 0.01 |
| 4 | 0.11214(97) | 0.002(15) | 0.02 |
| 6 | 0.07904(68) | 0.001(11) | 0.02 |
| 8 | 0.06057(54) | 0.0009(82) | 0.01 |

Table 7.6: The function g was fitted with $a + b/N_c^2$ for each value of the mass. In the table, the results of the fit and the reduced χ^2 .

| m | $a(\tilde{f})$ | $b(\tilde{f})$ | χ^2/dof |
|-------|----------------|----------------|---------------------|
| 0.012 | 0.2301(20) | -0.297(39) | 0.04 |
| 0.013 | 0.2302(17) | -0.295(30) | 0.04 |
| 0.014 | 0.2304(17) | -0.296(35) | 0.04 |
| 0.015 | 0.2305(17) | -0.296(33) | 0.05 |
| 0.016 | 0.2307(17) | -0.294(31) | 0.05 |
| 0.017 | 0.2309(16) | -0.294(28) | 0.06 |
| 0.018 | 0.2310(16) | -0.294(28) | 0.05 |
| 0.019 | 0.2311(16) | -0.295(31) | 0.05 |
| 0.02 | 0.2313(16) | -0.294(30) | 0.06 |
| 0.04 | 0.2343(10) | -0.288(21) | 0.08 |
| 0.06 | 0.23681(74) | -0.280(16) | 0.10 |
| 0.08 | 0.23905(57) | -0.273(13) | 0.12 |
| 0.1 | 0.24103(51) | -0.266(13) | 0.14 |
| 0.2 | 0.24770(31) | -0.2296(81) | 0.16 |
| 0.4 | 0.25116(27) | -0.1690(64) | 0.14 |
| 0.6 | 0.24735(27) | -0.1209(60) | 0.07 |
| 0.8 | 0.23977(22) | -0.0859(49) | 0.08 |
| 1 | 0.23023(19) | -0.0604(47) | 0.05 |
| 2 | 0.17878(15) | -0.0113(33) | 0.02 |
| 4 | 0.111997(73) | -0.0009(19) | 0.02 |
| 6 | 0.079090(44) | -0.0002(12) | 0.02 |
| 8 | 0.060642(41) | -0.00010(99) | 0.02 |

Table 7.7: The function \tilde{f} was fitted with $a + b/N_c^2$ for each value of the mass. In the table, the results of the fit and the reduced χ^2 .

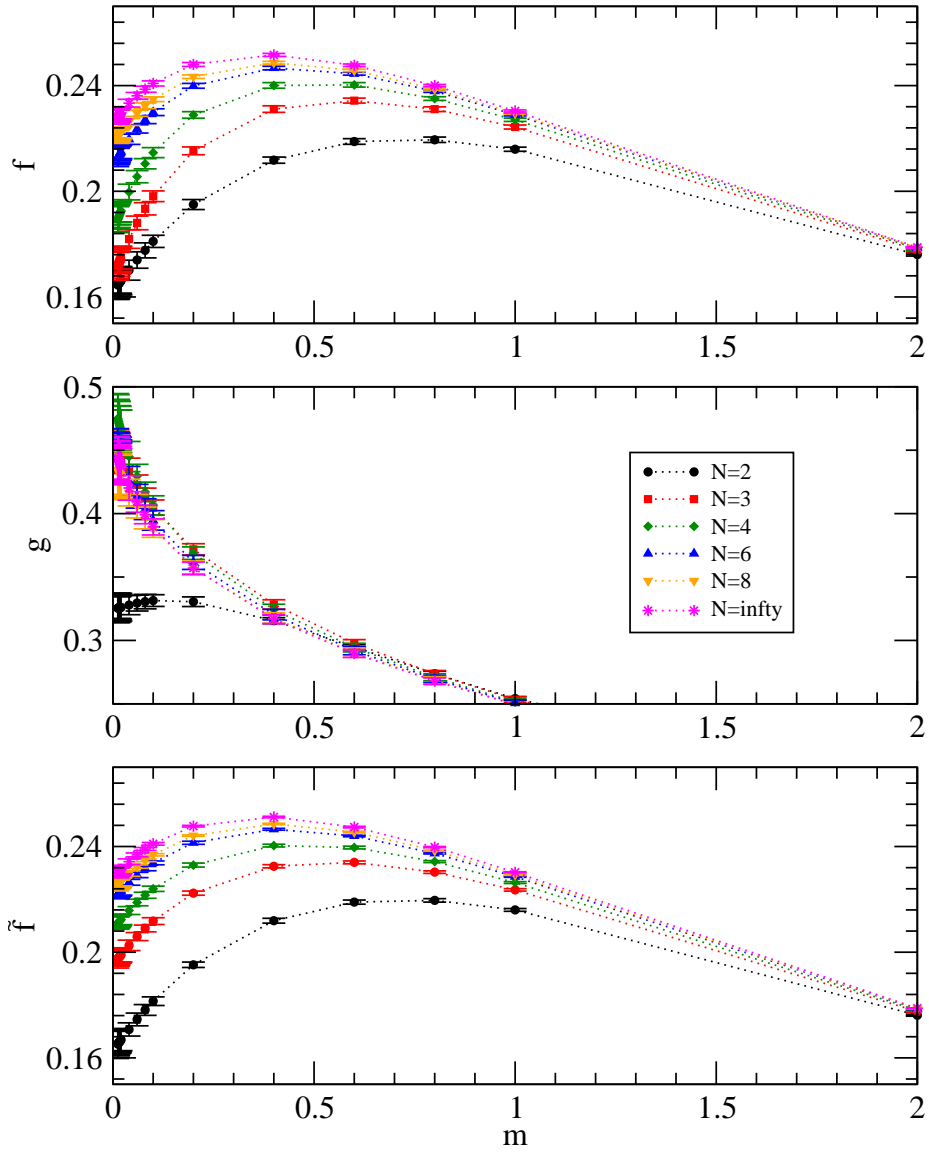
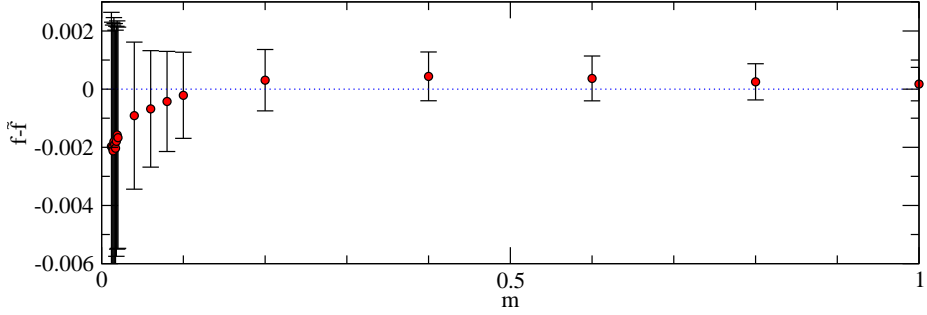


Figure 7.3: The f , g , \tilde{f} functions.


 Figure 7.4: The difference $f(0, m) - \tilde{f}(0, m)$.

| | c_0 | c_1 | χ^2/dof |
|----------------|------------|-----------|---------------------|
| $a(f)$ | 0.2269(26) | 0.144(81) | 0.09 |
| $b(f)$ | -0.550(55) | 1.60(43) | 0.01 |
| $a(g)$ | 0.449(17) | -0.62(32) | 0.05 |
| $b(g)$ | 0.12(24) | 0.4(1.1) | 0.01 |
| $a(\tilde{f})$ | 0.2290(20) | 0.123(46) | 0.10 |
| $b(\tilde{f})$ | -0.301(39) | 0.349(46) | 0.001 |

 Table 7.8: The LO and NLO of the functions f , g , \tilde{f} were fitted with $c_0 + c_1 m$ for masses in $0.012, \dots, 0.1$. In the table, the results of the fit and the reduced χ^2 . The stability of the first coefficient has been checked by adding a $c_2 m^2$ term. The errors of the second coefficient are underestimated.

| N | β | κ |
|---|---------|------------------------------------|
| 2 | 2.3715 | 0.156, 0.155, 0.154, 0.153, 0.152 |
| 3 | 5.8000 | 0.161, 0.160, 0.159, 0.1575, 0.156 |
| 4 | 10.6370 | 0.161, 0.160, 0.159, 0.1575, 0.156 |
| 6 | 24.5140 | 0.161, 0.160, 0.159, 0.1575, 0.156 |

Table 7.9: Bare parameters used the simulations of the mesonic spectrum.

7.3 Mesons at large- N_C

7.3.1 Details of the simulations

A Monte Carlo ensemble of gauge fields is generated using the Wilson action. The link variables are updated using a Cabibbo-Marinari algorithm [56], where each $SU(2)$ subgroup of $SU(N_c)$ is updated in turn. Microcanonical and heat-bath steps have been alternated in a ratio 4:1. I will call *sweep* the sequence of four microcanonical and one heat-bath update.

We chose the Wilson discretization of the Dirac operator:

$$\begin{aligned}
 D_m \phi(x) &= (D + m)\phi(x) = \\
 &= -\frac{1}{2} \left\{ \sum_{\mu} [(1 - \gamma_{\mu}) U_{\mu}(x)\phi(x + \hat{\mu}) + (1 + \gamma_{\mu}) U_{\mu}(x - \hat{\mu})^{\dagger} \phi(x - \hat{\mu})] - \right. \\
 &\quad \left. -(8 + 2m)\phi(x) \right\} . \tag{7.31}
 \end{aligned}$$

The bare mass is related to the hopping parameter used in the actual simulations by

$$1/(2\kappa) = 4 + m . \tag{7.32}$$

The complete set of bare parameters used in our simulations is summarized in table 7.9. For this work, we run simulations for $N_c = 2, 3, 4, 6$. We used a $N_s^3 \times N_t$ lattice with the spatial size $N_s = 16$ (which corresponds to about 2.3 fm) and the temporal size $N_t = 32$ (about 4.6 fm in physical units). For the quark masses used in this work, our calculation should be free from noticeable finite size effects. For the fermion fields we used periodic boundary conditions in the spatial directions and antiperiodic boundary conditions in the temporal direction. For the gauge field we used periodic boundary conditions in all directions.

| Particle | a_0 | π | ρ | a_1 | b_1 |
|----------|------------|------------------------------------------------|------------------------------------------------|-----------------------------|-----------------------------|
| Bilinear | $\bar{u}d$ | $\bar{u}\gamma_5 d, \bar{u}\gamma_0\gamma_5 d$ | $\bar{u}\gamma_i d, \bar{u}\gamma_0\gamma_i d$ | $\bar{u}\gamma_5\gamma_i d$ | $\bar{u}\gamma_i\gamma_j d$ |
| J^{PC} | 0^{++} | 0^{-+} | 1^- | 1^{++} | 1^{+-} |

Table 7.10: Bilinear operators for the computation of non-singlet meson masses.

We performed a chiral extrapolation using data from meson correlators at five values of κ for each N_c . The choice of values for κ relies on previous experience with $SU(3)$ simulations to yield pseudoscalar meson masses ≥ 450 MeV. The same values of κ were used for all values of $N_c \geq 3$, while for $SU(2)$ a different choice turned out to be necessary, since all κ 's but the lowest one were higher than κ_c . Because of the different additive renormalization, these values of κ yield different values for the bare PCAC mass as N_c is varied.

The mesonic spectrum is extracted from the zero-momentum two-point correlators of quark bilinears with the quantum numbers required to interpolate between a meson state and the vacuum. Let Γ_1 and Γ_2 be two generic products of Dirac γ matrices, a two-point correlator is defined as

$$C_{\Gamma_1, \Gamma_2}(t) = \sum_{\mathbf{x}} \left\langle (\bar{u}\Gamma_1 d)^\dagger(t, \mathbf{x}) (\bar{u}\Gamma_2 d)(0) \right\rangle, \quad (7.33)$$

where u and d are the fields corresponding to two different quark flavors, which from now on we take to be mass degenerate. All possible choices for the non-singlet quark bilinears and the quantum numbers of the corresponding physical states are summarized in table 7.10.

Performing the Wick contractions we can rewrite $C_{\Gamma_1, \Gamma_2}(t)$ in terms of the quark propagator $G(x, y) = (D_m)^{-1}(x, y)$ or, equivalently, of its hermitian version $H(x, y) = G(x, y)\gamma_5$:

$$\begin{aligned} C_{\Gamma_1, \Gamma_2}(t) &= - \sum_{\mathbf{x}} \left\langle \text{tr} \left[\gamma_0 \Gamma_1^\dagger \gamma_0 G(x, 0) \Gamma_2 \gamma_5 G(x, 0)^\dagger \gamma_5 \right] \right\rangle = \\ &= - \sum_{\mathbf{x}} \left\langle \text{tr} \left[\gamma_0 \Gamma_1^\dagger \gamma_0 H(x, 0) \gamma_5 \Gamma_2 H(x, 0) \gamma_5 \right] \right\rangle, \end{aligned} \quad (7.34)$$

(tr indicates the trace over spinor and color indices).

The propagator $G(x, 0)$ is obtained by inverting the Dirac operator D_m over point sources (capital roman letters A, B, \dots are used for collective indices over spin and color):

$$G(x, 0)_{AB} = (D_m)_{AC}^{-1}(x, y) \delta_{CB} \delta_{y,0} = (D_m)_{AC}^{-1}(x, y) \eta_C^{(B)}(y), \quad (7.35)$$

where the second equality defines the $4N_c$ point sources $\eta^{(B)}$.

The algorithm used for the inversion in (7.35), is a multishift QMR. This enables us to compute all the quark propagators corresponding to different masses simultaneously. We use a version of the QMR suitable for γ_5 -hermitian matrices with even-odd preconditioning of the Dirac matrix [60]. In the rare cases when the algorithm fails to converge, we continue the search for a solution using the MINRES algorithm, which is guaranteed to converge, on the hermitian version of the Dirac operator. For all the inversions we required a relative precision of 10^{-5} . To this accuracy, and for the parameters given above, the number of required applications of the Dirac operator to compute the propagator $G(x, 0)_{AB}$ at fixed values for the hopping parameters κ is found to become independent of N_c . We found that the average number of applications of the Dirac matrix required is about 7500, 5000, 5000 for $N_c = 3, 4, 6$ respectively (for $SU(2)$ we used different parameters).

From general large- N_c arguments, we expect the occurrence of exceptional configurations to be suppressed as N_c increases. This is confirmed by preliminary results reported in [55]. At the values of the parameters we have simulated, there is no sign of the presence of exceptional configurations.

7.3.2 Numerical results

Extracting masses from correlators

Masses can be extracted from the large- t behavior of $C_{\Gamma, \Gamma}(t)$. Inserting the energy eigenstates in the RHS of equation (7.33) yields

$$C_{\Gamma, \Gamma}(t) = \sum_i |c_i|^2 e^{-m_i t}, \quad (7.36)$$

where $c_i = (1/2m_i) \langle 0 | (\bar{u}\Gamma d)(0) | i \rangle$, Γ is one of the γ matrix products appearing in the bilinears in table 7.10, $|i\rangle$ is an eigenstate of the Hamiltonian with the same quantum numbers as the fermion bilinear, and m_i is the mass of the $|i\rangle$ eigenstate. In the limit $t \rightarrow \infty$, the previous equation becomes

$$C_{\Gamma, \Gamma}(t) \underset{t \rightarrow \infty}{=} |c_0|^2 e^{-m_0 t}, \quad (7.37)$$

i.e. at large time correlation functions decay in time as a single exponential with a typical time given by the inverse mass of the lowest-lying state in the spectrum with matching quantum numbers. The lowest mass in a given channel

can then be extracted as

$$m_0 = - \lim_{t \rightarrow \infty} \frac{\log C_{\Gamma, \Gamma}(t)}{t}. \quad (7.38)$$

Practically, one defines the effective mass $m_0(t)$ as

$$m_0(t) = - \log \frac{C_{\Gamma, \Gamma}(t)}{C_{\Gamma, \Gamma}(t-1)} \quad (7.39)$$

and obtains m_0 by fitting $m_0(t)$ to a constant at large enough t .

On a finite lattice the exponential in the large-time behavior of the propagator is replaced by a cosh and an effective mass can be defined as

$$m_0(t) = \text{acosh} \left(\frac{C_{\Gamma, \Gamma}(t+1) + C_{\Gamma, \Gamma}(t-1)}{2C_{\Gamma, \Gamma}(t)} \right). \quad (7.40)$$

Typical examples of correlation functions and effective masses as a function of the separation between source and sink are shown respectively in the plots 7.3.2 and 7.3.2.

We estimated the errors on the correlators using a jack-knife method, and checked that the bootstrap method gives similar results. With simple link operators, we have been able to extract an unambiguous signal for the pion and the rho mesons (to which we limit our analysis). Other correlators yielded a noisy signal, and we plan to investigate the possibility of improving the signal-to-noise ratio by more sophisticated measurements. Due to the small number of data points, often correlated fits proved to be unreliable, as already observed (see e.g. [61, 62]). Hence, masses have been extracted with uncorrelated fits and the error estimated with a jack-knife procedure. We have checked that the uncorrelated fit results coincide with the correlated fit results whenever the correlated fits give reasonable values for the parameters and the χ^2 .

Our results for the various N_c for the PCAC mass m_{PCAC} , the mass of the pion m_π , and the mass of the rho m_ρ are reported in tables 7.11-7.14. The details of our analysis are explained in the following two subsections.

In order to convert the results expressed in lattice units to masses in physical units, we note that

$$am = (aT_c)(m/T_c) = m/(5T_c) \quad (7.41)$$

(the last equality uses the fact that the lattice spacing has been fixed in such a way that the deconfinement phase transition corresponds to $N_t = 5$). As a reference scale, we can use T_c for $SU(3)$, which is approximately 270 MeV.

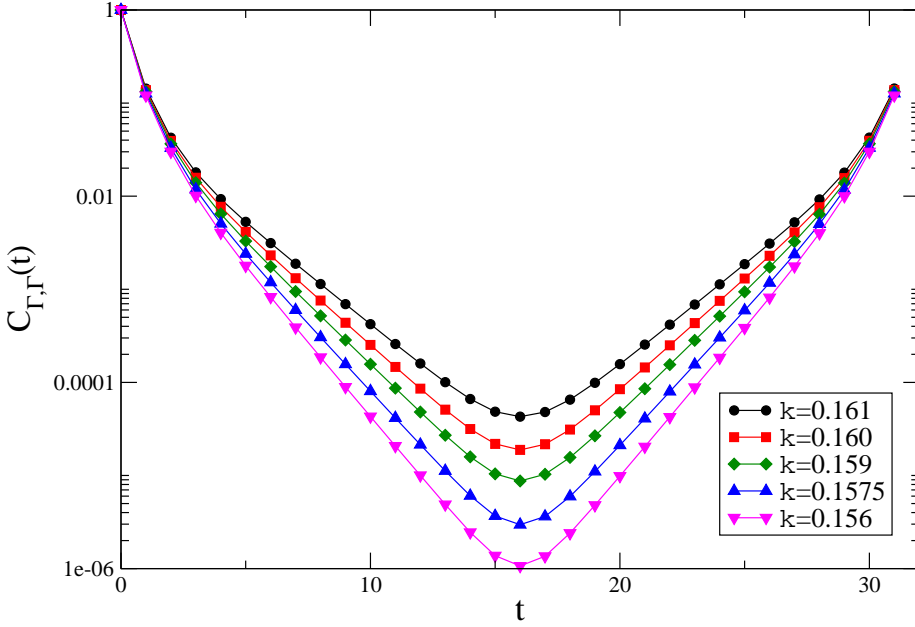


Figure 7.5: Correlators for $SU(4)$ and $\Gamma = \gamma_5$ at the values of κ shown. The correlators have been normalized in such a way that at $t = 0$ their value is 1. The lines joining the data are only guides for the eyes.

| κ | am_{PCAC} | m_{PCAC} (MeV) | am_π | m_π (MeV) | am_ρ | m_ρ (MeV) |
|----------|--------------------|-------------------------|----------|---------------|-----------|----------------|
| 0.152 | 0.0824(30) | 111(4) | 0.541(3) | 730(4) | 0.620(6) | 837(8) |
| 0.153 | 0.0669(28) | 90(4) | 0.492(4) | 664(5) | 0.584(7) | 788(9) |
| 0.154 | 0.0522(25) | 70(3) | 0.441(4) | 595(5) | 0.547(7) | 738(9) |
| 0.155 | 0.0396(24) | 53(3) | 0.389(4) | 525(5) | 0.510(10) | 789(13) |
| 0.156 | 0.0261(22) | 35(3) | 0.319(7) | 430(9) | 0.458(17) | 618(23) |

Table 7.11: Numerical results for $SU(2)$. Masses in lattice units have been converted to physical units by noting $a = 1/(5T_c)$.

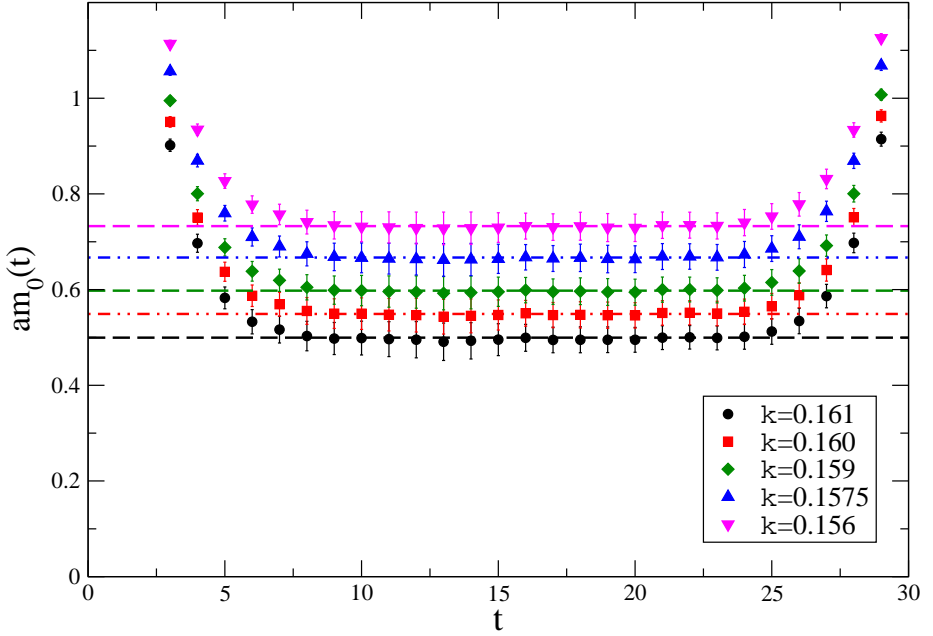


Figure 7.6: Effective masses from the correlators in figure 7.3.2. The straight lines are fits to the data at plateau.

| κ | am_{PCAC} | m_{PCAC} (MeV) | am_{π} | m_{π} (MeV) | am_{ρ} | m_{ρ} (MeV) |
|----------|--------------------|-------------------------|------------|-----------------|-------------|------------------|
| 0.156 | 0.1047(24) | 141(3) | 0.625(2) | 844(3) | 0.720(3) | 972(4) |
| 0.1575 | 0.0797(21) | 108(3) | 0.553(2) | 747(3) | 0.667(4) | 900(5) |
| 0.159 | 0.0574(17) | 77(2) | 0.476(2) | 643(3) | 0.616(5) | 832(7) |
| 0.160 | 0.0431(16) | 58(2) | 0.420(2) | 567(3) | 0.582(6) | 786(8) |
| 0.161 | 0.0299(14) | 40(2) | 0.362(3) | 489(4) | 0.550(7) | 743(9) |

Table 7.12: Numerical results for $SU(3)$. Masses in lattice units have been converted to physical units by noting $a = 1/(5T_c)$.

| κ | am_{PCAC} | m_{PCAC} (MeV) | am_π | m_π (MeV) | am_ρ | m_ρ (MeV) |
|----------|--------------------|-------------------------|----------|---------------|-----------|----------------|
| 0.156 | 0.1506(35) | 203(5) | 0.733(1) | 990(1) | 0.817(2) | 1103(3) |
| 0.1575 | 0.1234(29) | 167(4) | 0.667(1) | 900(1) | 0.766(2) | 1034(3) |
| 0.159 | 0.0981(22) | 132(3) | 0.598(1) | 807(1) | 0.714(2) | 964(3) |
| 0.160 | 0.0817(19) | 110(3) | 0.549(2) | 741(3) | 0.680(2) | 918(3) |
| 0.161 | 0.0659(17) | 89(2) | 0.499(2) | 674(3) | 0.646(3) | 872(4) |

Table 7.13: Numerical results for $SU(4)$. Masses in lattice units have been converted to physical units by noting $a = 1/(5T_c)$.

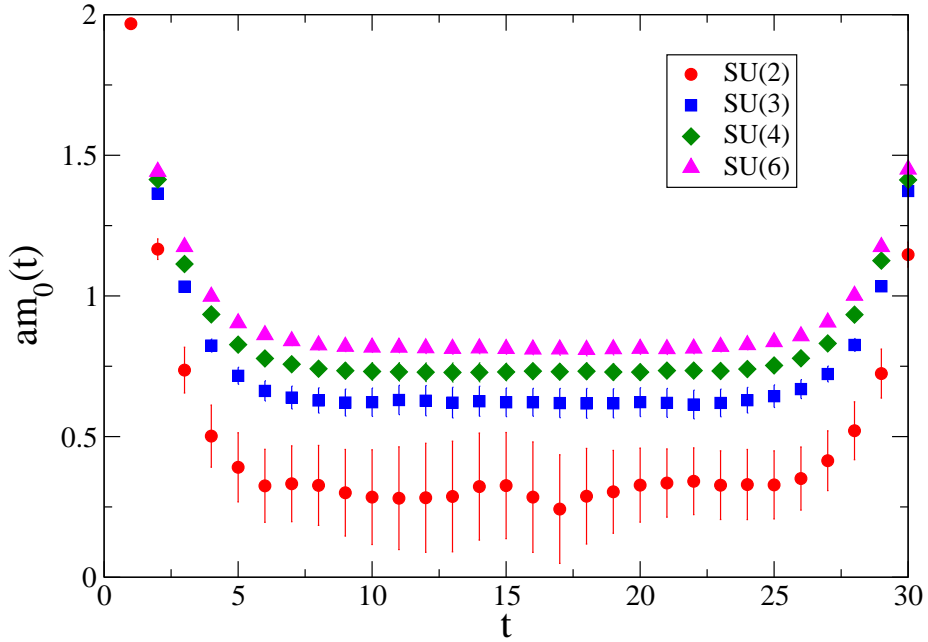


Figure 7.7: Effective masses from C_{γ_5, γ_5} at $\kappa = 0.156$.

| κ | am_{PCAC} | m_{PCAC} (MeV) | am_π | m_π (MeV) | am_ρ | m_ρ (MeV) |
|----------|--------------------|-------------------------|-----------|---------------|-----------|----------------|
| 0.156 | 0.1789(22) | 241(3) | 0.814(1) | 1099(1) | 0.889(2) | 1214(3) |
| 0.1575 | 0.1509(20) | 203(3) | 0.752(1) | 1015(1) | 0.838(2) | 1131(3) |
| 0.159 | 0.1248(18) | 168(2) | 0.687(1) | 927(1) | 0.786(2) | 1061(3) |
| 0.160 | 0.1078(17) | 146(2) | 0.6425(9) | 867(1) | 0.752(2) | 1015(3) |
| 0.161 | 0.0914(15) | 123(2) | 0.5952(9) | 804(1) | 0.718(2) | 969(3) |

Table 7.14: Numerical results for $SU(6)$. Masses in lattice units have been converted to physical units by noting $a = 1/(5T_c)$.

Meson masses at finite N_c

The pion is the would-be Goldstone boson of chiral symmetry breaking. Chiral perturbation theory at leading order predicts

$$m_\pi = A \left(\frac{1}{\kappa} - \frac{1}{\kappa_c} \right)^{1/2}. \quad (7.42)$$

Hence the value of κ corresponding to the chiral limit, κ_c , can be obtained by fitting the pion mass according to the equation (7.42). Equation (7.42) is modified for the quenched theory, where quenched chiral logs appear. For quenched $SU(N_c)$ gauge theory we expect

$$m_\pi = A \left(\frac{1}{\kappa} - \frac{1}{\kappa_c} \right)^{1/[2(1+\delta)]}, \quad (7.43)$$

where δ is positive, $\mathcal{O}(10^{-1})$ for $SU(3)$ and goes like $1/N_c$ [63].

The mass of the pion can be extracted by looking at correlators $C_{\Gamma,\Gamma}$ in which Γ is either γ_5 or $\gamma_0\gamma_5$. In the latter case, it was not possible to extract a signal for all κ 's in $SU(2)$. Hence, although in general mass plateau fits of $\gamma_0\gamma_5$ have a lower χ^2 , we will mostly focus on numerical results obtained with $\Gamma = \gamma_5$.

As N_c grows, so does m_π at fixed κ . A plot comparing numerical results for the effective mass extracted from C_{γ_5,γ_5} is shown in figure 7.3.2. A linear fit to the data according to the equation (7.42) enables us to extract the critical values of κ for the N_c at which we have simulated. Results are shown in table 7.15. The mass obtained from the $C_{\gamma_0\gamma_5,\gamma_0\gamma_5}$ correlator yields compatible results. Higher statistics and a careful study of the systematics are necessary for a more precise determination of the critical value of κ .

| N_c | κ_c | A |
|-------|-------------|------------|
| 2 | 0.15827(12) | 1.0583(99) |
| 3 | 0.16359(28) | 1.142(21) |
| 4 | 0.16556(23) | 1.201(14) |
| 6 | 0.16716(12) | 1.2422(69) |

Table 7.15: Fitted values for κ_c and A at various N_c .

Generally the reduced χ^2 of the fits according to the equation (7.42) varies between two and four. One can check whether this relatively high value of χ_r^2 is due to the fact that we are neglecting chiral logarithms. For $N \geq 2$, fits according to (7.43) yield a value of χ_r^2 that is below one, but δ is found to be negative. This agrees with the findings of [64], where the negative value is interpreted as a consequence of simulating far from the chiral limit. In fact, for $N = 2$, where we have the lightest pion mass, δ is found to be compatible with zero. As one would have expected, for $m_\pi \geq 450$ MeV there is no sensitivity to the chiral logarithms [63]. Instead of relying on phenomenological fits like in [64], we acknowledge the impossibility to determine δ and neglect the chiral logarithms, using the chiral behavior (7.43) to get an estimate for the systematic error associated with this approximation. For $SU(2)$, the three-parameter fit gives a value of κ_c that is higher than the fit with $\delta = 0$ by about 1%. Considering that $\delta \propto N^{-1}$, a conservative but safe estimate for the systematic error associated with the chiral logarithms is of the order of a few percent. This is in agreement with the literature for $SU(3)$ [64]. We will come back on issues associated with the chiral logarithms in the next subsection.

The mass of the rho has been extracted from C_{γ_i, γ_i} , after taking the average over the spatial direction i of the correlation functions. Fits in the $C_{\gamma_0 \gamma_i, \gamma_0 \gamma_i}$ channel also yield compatible results.

At small quark mass, m_ρ depends linearly on the quark mass and goes to a finite value in the chiral limit. Using (7.42), this can be rephrased into the following relationship between m_ρ and m_π

$$m_\rho = m_\rho^X + Bm_\pi^2, \quad (7.44)$$

where m_ρ^X is the mass of the rho meson at the chiral point. Note that the previous equation is not modified by chiral logarithms [63]. Assuming that the equation (7.44) holds in our case⁵, we can fit m_ρ^X and B at the various values of

⁵More sophisticated dependencies (e.g. the addition of a linear term in m_π to (7.44),

| N_c | am_ρ^X | B |
|-------|-------------|------------|
| 2 | 0.3890(75) | 0.797(31) |
| 3 | 0.4683(25) | 0.6455(84) |
| 4 | 0.5018(36) | 0.5905(88) |
| 6 | 0.5238(40) | 0.5533(77) |

 Table 7.16: Extrapolation of m_ρ to the chiral limit.

N_c from our data. Our results for those quantities are reported in table 7.16. The reduced χ^2 of the fits (which keep into account both the error on m_ρ and the error on m_π) is always less than one.

PCAC

As noted in the previous subsection, equation (7.42) only holds for the full theory, while it is modified at small masses, where quenched chiral logs become important. An alternative way of defining κ_c , which is free from these ambiguities, makes use of the partially conserved axial current (PCAC) relation. In the continuum, the PCAC relation reads

$$\partial_\mu A^\mu(x) = 2m_{\text{PCAC}} j(x), \quad (7.45)$$

with $A^\mu(x) = \bar{u}(x)\gamma_\mu\gamma_5 d(x)$ and $j = \bar{u}(x)\gamma_5 d(x)$. The previous equation allows us to determine m_{PCAC} as

$$m_{\text{PCAC}} = \frac{1}{2} \frac{\langle \int d\vec{x} (\partial_0 A^0(x)) j^\dagger(y) \rangle}{\langle \int d\vec{x} j(x) j^\dagger(y) \rangle}, \quad (7.46)$$

where y is an arbitrary point. On the lattice an effective mass $m_{\text{PCAC}}(t)$ can be defined as

$$m_{\text{PCAC}}(t) = \frac{1}{4} \frac{C_{\gamma_0\gamma_5,\gamma_5}(t+1) - C_{\gamma_0\gamma_5,\gamma_5}(t-1)}{C_{\gamma_5,\gamma_5}(t)} \quad (7.47)$$

and once again fitted at plateau. Note that with our choice for the discretized fermions PCAC holds on the lattice up to terms $\mathcal{O}(a)$. In practice, since $m_{\text{PCAC}}(t)$ defined through the equation (7.47) is antisymmetric around the

which is motivated by phenomenology) are also supported by our data. In the absence of any evidence against it, we chose to fit the parameters using the simple chiral functional behavior.

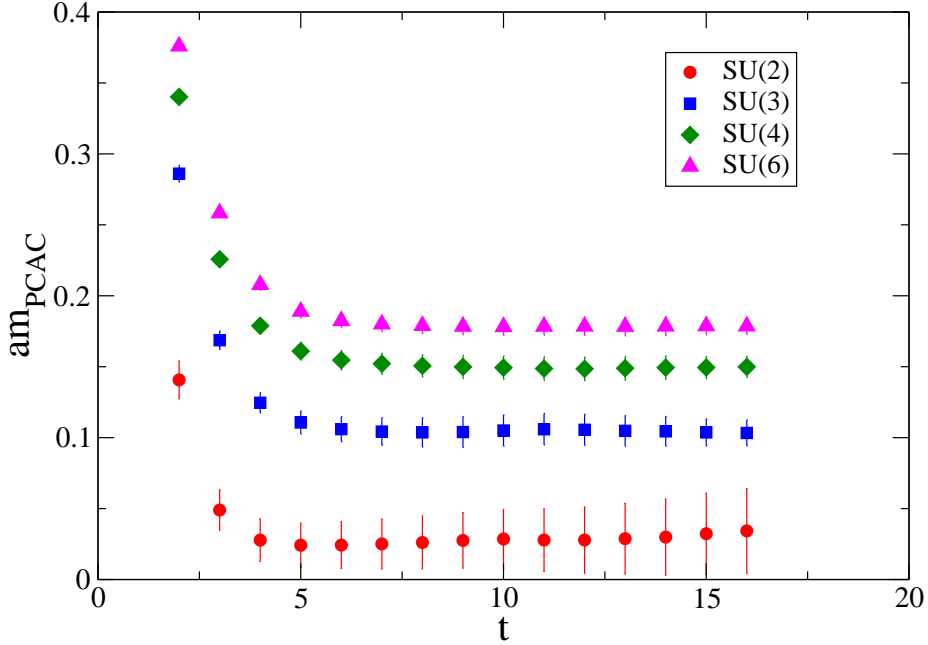


Figure 7.8: $m_{\text{PCAC}}(t)$ as a function of t for $\kappa = 0.156$.

point $N_t/2$, one averages the absolute values at points t and $N_t - t$. An example of an effective mass plateau obtained using the formula (7.47) is given in the figure 7.3.2.

Since $m_{\text{PCAC}} = Z_m(1/\kappa - 1/\kappa_c)$, we can determine κ_c as the value for which $m_{\text{PCAC}} = 0$. A linear fit to the data enables us to extract κ_c . Results for $N = 2, 3, 4, 6$ are reported in table 7.17. Comparing with the similar fits from m_π (table 7.15), it is immediate to see that using m_{PCAC} we get values for κ_c that are systematically lower⁶. Although this effect is below half a percent, it is by far larger than the statistical errors. This discrepancy might be due to the different chiral behavior of the two definitions of the quark mass for the quenched theory or be a consequence of the underestimation of the errors due to

⁶This should be contrasted with fits that keep into account chiral logarithms, for which we find values of κ_c systematically higher.

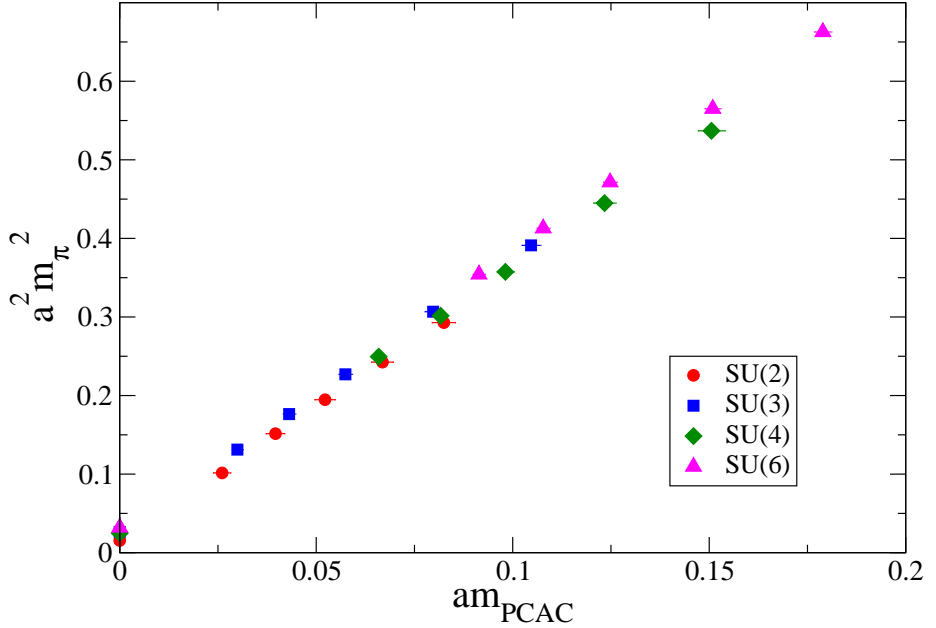


Figure 7.9: m_π^2 as a function of m_{PCAC} at the various N_c . The values of m_π at $m_{\text{PCAC}} = 0$ have been obtained with a linear fit to the data, as discussed in the text.

the use of uncorrelated fits, as we have discussed above. However, at our value of the lattice spacing discretization errors also play a relevant part. In order to investigate these issues, we have analyzed m_π as a function of m_{PCAC} . Our results are reported in figure 7.9, where m_π is plotted as a function of m_{PCAC} .

The expected quadratic behavior

$$m_\pi^2 = C m_{\text{PCAC}} \quad (7.48)$$

is not obeyed by our data. To extrapolate to the chiral limit, we need to correct the above relationship by allowing for a non-zero value for m_π when m_{PCAC} is zero:

$$m_\pi^2 = C m_{\text{PCAC}} + B, \quad (7.49)$$

where B and C depend on N_c . B (obtained from a fit according to the previous equation keeping into account both the errors on m_π and on m_{PCAC}) is roughly

| N_c | κ_c | A |
|-------|-------------|-----------|
| 2 | 0.15792(25) | 0.331(15) |
| 3 | 0.16306(10) | 0.372(10) |
| 4 | 0.16513(15) | 0.422(12) |
| 6 | 0.16657(15) | 0.438(11) |

Table 7.17: Extrapolation of κ to the chiral limit using m_{PCAC} .

of order 10^{-2} and independent of N_c . If the existence of a constant (as a function of N_c) residual m_π as $m \rightarrow 0$ were a sign of the failure of the quenched approximation, we would have expected B to go to zero as $N_c \rightarrow \infty$. This expectation is not supported by our data. On the other hand, having fixed the lattice spacing across the gauge groups, any discretization artifact would be constant in N_c . Hence, it is likely that this residual mass is (mostly) due to the violation of PCAC on the lattice. If this is correct, also the systematic discrepancy between the two sets of κ_c should be due to lattice artifacts. In order to settle this issue, a systematic study at different lattice spacings needs to be performed.

7.3.3 Extrapolation to $SU(\infty)$

Using data at finite N_c , we can estimate the behavior of the lowest-lying meson masses at $N_c = \infty$. Following similar analysis performed in pure gauge [12, 17, 18, 14, 15, 21, 65], we use predictions from the large- N_c expansion to see whether they hold in the non-perturbative regime. In practice, we take the asymptotic expansion for an observable O in the quenched case [1]

$$O(N_c) = O(\infty) + \sum_i \frac{\alpha_i}{N^{2i}} \quad (7.50)$$

and we check whether a reasonable (as dictated by the number of data) truncation of this series accommodates our numerical values. In the pure gauge case, a precocious onset of the large- N_c behavior has been found for all the observables that have been studied (which include glueball masses, deconfining temperature and topological susceptibility): the $\mathcal{O}(1/N^2)$ correction correctly describes the data down to at least $N_c = 3$, often including also the case $N_c = 2$. From a qualitative point of view, it is already clear from what we have seen so far that the quantities we have investigated have a mild dependence on N_c . In this

section, we want to study whether this dependence is correctly described by a large- N_c -inspired expansion.

κ_c can be computed in lattice perturbation theory [66]. The result at one loop is in agreement with the predictions of the large- N_c limit: this quantity receives a correction $\mathcal{O}(1/N^2)$. This motivates the fit

$$\kappa_c(N_c) = \kappa_c(\infty) + \frac{a}{N_c^2} . \quad (7.51)$$

For κ_c obtained via the equation (7.42), we get $\kappa_c(\infty) = 0.1682(1)$ and $a = -0.0398(6)$, with $\chi_r^2 = 0.6$. The quality of the fit is good, and the coefficient of the $1/N_c^2$ correction is small, as one would expect for a series expansion. Similarly to the pure gauge case, we observe an early onset of the asymptotic behavior, which captures also the $SU(2)$ value. Our data and the large- N_c extrapolation are plotted in figure 7.10. The same extrapolation for the critical value of κ obtained using the PCAC relation yields $\kappa_c(\infty) = 0.1675(2)$, $a = -0.039(1)$ and $\chi_r^2 = 1.3$. The discrepancy between the values of $\kappa_c(\infty)$ could be due to lattice discretization artifacts, as discussed in subsection 7.3.2. We take the difference between the two determinations should be seen as an estimate of the systematic error. The fact that the angular coefficient a has the same value seems to corroborate this hypothesis. A more precise determination of κ_c is beyond the scope of this work.

The slope A in (7.42) can also be extrapolated to the $N_c = \infty$ limit, with corrections that are $\mathcal{O}(1/N_c^2)$:

$$A(N_c) = A(\infty) + a/N_c^2 . \quad (7.52)$$

For the C_{γ_5, γ_5} results, the fit gives $A(\infty) = 1.262(8)$ and $a = -0.82(6)$ with $\chi_r^2 = 1.2$. This allows us to write the mass of the pion as a function of κ at $N_c = \infty$ as

$$m_\pi = 1.262(8) (1/\kappa - 5.945(4))^{1/2} , \quad (7.53)$$

where the values of κ_c obtained from fits to C_{γ_5, γ_5} have been used (using the PCAC value gives a slightly discrepant result, for the reasons discussed in subsection 7.3.2). We plot in figure 7.11 the data for the dependence of m_π^2 as a function of κ , with a fit according to (7.42). We also plot in the same figure the squared pion mass as a function of κ at the critical coupling κ_c and the critical coupling κ_c as a function of κ .

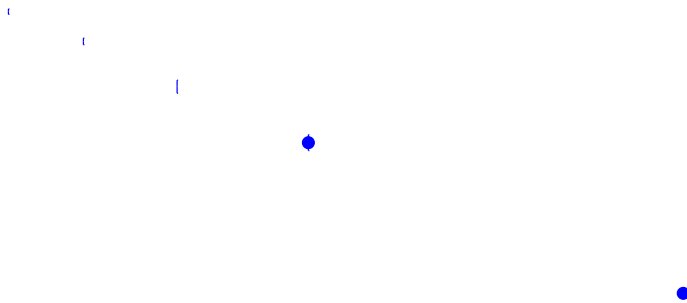


Figure 7.10: Extrapolation of κ_c to $N_c = \infty$.

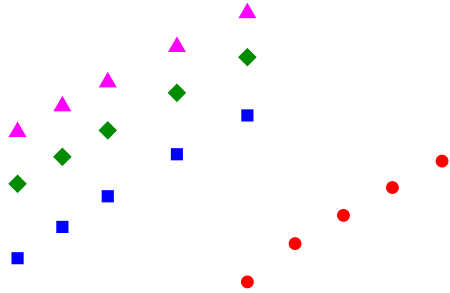


Figure 7.11: m_π as a function of $1/\kappa$. The curves through the data are obtained from a fit assuming the expected leading dependence from chiral perturbation theory. Also shown is the extrapolation to $N_c = \infty$.

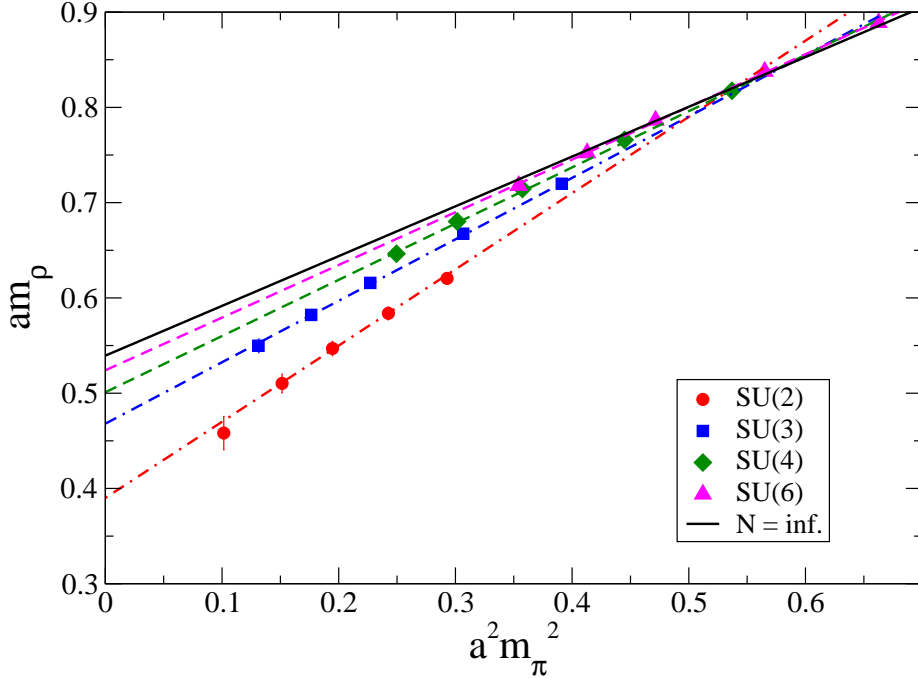


Figure 7.12: m_ρ vs. m_π^2 . Lines through the data have been obtained with a plot inspired by chiral perturbation theory. Also shown is the extrapolation to $N_c = \infty$.

The tiny χ_r^2 for $B(\infty)$ is particularly surprising, given the statistical independence of the measured values of $B(N_c)$. We see that once again the leading behavior describes very well the parameters and that the coefficient of the $1/N_c^2$ correction is order one.

As a result of this analysis, at $N_c = \infty$ we can describe m_ρ as a function of m_π as

$$m_\rho = 0.539(3) + 0.5224(8)m_\pi^2. \quad (7.55)$$

This relationship, together with the data and the fits at finite N_c , is plotted in figure 7.12.

7.3.4 Discussion

The masses of the rho and pi in the large- N_c limit of QCD have been computed, by extrapolating from the quenched data at $N_c = 2, 3, 4, 6$ and by using the large- N_c behavior deduced from arguments inspired by a diagrammatic expansion. We find that the extrapolation works well in its simplest form, i.e. using only the leading correction to the large- N_c value. This allows us to determine the behavior at $N_c = \infty$ of the mass of the pion as a function of the renormalized quark mass and of the mass of the rho as a function of the mass of the pion (chiral perturbation theory has also been used as an input).

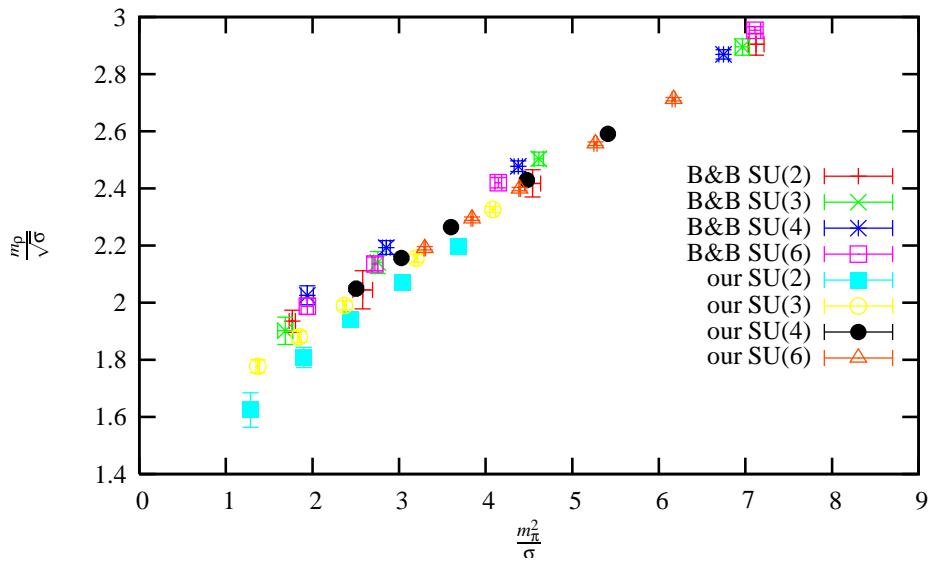


Figure 7.13: $m_\rho/\sqrt{\sigma}$ vs. m_π^2/σ . In this plot, the data of Bali and Bursa (B&B) and ours are reported. Courtesy of Francis Bursa.

(after normalizing the mass of the rho in the chiral limit to our data) finds for the coefficient of m_π^2 (see equation (7.44)) 0.57. This number is in agreement with our calculations within 5%. However, before we can draw any conclusion from the comparison with the lattice, an extrapolation of the lattice data to the continuum limit is needed.

Beyond the specific numerical details, our calculation seems to indicate that (a) the large- N_c theory is a well defined theory; (b) lattice calculations can be successfully exploited to compute the parameters of this theory; (c) at least in the quenched theory, to describe results at any finite N_c only the first term in the expected power series in $1/N_c^2$ is required; (d) the coefficient of the correction is at most order one, justifying the idea of a power expansion. All these indications are perfectly in line with what we have already learned for the $SU(N_c)$ theory without fermionic matter. Although this can be considered obvious, since our calculation is quenched, we stress that the $N_c = \infty$ limit is also quenched. In other words, to describe the limiting theory a quenched calculation suffices. The inclusion of the full fermion determinant becomes mandatory if one is interested in the actual size of the finite N_c corrections. In particular, one expects larger corrections ($\mathcal{O}(n_f/N_c)$) in the unquenched theory.

As I have stressed several times, one of the main limitations of this calculation is that our chiral extrapolations are not sensitive to the expected chiral log behavior. We have conservatively estimated that this approximation produces a 3% systematic error. This error does not affect our conclusions. Moreover, we note that chiral logarithms do not modify the formula (7.57). In any case, in order to make more robust estimates, better control on the chiral extrapolation should be achieved. This requires simulating at smaller pion masses. It would also be nice to check that the chiral log effects decrease as N_c increases.

Another source of systematic error in our calculation is the fact that simulations have been performed at one single lattice spacing. For this reason we

Chapter 8

Towards dynamical fermions – the HiRep code

As already pointed out in the Introduction, performing simulations at large number of colours with dynamical fermions in a two-index representation is computationally a hard task.

If a Hybrid Monte Carlo (HMC) algorithm is used, the computation of the gluonic part of both the action and the force requires the multiplication of link variables; these operations take a time (asymptotically) proportional to N_c^3 . The computation of the fermionic action and force requires the multiplication of the inverse Dirac operator times a random source. The inverse Dirac operator is usually computed with some iterative method. At each step, the Dirac operator is applied to a spinor. If d_R is the dimension of the fermionic representation, this operation take a time proportional to d_R^2 . Moreover, the number of steps in the iterative process do not seem to depend significantly on the number of colours. This means that, if quarks in the fundamental representation are simulated, the computation of the fermionic part of the action and the force take a time proportional to N_c^2 . At very large N_c , this should become irrelevant with respect the computation of the gauge part. But at some reasonable N_c , the computation of the fermionic terms usually dominate, since the number of iterative steps in the inversion algorithm is high. The situation gets worse when fermions in a two-index representation are considered. In this case, the computation of the fermionic terms takes a time proportional to N_c^4 (since d_R goes like N_c^2).

It is clear that a well-optimized and parallel code needs to be developed in

order to simulate dynamical fermions in a two-index representation. At present, no codes are available for simulating higher representations at various N_c . For these reasons we¹ have preferred to develop a bespoke code (HiRep), starting from scratch.

In what follows, the main features of the HiRep code (also presented in [70]), that are currently implemented, are summarized.

- HiRep can simulate $SU(N_c)$ pure Yang-Mills theories. A Monte Carlo ensemble of gauge fields is generated via the Cabibbo-Marinari algorithm [56]. This is a standard feature, already implemented in other available codes.
- HiRep can simulate $SU(N_c)$ gauge theories with Wilson fermions (Wilson action for the gauge field + one-link Wilson-Dirac pseudofermion action) in the following representations: fundamental, adjoint, antisymmetric, symmetric. Optimized code has been developed for each one of these representations. A Monte Carlo ensemble of gauge fields is generated via the RHMC algorithm [71].
- The computation of the isotriplet mesonic correlators with Wilson fermions is implemented, with the method of the point-to-all propagator.
- The computation of the fermionic condensate with staggered fermions is implemented.

Here, the features that are currently under development follow.

- Parallel computation. This feature is being implemented in two steps: definition of the geometry (how the lattice is distributed over the nodes, which are the boundaries of the sublattices, which are the buffers needed for the communication between the nodes); implementation of the communication between nodes (by using the MPI – Message Passing Interface – library) in the existing code, where nearest neighbours or global operations are required.
- All-to-all propagators techniques for the computation of isosinglet mesonic correlators. In particular, the algorithms described in [72] are being implemented.

¹Until the present stage, the code is developed in collaboration with Luigi Del Debbio (Edinburgh), Biagio Lucini (Swansea), Claudio Pica (BNL).

| N | time | Dirac op's per config. |
|---|------|------------------------|
| 2 | 3d | n.a. |
| 3 | 10d | 7500 |
| 4 | 21d | 5000 |
| 6 | 50d | 5000 |

Table 8.1: This table refers to the computation of the mesonic correlators (fermions in the fundamental representation), described in section 7.3. An ensemble of 100 gauge fields were generated on a 32×16^3 lattice, with the Cabibbo-Marinari algorithm. The correlators were computed with a multishift inverter, at $\kappa = 0.156, 0.155, 0.154, 0.153, 0.152$ for $SU(2)$, and $\kappa = 0.161, 0.160, 0.159, 0.1575, 0.156$ for the others. The total time required for the simulations is reported, as well as the number of applications of the Dirac matrix per configuration. The time required to generate the gauge fields was approximately 10% of the total time.

- The sign function of determinant of the Dirac operator, in order to simulate one dynamical flavour.

The numerical results presented in chapter 7 were obtained by running the HiRep code, in its non-parallel form. In tables 8.1, 8.2, the time required by those simulations is summarized. All these times refers to quenched simulations. We can roughly estimate the time required for dynamical simulations with the same parameters, by computing the average time per each inversion of the Dirac operator and multiplying it by 100 configurations, 100 steps of molecular dynamics (MD) per each configuration, 3 inversions of the Dirac operator per each MD step. If the computation is spread over the 60 processors available at Swansea University (the time for the communication among the processors is not taken into account; however this estimate should give a reasonable order of magnitude), the time required is reported in tables 8.3, 8.4. Clearly these computations need a large amount of computing resources; however from these estimates we conclude that dynamical simulations can be reasonably faced with the presently available resources at not too large volumes (14^4 is a realistic size) and not too large N_c ($N_c = 6$ is a realistic value).

In the following sections, I will describe in some details the algorithms implemented in the HiRep code.

| N | repr. | time | Dirac op's per config. | Smallest mass |
|---|-------|------|------------------------|----------------------|
| 2 | Adj | 30h | 25000 | 10^{-3} |
| 3 | Adj | 130h | 26000 | 10^{-3} |
| 4 | Adj | 47h | 2200 | 1.2×10^{-2} |
| 6 | Adj | 150h | 2200 | 1.2×10^{-2} |
| 8 | Adj | 850h | 2200 | 1.2×10^{-2} |
| 2 | S | 53h | 26000 | 10^{-3} |
| 3 | S | 140h | 26000 | 10^{-3} |
| 4 | S | 30h | 2200 | 1.2×10^{-2} |
| 6 | S | 140h | 2200 | 1.2×10^{-2} |
| 8 | S | 350h | 2200 | 1.2×10^{-2} |
| 3 | AS | 14h | 5900 | 10^{-3} |
| 4 | AS | 14h | 2100 | 1.2×10^{-2} |
| 6 | AS | 65h | 2200 | 1.2×10^{-2} |
| 8 | AS | 210h | 2200 | 1.2×10^{-2} |

Table 8.2: This table refers to the computation of the fermionic condensate, described in section 7.2. An ensemble of 100 gauge fields were generated on a 14^4 lattice, with the Cabibbo-Marinari algorithm. The condensate was computed with a multishift inverter at various values of the mass (the smallest one is reported in the table for each simulation). The total time required for the simulations is reported, as well as the number of applications of the Dirac matrix per configuration.

| N | time using 1 proc. | time using 60 proc.s |
|---|--------------------|----------------------|
| 2 | 75d | 2d |
| 3 | 250d | 5d |
| 4 | 400d | 7d |
| 6 | 630d | 11d |

Table 8.3: The time required for generating an ensemble of 100 gauge field interacting with dynamical fermions is estimated. The parameter are the same as in the computation of the mesonic masses (Wilson fermions in the fundamental representation, 32×16^3 lattice, $aT_c = 0.2$, $\kappa = 0.156, 0.155, 0.154, 0.153, 0.152$ for $SU(2)$, and $\kappa = 0.161, 0.160, 0.159, 0.1575, 0.156$ for the others).

| N | repr. | time using 1 proc. | time using 60 proc.s | Smallest mass |
|---|-------|--------------------|----------------------|----------------------|
| 2 | Adj | 380d | 7d | 10^{-3} |
| 3 | Adj | 1700d | 29d | 10^{-3} |
| 4 | Adj | 590d | 10d | 1.2×10^{-2} |
| 6 | Adj | 1900d | 32d | 1.2×10^{-2} |
| 8 | Adj | 11000d | 180d | 1.2×10^{-2} |
| 2 | S | 670d | 12d | 10^{-3} |
| 3 | S | 1800d | 30d | 10^{-3} |
| 4 | S | 380d | 7d | 1.2×10^{-2} |
| 6 | S | 1800d | 30d | 1.2×10^{-2} |
| 8 | S | 3600d | 73d | 1.2×10^{-2} |
| 3 | AS | 180d | 3d | 10^{-3} |
| 4 | AS | 180d | 3d | 1.2×10^{-2} |
| 6 | AS | 820d | 14d | 1.2×10^{-2} |
| 8 | AS | 2700d | 45d | 1.2×10^{-2} |

Table 8.4: The time required for generating an ensemble of 100 gauge field interacting with dynamical fermions is estimated. The parameter are the same as in the computation of the fermionic condensate (staggered fermions, the smallest mass and the fermionic representation are in the table, 14^4 lattice, $aT_c = 0.2$).

8.1 The HMC algorithm

The main idea of the Hybrid Monte Carlo (HMC) is that the probability distribution e^{-S} of the functional integral of a quantum field theory in 4 Euclidean dimensions can be generated as the thermal distribution of a 4+1 classical field theory, and this one can be obtained as the limit probability of a Markov chain. Let us see how this works in some details.

8.1.1 Bosonic fields

Given the action $S(\phi)$ of a system of bosonic fields ϕ , the HMC algorithm produces a sequence of fields $(\phi_1, \dots, \phi_n, \dots)$ that approximates the probability distribution $P_S(\phi) = 1/Z \exp[-S(\phi)]$. More precisely, if $f(\phi)$ is an observable, its expectation value is given by:

$$\langle f(\phi) \rangle \equiv \int f(\phi) P_S(\phi) d\phi = \lim_{n \rightarrow \infty} \frac{1}{n} \sum_{i=1}^n f(\phi_i). \quad (8.1)$$

The sequence above is generated as a Markov process, i.e. each configuration is obtained from the previous one, by means of a stochastic evolution characterised by a time-invariant transition probability $P_T(\phi \rightarrow \phi')$. From the general theory of the Markov chains, if the process is ergodic and the transition probability satisfies the detailed balance:

$$P_S(\phi) P_T(\phi \rightarrow \phi') = P_S(\phi') P_T(\phi' \rightarrow \phi), \quad (8.2)$$

then the Markov process reproduces correctly the probability $P_S(\phi)$.

The transition probability $P_T(\phi \rightarrow \phi')$ is defined by means of the following three-steps process.

1. Expand the configuration space with additional fields, the "momenta" π randomly chosen with probability $P_k(\pi)$ such that $P_k(\pi) = P_k(-\pi)$. Usually one takes $P_k(\pi) \propto \exp[-\pi^2/2]$.
2. (*Molecular dynamics.*) In the extended configuration space (ϕ, π) , generate a new configuration (ϕ', π') , by evolving for a fixed "time" the starting configuration along the flow defined by the Hamiltonian:

$$H(\pi, \phi) = -\ln[P_k(\pi)P_S(\phi)] = \pi^2/2 + S(\phi),$$

where π and ϕ are considered as classical conjugate variables. This step is characterised by a deterministic transition probability (it is a delta-function) $P_h((\phi, \pi) \rightarrow (\phi', \pi'))$. Of course, the Hamilton equation are integrated numerically and the transition can result distorted. One must just assure that it satisfies the reversibility condition:

$$P_h((\phi, \pi) \rightarrow (\phi', \pi')) = P_h((\phi', -\pi') \rightarrow (\phi, -\pi)) .$$

3. (*Metropolis test.*) Accept the new configuration ϕ' with probability

$$P_m((\phi, \pi) \rightarrow (\phi', \pi')) = \min \left\{ 1, \frac{P_S(\phi')P_k(\pi')}{P_S(\phi)P_k(\pi)} \right\} .$$

If the Hamiltonian H were exactly conserved in the previous step, this probability would be exactly 1. An acceptance rate less than 1 corrects the systematic errors due to the numerical errors.

It is easy to see that the resulting probability

$$P_T(\phi \rightarrow \phi') = \int d\pi d\pi' P_k(\pi) P_h((\phi, \pi) \rightarrow (\phi', \pi')) P_m((\phi, \pi) \rightarrow (\phi', \pi')) , \quad (8.3)$$

satisfies the detailed balance. The choice of $P_k(\pi)$ as a Gaussian distribution is generally believed to guarantee ergodicity.

8.1.2 Fermionic fields

When fermionic degrees of freedom are present in the action, we can first integrate them out, resulting in a non-local bosonic action and then apply the above scheme. In practice, to deal with a non-local action is not convenient from a numerical point a view and stochastic estimates are used.

Consider a quadratic fermionic term in the action: $S(\bar{\psi}, \psi) = \bar{\psi} M \psi$ with a generic interaction matrix $M(\phi)$ function of the bosonic fields ϕ . The contribution of this term to the partition function is

$$\int d\bar{\psi} d\psi \exp[-S(\bar{\psi}, \psi)] = \det[M(\phi)] .$$

Assuming that the matrix $M(\phi)$ is positive definite, we can rewrite

$$\det[M] = \int d\bar{\eta} d\eta \exp[\bar{\eta}(M)^{-1}\eta] ,$$

where $\bar{\eta}, \eta$ are two new complex bosonic fields, called pseudofermions. This term can be taken into account generating random pseudofermions $\bar{\eta}, \eta$ with the desired probability distribution and keeping them fixed during the above HMC configuration generation for the remaining bosonic fields ϕ .

8.2 $SU(N_c)$ notation

The generators of the $SU(N_c)$ group are taken hermitian:

$$T^{a\dagger} = T^a . \quad (8.4)$$

For the fundamental representation, the normalization of the generators is such that:

$$\text{tr} (T^a T^b) = \frac{1}{2} \delta^{ab} . \quad (8.5)$$

For a generic representation R , we define $R[T^a]$ to be the generator in such a representation R , with the normalizations:

$$\text{tr} (R[T^a] R[T^b]) = T_R \delta^{ab} , \quad (8.6)$$

$$\sum_a (R[T^a] R[T^a])_{AB} = C_2(R) \delta_{AB} , \quad (8.7)$$

which imply:

$$T_R = \frac{1}{N_c^2 - 1} C_2(R) d_R , \quad (8.8)$$

where d_R is the dimension of the representation R . The computation of the quantities $T_R, C_2(R), d_R$ is a standard issue of the representation theory. For the representations we are interested to, those are listed in table 8.5. A generic

Table 8.5: Group invariants

| R | d_R | T_R | $C_2(R)$ |
|------|-----------------------------|---------------------|-------------------------------------|
| fund | N_c | $\frac{1}{2}$ | $\frac{N_c^2 - 1}{2N_c}$ |
| Adj | $N_c^2 - 1$ | N_c | N_c |
| 2S | $\frac{1}{2} N_c (N_c + 1)$ | $\frac{N_c + 2}{2}$ | $C_2(f) \frac{2(N_c + 2)}{N_c + 1}$ |
| 2AS | $\frac{1}{2} N_c (N_c - 1)$ | $\frac{N_c - 2}{2}$ | $C_2(f) \frac{2(N_c - 2)}{N_c - 1}$ |

element of the Lie algebra can be equivalently thought as a $N_c \times N_c$ antihermitian

matrix $X = iX^a T^a$ or as $N_c^2 - 1$ vector X^a . The scalar product in the algebra is defined as:

$$(X, Y) = \text{tr} (X^\dagger Y) = T_f X^a Y^a . \quad (8.9)$$

8.3 The fermionic action

We used the Dirac operator in the Wilson discretization:

$$D_m = m - \frac{1}{2} \{ \gamma_\mu (\nabla_\mu + \nabla_\mu^*) - \nabla_\mu^* \nabla_\mu \} , \quad (8.10)$$

with the Lie derivative ∇_μ defined as:

$$\nabla_\mu \psi(x) = R[U_\mu(x)]\psi(x + \mu) - \psi(x) \quad (8.11)$$

$$\nabla_\mu^* \psi(x) = \psi(x) - R[U_\mu(x - \hat{\mu})]^\dagger \psi(x - \hat{\mu}) . \quad (8.12)$$

In order to implement the fermionic action with the pseudofermion technique described in subsection 8.1.2, we need a positive definite operator. A hermitian Dirac operator is obtained as:

$$Q_m = \gamma_5 D_m , \quad (8.13)$$

therefore, Q_m^2 is a positive definite operator. The following relationships among the determinants hold:

$$\text{Det } Q_m^2 = (\text{Det } Q_m)^2 = (\text{Det } D_m)^2 . \quad (8.14)$$

In general, $\text{Det } D_m$ is real but not positive, thus we need care in taking the square root:

$$(\text{Det } D_m)^{N_f} = (\text{Det } Q_m^2)^{N_f/2} \text{sgn} (\text{Det } D_m)^{N_f} . \quad (8.15)$$

If the number of flavours is even, we can neglect the sign function. I will make this assumption from this point. The determinant can be estimated now by introducing the pseudofermion ϕ .

$$(\det D_m)^{N_f} \propto \int \mathcal{D}\phi \mathcal{D}\phi^\dagger e^{-\phi^\dagger (Q_m^2)^{-N_f/2} \phi} . \quad (8.16)$$

The pseudofermion ϕ is generated randomly with the correct probability distribution at the beginning of each update procedure. This can be done generating a random pseudofermion R with a Gaussian distribution $\propto \exp(-R^\dagger R)$,

and then computing $\phi = (Q_m^2)^{N_f/4} R$. The fractional power of the matrix Q_m^2 can be approximated with a rational function:

$$(Q_m^2)^{N_f/4} \simeq r_a(Q_m^2) = \alpha_0^a + \sum_{n=1}^{d_a} \alpha_n^b (Q_m^2 - \beta_n^a)^{-1}. \quad (8.17)$$

The d_a inversions can be obtained by means of a standard multishift algorithm.

8.4 Molecular dynamics

8.4.1 Computation of the force

The HMC Hamiltonian is given by the sum of the momenta, gauge field and pseudofermion Hamiltonians:

$$\mathcal{H} = \mathcal{H}_\pi + \mathcal{H}_G + \mathcal{H}_F, \quad (8.18)$$

where

$$\mathcal{H}_\pi = \frac{1}{2} \sum_{x,\mu} \text{tr} [\pi_\mu(x)^\dagger \pi_\mu(x)] = \frac{1}{2} T_f \sum_{a,x,\mu} \pi_\mu^a(x)^2, \quad (8.19a)$$

$$\mathcal{H}_G = \frac{N_c^2}{\lambda} \sum_{p \in \mathcal{L}_\square} \left(1 - \frac{1}{N_c} \text{tr} U(p) \right), \quad (8.19b)$$

$$\mathcal{H}_F = \phi^\dagger (Q_m^2)^{-N_f/2} \phi, \quad (8.19c)$$

and we have introduced for each link variable a conjugate momentum $\pi_\mu(x) = i\pi_\mu^a(\mu) T_f^a$ in the algebra of the gauge group.

The equation of motion for the link variables are given by (the dot indicates the derivative with respect to the molecular dynamics time τ):

$$\dot{U}_\mu(x) = \pi_\mu(x) U_\mu(x), \quad (8.20)$$

while the equation of motion for the momenta can be obtain as follows from the requirement that the Hamiltonian \mathcal{H} is conserved:

$$0 = \dot{\mathcal{H}} = \dot{\mathcal{H}}_\pi + \dot{\mathcal{H}}_G + \dot{\mathcal{H}}_F. \quad (8.21)$$

For the first two derivatives we have:

$$\dot{\mathcal{H}}_\pi = T_f \sum_{x,\mu} \sum_a \pi_\mu^a(x) \dot{\pi}_\mu^a(x) , \quad (8.22)$$

$$\begin{aligned} \dot{\mathcal{H}}_G &= \sum_{x,\mu} -\frac{\beta}{N} \Re \text{tr} \left[\dot{U}_\mu(x) V_\mu^\dagger(x) \right] = \\ &= \sum_{x,\mu} -\frac{\beta}{N} \Re \text{tr} \left[\pi_\mu(x) U_\mu(x) V_\mu^\dagger(x) \right] = \\ &= \sum_{x,\mu} \sum_a -\frac{\beta}{N} \pi_\mu^a(x) \Re \text{tr} \left[iT^a U_\mu(x) V_\mu^\dagger(x) \right] , \end{aligned} \quad (8.23)$$

where $V_\mu(x)$ is the sum of the staples around the link $U_\mu(x)$.

Before computing the fermionic force, it is useful to estimate the fractional power of the matrix Q_m^2 again with a rational function:

$$(Q_m^2)^{-N_f/2} \simeq r_b(Q_m^2) = \alpha_0^b + \sum_{n=1}^{d_2} \alpha_n^b (Q_m^2 - \beta_n^b)^{-1} . \quad (8.24)$$

The fermionic Hamiltonian becomes:

$$\mathcal{H}_F = \sum_{n=1}^{d_2} \alpha_n^b \phi^\dagger (Q_m^2 - \beta_n^b)^{-1} \phi . \quad (8.25)$$

Now, the computation of the fermionic force goes as follows:

$$\begin{aligned} \dot{\mathcal{H}}_F &= -2 \sum_{n=1}^{d_2} \alpha_n^b \phi^\dagger (Q_m^2 - \beta_n^b)^{-1} \dot{Q}_m (Q_m^2 - \beta_n^b)^{-1} \phi = \\ &= -2 \sum_{n=1}^{d_2} \alpha_n^b \xi_n^\dagger \dot{Q}_m \eta_n , \end{aligned} \quad (8.26)$$

where I have defined:

$$\eta_n = (Q_m^2 - \beta_n^b)^{-1} \phi , \quad (8.27)$$

$$\xi_n = Q_m \eta_n . \quad (8.28)$$

Inserting the explicit form of Q_m , we obtain:

$$\begin{aligned}
 \dot{\mathcal{H}}_F &= \sum_{n=1}^{d_2} \alpha_n^b \sum_{x,\mu} \left\{ \xi_n(x)^\dagger \frac{d}{d\tau} R[U_\mu(x)] \gamma_5 (1 - \gamma_\mu) \eta_n(x + \hat{\mu}) + \right. \\
 &\quad \left. + \xi_n(x + \hat{\mu})^\dagger \frac{d}{d\tau} R[U_\mu(x)]^\dagger \gamma_5 (1 + \gamma_\mu) \eta_n(x) \right\} = \\
 &= \Re \sum_{n=1}^{d_2} \alpha_n^b \sum_{x,\mu} \left\{ \xi_n(x)^\dagger \frac{d}{d\tau} R[U_\mu(x)] \gamma_5 (1 - \gamma_\mu) \eta_n(x + \hat{\mu}) + \right. \\
 &\quad \left. + \eta_n(x)^\dagger \frac{d}{d\tau} R[U_\mu(x)] \gamma_5 (1 - \gamma_\mu) \xi_n(x + \hat{\mu}) \right\} \quad (8.29)
 \end{aligned}$$

where I made explicit the fact the the whole expression is real. I now use the fact that

$$\frac{d}{d\tau} R[U_\mu(x)] = R[\pi_\mu(x)] R[U_\mu(x)] = i\pi_\mu^a(x) R[T^a] R[U_\mu(x)] , \quad (8.30)$$

and obtain for the derivative of the fermionic Hamiltonian:

$$\begin{aligned}
 \dot{\mathcal{H}}_F &= \sum_{x,\mu} \sum_a \pi_\mu^a(x) \Re \text{tr} \left\{ i R[T^a] R[U_\mu(x)] \gamma_5 (1 - \gamma_\mu) \times \right. \\
 &\quad \left. \times \sum_{n=1}^{d_2} \alpha_n^b [\eta_n(x + \hat{\mu}) \otimes \xi_n(x)^\dagger + \xi_n(x + \hat{\mu}) \otimes \eta_n(x)^\dagger] \right\} . \quad (8.31)
 \end{aligned}$$

Inserting equations (8.22), (8.23), (8.31) into (8.21) we obtain the equation of motion for the momenta $\pi^a(x, \mu)$

$$\dot{\pi}_\mu^a(x) = \dot{\pi}_{G\mu}^a(x) + \dot{\pi}_{F\mu}^a(x) , \quad (8.32)$$

$$\dot{\pi}_{G\mu}^a(x) = \frac{\beta}{N} \frac{1}{T_f} \Re \text{tr} [i T_f^a U(x, \mu) V^\dagger(x, \mu)] , \quad (8.33)$$

$$\begin{aligned}
 \dot{\pi}_{F\mu}^a(x) &= - \Re \text{tr} \left\{ i R[T^a] R[U_\mu(x)] \gamma_5 (1 - \gamma_\mu) \times \right. \\
 &\quad \left. \times \sum_{n=1}^{d_2} \alpha_n^b [\eta_n(x + \hat{\mu}) \otimes \xi_n(x)^\dagger + \xi_n(x + \hat{\mu}) \otimes \eta_n(x)^\dagger] \right\} . \quad (8.34)
 \end{aligned}$$

8.4.2 Integration of the Hamilton equations

The molecular dynamics is obtained with a second-order expansion of the Omelyan integrator [73], which is given formally by:

$$U(\delta\tau) = e^{\lambda \delta\tau Q} e^{\delta\tau P/2} e^{(1-2\lambda) \delta\tau Q} e^{\delta\tau P/2} e^{\lambda \delta\tau Q}, \quad (8.35)$$

where P and Q are the update operators of the momenta and of the links respectively. The optimal value for λ found in [74] is used.

8.5 Metropolis test

In order to perform the Metropolis test, the computation of the Hamiltonian is required. The computation of the momenta and gauge terms is straightforward. While the fermionic part is computed as:

$$\mathcal{H}_F = X^\dagger X, \quad \text{with } X = (Q_m^2)^{-N_f/4} \phi, \quad (8.36)$$

and the last rational approximation is used:

$$(Q_m^2)^{-N_f/4} \simeq r_c(Q_m^2) = \alpha_0^c + \sum_{n=1}^{d_c} \alpha_n^b (Q_m^2 - \beta_n^c)^{-1}. \quad (8.37)$$

8.6 Notes on the rational approximations

In order to compute the coefficients α_n , β_n appearing in the rational approximations the Remez algorithm is needed. In our implementation we do not compute those coefficients "on the fly", but rather we use a precomputation step to generate a table of coefficients from which we pick up the right values when needed. The generation of this table goes as follows.

First note that we need to compute rational approximations for a function $f(x)$ of the form $f(x) = x^l$ and the approximation must be accurate over the spectral range of the operator Q_m^2 . To simplify the computation of the table we note that the following proposition holds: if $f(x)$ is a homogeneous function of degree l and $r(x)$ is an optimal (in the sense of relative error) rational approximation to $f(x)$ over the interval $[\epsilon, \mathfrak{h}]$ to a given accuracy then $r(kx)/k^l$ is an optimal rational approximation for the same function and the same accuracy over the interval $[\epsilon/k, \mathfrak{h}/k]$. Notice that the coefficients of the "rescaled" rational approximation are easily obtained from that of the original approximation.

A simple corollary is that, given a homogeneous function $f(x)$, we can divide the rational approximations with the same accuracy in classes distinguished by the ratio ϵ/h ; within each class the coefficients of the rational approximations are easily related to each other, so that we only need to compute one rational approximation in each class. This is what is done in our implementation.

In detail: we generate a table containing the coefficients for the rational approximations belonging in different classes distinguished by the function $f(x)$ which we want to approximate and the accuracy which is required. We arbitrary set h to a fixed value equal to the absolute upper bound on the spectrum of the matrix Q_m^2 . This choice fixes the representative of each class, because the lower bound of the approximation is now a function of h .

At run-time this table is used to generate optimal rational approximations rescaling the precomputed coefficients to the desired interval containing the spectrum of the matrix Q_m^2 . This interval is obtained by computing the maximum and minimum eigenvalue of Q_m^2 on each configuration when needed. In our code we update this interval only before the metropolis test, while we keep it fixed during the molecular dynamics.

8.7 Conventions used in the code

8.7.1 Representations

The hermitian generators T_f^a for the fundamental representation used are of the form:

$$\begin{pmatrix} 0 & 1 & 0 & \dots \\ 1 & 0 & 0 & \dots \\ 0 & 0 & 0 & \dots \\ \dots & \dots & \dots & \dots \end{pmatrix}, \begin{pmatrix} 0 & i & 0 & \dots \\ -i & 0 & 0 & \dots \\ 0 & 0 & 0 & \dots \\ \dots & \dots & \dots & \dots \end{pmatrix}, \begin{pmatrix} 1 & 0 & 0 & \dots \\ 0 & 1 & 0 & \dots \\ 0 & 0 & -2 & \dots \\ \dots & \dots & \dots & \dots \end{pmatrix}, \quad (8.38)$$

normalized so that $T_f = 1/2$. The generators for the other representations will be obtained in the following.

We first give the explicit form for the representation functions R which map $U \rightarrow U^R$. We define for each representation an orthonormal base e_R for the appropriate vector space of matrices.

For the Adjoint representation we define the base e_{Adj} for the $N \times N$ traceless hermitean matrices to be $e_{Adj}^a = T_f^a / \sqrt{T_f}$, $a = 1, \dots, N^2 - 1$ (i.e. proportional to the generators of the fundamental representation and normalized to 1.)

For the two-index Symmetric representation the base $e_S^{(ij)}$, with $i \leq j$, for the $N \times N$ symmetric matrices is given by:

$$i \neq j, \quad e_S^{(ij)} = \frac{1}{\sqrt{2}} \begin{pmatrix} 0 & 1 & 0 & \dots \\ 1 & 0 & 0 & \dots \\ 0 & 0 & 0 & \dots \\ \dots & \dots & \dots & \dots \end{pmatrix}, \quad (8.39)$$

$$i = j, \quad e_S^{(ii)} = \begin{pmatrix} 0 & 0 & 0 & \dots \\ 0 & 1 & 0 & \dots \\ 0 & 0 & 0 & \dots \\ \dots & \dots & \dots & \dots \end{pmatrix}, \quad (8.40)$$

where the non zero entries are at position (i, j) , etc.

For the two-index Antisymmetric representation the base $e_{AS}^{(ij)}$, with $i < j$, for the $N \times N$ symmetric matrices is given by:

$$e_{AS}^{(ij)} = \frac{1}{\sqrt{2}} \begin{pmatrix} 0 & 1 & 0 & \dots \\ -1 & 0 & 0 & \dots \\ 0 & 0 & 0 & \dots \\ \dots & \dots & \dots & \dots \end{pmatrix}, \quad (8.41)$$

where, as above, the non zero entries are at position (i, j) .

The maps R are explicitly given by:

$$(R^{Adj}U)_{ab} = U_{ab}^{Adj} = \text{tr} [e_{Adj}^a U e_{Adj}^b U^\dagger], \quad a, b = 1, \dots, N^2 - 1, \quad (8.42)$$

$$(R^S U)_{(ij)(lk)} = U_{(ij)(lk)}^S = \text{tr} [(e_S^{(ij)})^\dagger U e_S^{(lk)} U^T], \quad i \leq j, l \leq k, \quad (8.43)$$

$$(R^A U)_{(ij)(lk)} = U_{(ij)(lk)}^A = \text{tr} [(e_A^{(ij)})^\dagger U e_A^{(lk)} U^T], \quad i < j, l < k. \quad (8.44)$$

The generators T_R^a used are defined as the image of the generators in the fundamental under the differential of the maps R defined above: $T_R^a = R_* T_f^a$. Explicit expression can easily be worked out from the definition above. The invariants T_R and $C_2(R)$ for the generators defined in this way are given in table 8.5.

8.7.2 γ matrices

We use the chiral representation for the Dirac γ matrices:

$$\gamma_\mu = \begin{pmatrix} 0 & e_\mu \\ e_\mu^\dagger & 0 \end{pmatrix}, \quad (8.45)$$

where e_μ are 2×2 matrices given by: $e_0 = -1$, $e_k = -i\sigma_k$,

$$\sigma_1 = \begin{pmatrix} 0 & 1 \\ 1 & 0 \end{pmatrix}, \quad \sigma_2 = \begin{pmatrix} 0 & -i \\ i & 0 \end{pmatrix}, \quad \sigma_3 = \begin{pmatrix} 1 & 0 \\ 0 & -1 \end{pmatrix}. \quad (8.46)$$

We have:

$$\gamma_5 = \gamma_0\gamma_1\gamma_2\gamma_3 = \begin{pmatrix} 1 & 0 \\ 0 & -1 \end{pmatrix}. \quad (8.47)$$

Chapter 9

Conclusions and outlook

The orientifold large- N_c limit of QCD and the orientifold planar equivalence have been discussed in this work, mainly from a lattice point of view. The orientifold planar equivalence is indeed expected to be valid also at fixed lattice spacing. Some debated points, raised in the past against the orientifold planar equivalence, have been discussed and actually resolved in its favour.

Summarizing, a multicolour version of QCD can be defined by taking some of the quarks in the antisymmetric two-index representation of the gauge group (OrientiQCD). In the large- N_c limit, this theory is found to be equivalent to a gauge theory with the same number of Majorana fermions in the adjoint representation (AdjQCD).

In this work, I have proved that the orientifold planar equivalence holds on the lattice in the strong-coupling and large-mass phase (chapter 4). Unfortunately, this phase is expected to be disconnected from the physical one (the weak-coupling and small-mass phase, where the continuum limit is defined), as it happens in the well-known case of the large- N_c limit of 2d Yang-Mills. This proof can be refined (section 3.4), and it has been shown that the equivalence holds in the large-mass phase (no restriction for the coupling constant) under the (commonly accepted) hypothesis that in pure Yang-Mills the charge conjugation symmetry is not spontaneously broken. Whether the large-mass phase is analytically connected to the physical one or not, is still an open point for both OrientiQCD and AdjQCD, and deserves some future investigation.

It was proved in [26] that the orientifold planar equivalence holds if and only if the charge conjugation symmetry is not spontaneously broken in OrientiQCD. It was shown that on a space with one small compact dimension and periodic

boundary conditions for the fermions the charge conjugation is broken and the equivalence actually is not valid. Therefore the validity of the equivalence requires a phase transition as the size of the compact dimension grows, and the restoration of the charge conjugation. In this work, I have shown as the breaking of the charge conjugation implies the presence of a baryonic current flowing along the compact dimension (chapter 6) and thus it is intimately related to the (explicit) breaking of the Lorentz symmetry. This picture (besides the CPT breaking and the dependence on the boundary condition) strongly supports the idea that the charge conjugation is restored at large enough size.

It was questioned in [24] that OrientiQCD and AdjQCD cannot be equivalent, because these theories have different symmetry groups even at large- N_c . Actually, the equivalence is claimed not to hold between the two full theories, but just between the two sectors (the *neutral sectors*) of all the charge conjugation invariant and bosonic states. Although both the chiral symmetry group (section 3.1) and the center symmetry group (chapter 5) are different in the two theories, only some subgroups map the neutral sector into itself. And in this work it was shown that these subgroups are exactly the same in the two theories, according with the orientifold planar equivalence.

All the pieces discussed here perfectly fit together in a puzzle that strongly support the orientifold planar equivalence, and this analysis was one of the two main goals of this work.

The other one concerns the numerical simulation of OrientiQCD and AdjQCD. Since the $1/N_c$ corrections are generally hard to handle analytically, numerical simulation is the natural tool to quantify them. The HiRep code (chapter 8) was developed for simulating gauge theories with fermions in the two-index representations at generic N_c . At present, a single-processor version is ready, while the parallel version is being developing. As I highlighted several times, the simulations of dynamical fermions in the two-index representations requires large computing resources and a parallel code. However, some preliminary analyses of the performance of the HiRep code suggest that it will be able to simulate dynamical fermions on lattices of the order of 14^4 sites and up to $N_c = 6$ with the resources already available (a 60-core cluster at the Swansea University) in a reasonable time. $N_c = 8$ is harder, but it could be still reliable at least in the antisymmetric case.

It was shown in this work that in some cases, i.e. the computation of the pion and rho masses in the quenched theory (section 7.3), $N_c = 6$ is enough in order to obtain very good extrapolations at $N_c = \infty$. The fermionic condensate with fermions in the two-index representations was also computed in the quenched theory (section 7.2), but also $N_c = 8$ was used in this case.

The parallel version of the HiRep code is being developed in collaboration with Luigi Del Debbio (Edinburgh), Biagio Lucini (Swansea), Claudio Pica (BNL), Antonio Rago (Swansea), and it will be used more than one project:

- to compute the spectra of OrientiQCD and AdjQCD, and evaluate the subleading corrections to the orientifold planar equivalence;
- to compute the masses of the isosinglet mesons in the 't Hooft large- N_c limit (in collaboration with Gregory Moraitis (Swansea), Francis Bursa (Oxford), Gunnar Bali (Regensburg));
- to investigate the softly broken supersymmetric Yang-Mills;
- to simulate models for the breaking of the electroweak symmetry via strong interaction (technicolor).

Bibliography

- [1] G. 't Hooft, *A planar diagram theory for strong interactions*, *Nucl. Phys.* **B72** (1974) 461.
- [2] J. M. Maldacena, *The large N limit of superconformal field theories and supergravity*, *Adv. Theor. Math. Phys.* **2** (1998) 231–252 [[hep-th/9711200](#)].
- [3] A. Armoni, M. Shifman and G. Veneziano, *SUSY relics in one-flavor QCD from a new $1/N$ expansion*, *Phys. Rev. Lett.* **91** (2003) 191601 [[hep-th/0307097](#)].
- [4] A. Armoni, M. Shifman and G. Veneziano, *Exact results in non-supersymmetric large N orientifold field theories*, *Nucl. Phys.* **B667** (2003) 170–182 [[hep-th/0302163](#)].
- [5] A. Armoni, M. Shifman and G. Veneziano, *From super-Yang-Mills theory to QCD: Planar equivalence and its implications*, [hep-th/0403071](#).
- [6] A. Armoni, M. Shifman and G. Veneziano, *Exact results in a non-supersymmetric gauge theory*, *Fortsch. Phys.* **52** (2004) 453–457.
- [7] A. Armoni, G. Shore and G. Veneziano, *Quark condensate in massless QCD from planar equivalence*, *Nucl. Phys.* **B740** (2006) 23–35 [[hep-ph/0511143](#)].
- [8] A. Sagnotti, *Some properties of open string theories*, [hep-th/9509080](#).
- [9] A. Sagnotti, *Surprises in open-string perturbation theory*, *Nucl. Phys. Proc. Suppl.* **56B** (1997) 332–343 [[hep-th/9702093](#)].

BIBLIOGRAPHY

- [10] E. Corrigan and P. Ramond, *A note on the quark content of large color groups*, *Phys. Lett.* **B87** (1979) 73.
- [11] R. Narayanan and H. Neuberger, *Universality of large N phase transitions in wilson loop operators in two and three dimensions*, [arXiv:0711.4551](#) [[hep-th](#)].
- [12] B. Lucini and M. Teper, *$SU(N)$ gauge theories in four dimensions: Exploring the approach to $N = \text{infinity}$* , *JHEP* **06** (2001) 050 [[hep-lat/0103027](#)].
- [13] L. Del Debbio, H. Panagopoulos, P. Rossi and E. Vicari, *k -string tensions in $SU(N)$ gauge theories*, *Phys. Rev.* **D65** (2002) 021501 [[hep-th/0106185](#)].
- [14] L. Del Debbio, H. Panagopoulos, P. Rossi and E. Vicari, *Spectrum of confining strings in $SU(N)$ gauge theories*, *JHEP* **01** (2002) 009 [[hep-th/0111090](#)].
- [15] L. Del Debbio, H. Panagopoulos and E. Vicari, *Theta dependence of $SU(N)$ gauge theories*, *JHEP* **08** (2002) 044 [[hep-th/0204125](#)].
- [16] B. Lucini, M. Teper and U. Wenger, *The deconfinement transition in $SU(N)$ gauge theories*, *Phys. Lett.* **B545** (2002) 197–206 [[hep-lat/0206029](#)].
- [17] B. Lucini, M. Teper and U. Wenger, *The high temperature phase transition in $SU(N)$ gauge theories*, *JHEP* **01** (2004) 061 [[hep-lat/0307017](#)].
- [18] B. Lucini, M. Teper and U. Wenger, *Topology of $SU(N)$ gauge theories at $T \text{ approx. } 0$ and $T \text{ approx. } T(c)$* , *Nucl. Phys.* **B715** (2005) 461–482 [[hep-lat/0401028](#)].
- [19] B. Lucini, M. Teper and U. Wenger, *Glueballs and k -strings in $SU(N)$ gauge theories: Calculations with improved operators*, *JHEP* **06** (2004) 012 [[hep-lat/0404008](#)].
- [20] R. Narayanan and H. Neuberger, *Chiral symmetry breaking at large $N(c)$* , *Nucl. Phys.* **B696** (2004) 107–140 [[hep-lat/0405025](#)].
- [21] L. Del Debbio, H. Panagopoulos and E. Vicari, *Topological susceptibility of $SU(N)$ gauge theories at finite temperature*, *JHEP* **09** (2004) 028 [[hep-th/0407068](#)].

-
- [22] B. Lucini, M. Teper and U. Wenger, *Properties of the deconfining phase transition in $SU(N)$ gauge theories*, *JHEP* **02** (2005) 033 [[hep-lat/0502003](#)].
- [23] A. Armoni, M. Shifman and G. Veneziano, *Refining the proof of planar equivalence*, *Phys. Rev.* **D71** (2005) 045015 [[hep-th/0412203](#)].
- [24] F. Sannino, *Higher representations: Confinement and large N* , *Phys. Rev.* **D72** (2005) 125006 [[hep-th/0507251](#)].
- [25] A. Patella, *An insight on the proof of orientifold planar equivalence on the lattice*, *Phys. Rev.* **D74** (2006) 034506 [[hep-lat/0511037](#)].
- [26] M. Unsal and L. G. Ya e, *(In)validity of large N orientifold equivalence*, *Phys. Rev.* **D74** (2006) 105019 [[hep-th/0608180](#)].
- [27] T. DeGrand and R. Hoffmann, *QCD with one compact spatial dimension*, *JHEP* **02** (2007) 022 [[hep-lat/0612012](#)].
- [28] A. Armoni, M. Shifman and G. Veneziano, *A note on C -parity conservation and the validity of orientifold planar equivalence*, *Phys. Lett.* **B647** (2007) 515–518 [[hep-th/0701229](#)].
- [29] B. Lucini, A. Patella and C. Pica, *Baryon currents in QCD with compact dimensions*, *Phys. Rev.* **D75** (2007) 121701 [[hep-th/0702167](#)].
- [30] A. Armoni, M. Shifman and M. Unsal, *Planar limit of orientifold field theories and emergent center symmetry*, [arXiv:0712.0672](#) [[hep-th](#)].
- [31] E. Witten, *Baryons in the $1/N$ expansion*, *Nucl. Phys.* **B160** (1979) 57.
- [32] G. Veneziano, *$U(1)$ without instantons*, *Nucl. Phys.* **B159** (1979) 213–224.
- [33] E. Witten, *Current algebra theorems for the $U(1)$ goldstone boson*, *Nucl. Phys.* **B156** (1979) 269.
- [34] G. Veneziano, *Some aspects of a unified approach to gauge, dual and gribov theories*, *Nucl. Phys.* **B117** (1976) 519–545.
- [35] L. G. Ya e, *Large N limits as classical mechanics*, *Rev. Mod. Phys.* **54** (1982) 407.

BIBLIOGRAPHY

- [36] P. Kovtun, M. Unsal and L. G. Ya e, *Necessary and sufficient conditions for non-perturbative equivalences of large $N(c)$ orbifold gauge theories*, *JHEP* **07** (2005) 008 [[hep-th/0411177](#)].
- [37] Y. M. Makeenko and A. A. Migdal, *Exact equation for the loop average in multicolor QCD*, *Phys. Lett.* **B88** (1979) 135.
- [38] P. Kovtun, M. Unsal and L. G. Ya e, *Non-perturbative equivalences among large $N(c)$ gauge theories with adjoint and bifundamental matter fields*, *JHEP* **12** (2003) 034 [[hep-th/0311098](#)].
- [39] D. J. Gross and E. Witten, *Possible third order phase transition in the large N lattice gauge theory*, *Phys. Rev.* **D21** (1980) 446–453.
- [40] T. J. Hollowood and A. Naqvi, *Phase transitions of orientifold gauge theories at large N in finite volume*, *JHEP* **04** (2007) 087 [[hep-th/0609203](#)].
- [41] R. Narayanan and H. Neuberger, *Phases of planar QCD on the torus*, *PoS LAT2005* (2006) 005 [[hep-lat/0509014](#)].
- [42] I. Montvay, *Majorana fermions on the lattice*, [hep-lat/0108011](#).
- [43] G. 't Hooft, *Large N* , [hep-th/0204069](#).
- [44] C. Vafa and E. Witten, *Parity conservation in QCD*, *Phys. Rev. Lett.* **53** (1984) 535.
- [45] P. van Baal, *The small volume expansion of gauge theories coupled to massless fermions*, *Nucl. Phys.* **B307** (1988) 274.
- [46] M. Unsal, *Phases of $N(c) = \text{infinity}$ QCD-like gauge theories on $S^1 \times S^1$ and nonperturbative orbifold-orientifold equivalences*, *Phys. Rev.* **D76** (2007) 025015 [[hep-th/0703025](#)].
- [47] B. Lucini, A. Patella and C. Pica, *Spontaneous breaking of discrete symmetries in QCD on a small volume*, *AIP Conf. Proc.* **957** (2007) 229–232 [[arXiv:0709.0909](#) [[hep-lat](#)]].
- [48] T. DeGrand, R. Hoffmann and J. Najjar, *More about QCD on compact spaces*, [arXiv:0711.4290](#) [[hep-lat](#)].
- [49] J. L. F. Barbon and C. Hoyos-Badajoz, *Dynamical Higgs potentials with a landscape*, *Phys. Rev.* **D73** (2006) 126002 [[hep-th/0602285](#)].

-
- [50] T. DeGrand, R. H., S. Schaefer and Z. Liu, *Quark condensate in one-flavor QCD*, *Phys. Rev.* **D74** (2006) 054501 [[hep-th/0605147](#)].
- [51] R. Sommer, *A new way to set the energy scale in lattice gauge theories and its applications to the static force and alpha-s in SU(2) yang-mills theory*, *Nucl. Phys.* **B411** (1994) 839–854 [[hep-lat/9310022](#)].
- [52] A. Armoni, B. Lucini, A. Patella and C. Pica, *Lattice study of planar equivalence: The quark condensate*, *Phys. Rev.* **D78** (2008) 045019 [[0804.4501](#)].
- [53] L. Del Debbio, B. Lucini, A. Patella and C. Pica, *Quenched mesonic spectrum at large N*, [arXiv:0712.3036](#) [[hep-th](#)].
- [54] R. Narayanan and H. Neuberger, *The quark mass dependence of the pion mass at infinite N*, *Phys. Lett.* **B616** (2005) 76–84 [[hep-lat/0503033](#)].
- [55] G. Bali and F. Bursa, *Meson masses at large N(c)*, [arXiv:0708.3427](#) [[hep-lat](#)].
- [56] N. Cabibbo and E. Marinari, *A new method for updating SU(N) matrices in computer simulations of gauge theories*, *Phys. Lett.* **B119** (1982) 387–390.
- [57] J. B. Kogut *et. al.*, *Studies of chiral symmetry breaking in SU(2) lattice gauge theory*, *Nucl. Phys.* **B225** (1983) 326.
- [58] S. J. Hands and M. Teper, *On the value and origin of the chiral condensate in quenched SU(2) lattice gauge theory*, *Nucl. Phys.* **B347** (1990) 819–853.
- [59] P. Kovtun, M. Unsal and L. G. Ya e, *Volume independence in large N(c) QCD-like gauge theories*, *JHEP* **06** (2007) 019 [[hep-th/0702021](#)].
- [60] A. Frommer, B. Nockel, S. Gusken, T. Lippert and K. Schilling, *Many masses on one stroke: Economic computation of quark propagators*, *Int. J. Mod. Phys.* **C6** (1995) 627–638 [[hep-lat/9504020](#)].
- [61] C. Michael, *Fitting correlated data*, *Phys. Rev.* **D49** (1994) 2616–2619 [[hep-lat/9310026](#)].
- [62] C. Michael and A. McKerrell, *Fitting correlated hadron mass spectrum data*, *Phys. Rev.* **D51** (1995) 3745–3750 [[hep-lat/9412087](#)].

BIBLIOGRAPHY

- [63] S. R. Sharpe, *Quenched chiral logarithms*, *Phys. Rev.* **D46** (1992) 3146–3168 [[hep-lat/9205020](#)].
- [64] M. Gockeler *et al.*, *Scaling of non-perturbatively $O(a)$ improved Wilson fermions: Hadron spectrum, quark masses and decay constants*, *Phys. Rev.* **D57** (1998) 5562–5580 [[hep-lat/9707021](#)].
- [65] L. Del Debbio, G. M. Manca, H. Panagopoulos, A. Skouroupathis and E. Vicari, *Theta-dependence of the spectrum of $SU(N)$ gauge theories*, *JHEP* **06** (2006) 005 [[hep-th/0603041](#)].
- [66] J. Stehr and P. H. Weisz, *Note on gauge fixing in lattice QCD*, *Lett. Nuovo Cim.* **37** (1983) 173–177.
- [67] J. Babington, J. Erdmenger, N. J. Evans, Z. Guralnik and I. Kirsch, *Chiral symmetry breaking and pions in non-supersymmetric gauge / gravity duals*, *Phys. Rev.* **D69** (2004) 066007 [[hep-th/0306018](#)].
- [68] J. Erdmenger, N. Evans, I. Kirsch and E. Threlfall, *Mesons in gauge/gravity duals - a review*, [arXiv:0711.4467](#) [[hep-th](#)].
- [69] N. R. Constable and R. C. Myers, *Exotic scalar states in the AdS/CFT correspondence*, *JHEP* **11** (1999) 020 [[hep-th/9905081](#)].
- [70] L. Del Debbio, A. Patella and C. Pica, *Higher representations on the lattice: numerical simulations. $SU(2)$ with adjoint fermions*, [0805.2058](#).
- [71] A. D. Kennedy, I. Horvath and S. Sint, *A new exact method for dynamical fermion computations with non-local actions*, *Nucl. Phys. Proc. Suppl.* **73** (1999) 834–836 [[hep-lat/9809092](#)].
- [72] S. Collins, G. Bali and A. Schafer, *Disconnected contributions to hadronic structure: a new method for stochastic noise reduction*, [arXiv:0709.3217](#) [[hep-lat](#)].
- [73] I. P. Omelyan, I. M. Mryglod and F. R. *Comp. Phys. Comm* **151** (2003) 272.
- [74] T. Takaishi and P. de Forcrand, *Testing and tuning new symplectic integrators for hybrid monte carlo algorithm in lattice QCD*, *Phys. Rev.* **E73** (2006) 036706 [[hep-lat/0505020](#)].